ABSTRACT

BACTERIAL MOTION AND SPREAD IN POROUS
ENVIRONMENTS

by
Yasser Almoteri

Micro-swimmers are ubiquitous in nature from soil and water to mammalian bodies and even many technological processes. Common known examples are microbes such as bacteria, micro-algae and micro-plankton, cells such as spermatozoa and organisms such as nematodes. These swimmers live and have evolved in multiplex environments and complex flows in the presence of other swimmers and types, inert particles and fibers, interfaces and non-trivial confinements and more. Understanding the locomotion and interactions of these individual micro-swimmers in such impure viscous fluids is crucial to understanding the emergent dynamics of such complex systems, and to further enabling us to control and direct this dynamics.

The focus is on studying through mathematical modeling, analysis and computer simulations, the collective dynamics and chemotactic aggregation of a suspension of micro-swimmers immersed in a fluid that also contains inert impurities or stationary obstacles. Such an environment can be regarded as a wet porous medium. A continuum model for micro-swimmers in such a wet porous medium that accounts for the presence of the impurities or obstacles through the Brinkman approximation, which encompasses their effect using a resistance or friction parameter in the fluid flow equations is presented. This resistance introduces supplementary friction in the individual locomotion and alters the way each swimmer disturbs the surrounding fluid and the hydrodynamic interaction with its neighbors. The analysis of the linearized system reveals that the resistance affects and hinders the hydrodynamic interactions and collective swimming. Asymptotic analysis and the numerical solution of the dispersion relations help compose a parameter phase space for four predicted

and distinct types of dynamics: hydrodynamic collective swimming, chemotactic aggregation, dynamic aggregation, and uniform motion. Simulations of the full nonlinear system show that resistance impacts the collective dynamics for each of these dynamics states.

Firstly, resistance inhibits the collective motion of the swimmers. In an environment where resistance is strong, the swimmers find it challenging to synchronize their movements and form cohesive groups. The presence of obstacles and the associated resistance disrupt the fluid flow patterns collectively generated by the swimmers, leading to a less organized or coherent collective behavior.

Secondly and surprisingly, resistance hampers the chemotactic behavior of swimmers. Chemotaxis is the process by which micro-swimmers respond to chemical gradients and move towards regions of higher concentration; if the chemical is produced by the swimmers themselves as in quorum sensing scenarios, this leads to aggregation. However resistance hinders the ability of pusher swimmers to aggregate and form dense clusters because it impedes their ability to efficiently navigate towards chemotactic cues and assemble into concentrated populations. Simulations also reveal unexpected dynamics far from the parameter regimes predicted by the linear analysis, ultimately showcasing the nonlinear couplings in this complex system.

Lastly, resistance restricts the spreading of an already accumulated swimmer suspension, for example a bacterial cluster. When swimmers are already clustered or perhaps introduced into a specific region, resistance impedes their ability to disperse to other areas of the medium, effectively detaining them to localized regions and reducing their ability to spread out and cover larger distances. These findings show that complex emergent dynamics also depends on the initial state of the system, and ultimately help towards better understanding of recent experimental observations.

BACTERIAL MOTION AND SPREAD IN POROUS ENVIRONMENTS

by
Yasser Almoteri

A Dissertation
Submitted to the Faculty of
New Jersey Institute of Technology and
Rutgers, The State University of New Jersey – Newark
in Partial Fulfillment of the Requirements for the Degree of
Doctor of Philosophy in Mathematical Sciences

Department of Mathematical Sciences
Department of Mathematics and Computer Science, Rutgers-Newark

August 2023

APPROVAL PAGE

BACTERIAL MOTION AND SPREAD IN POROUS ENVIRONMENTS

Yasser Almoteri

Dr. Enkeleida Lushi, Dissertation Advisor   Date
Assistant Professor of Mathematical Sciences, NJIT

Dr. Lou Kondic, Committee Member   Date
Professor of Mathematical Sciences, NJIT

Dr. Victor Matveev, Committee Member   Date
Professor of Mathematical Sciences, NJIT

Dr. Yuan-Nan Young, Committee Member   Date
Professor of Mathematical Sciences, NJIT

Dr. Sujit S. Datta, Committee Member   Date
Assistant Professor of Chemical and Biological Engineering, Princeton University

BIOGRAPHICAL SKETCH

Author: Yasser Almoteri

Degree: Doctor of Philosophy

Date: August 2023

Undergraduate and Graduate Education:

- Doctor of Philosophy in Mathematical Sciences,
  New Jersey Institute of Technology, NJ, 2023

- Master in Mathematics,
  New York University, NY, 2016

- Bachelor of Science in Applied Mathematics,
  Al-Imam Mohammad Ibn Saud Islamic University, Riyadh, 2011

Major: Mathematical Sciences

Presentations and Publications:

Yasser Almoteri, Enkeleida Lushi "Bacterial motion and spread in porous media,"
Conference Presentation, APS March Meeting, 2021.

Yasser Almoteri, "Bacterial motion and spread in porous media,"
Conference Presentation, Dana Knox Research Showcase at NJIT, 2021.

Yasser Almoteri, Enkeleida Lushi "Collective motion of micro-swimmers in impure flow,"
Conference Presentation, APS Division of Fluid Dynamics, 2021.

Yasser Almoteri, Enkeleida Lushi "Collective motion of interacting swimmers in impure flows,"
Conference Presentation, APS March Meeting, 2022.

Yasser Almoteri, Enkeleida Lushi "Bacterial collective motion and spread in porous media."
Conference Presentation, ICIAM, 2023.

In dedication to my mother and family.

ACKNOWLEDGMENTS

TABLE OF CONTENTS

TABLE OF CONTENTS
(Continued)

LIST OF FIGURES

Figure   **Page**

CHAPTER 1

INTRODUCTION

1.1   Micro-swimmers and Their Environment

Micro-swimmers, or microscopic objects that are "active" and have the ability to swim, are naturally found in many environments in our world, from phytoplankton in the oceans, to microbes in soil and volcanic hot springs, to microbes in the bodies of plants and animals [93, 135, 141, 112, 149, 160]. Micro-swimmers such as bacteria are important in many phenomena such as nutrient recycling, digestion, fermentation, bioremediation, fixation of nitrogen from the atmosphere, and some pathogenic ones cause many infectious diseases. Micro-swimmers such as algae can produce the oxygen we consume. Micro-swimmers such as spermatozoa are a crucial step in the propagation of many species of animals. Examples of micro-swimmers can also be artificial active particles such as phoretic colloids or driven colloids [132, 119, 47, 76]. Given their ubiquity and importance in nature and technology, studying microorganisms' behavior, locomotion, collective dynamics, interactions with each-other and other particles, their response to nutrients or toxins, is of paramount importance to understanding many of the phenomena they are involved in. Better understanding of their emerging dynamics and the factors that lead to it and affect it can lead to better understanding ways of controlling and directing it.

Microscopic swimmers naturally live and move through complex fluids and environments [160, 114, 98]. The ability of microorganisms to move through such complex fluids is of great significance in various biological processes such as fertilization and infection, but the environment complexity and inhomogeneity is also being recognized as significant effect for artificial active particles which have great potential for technological applications [11].

1

Microorganism locomotion and at the micron scale are dominated by viscous dissipation over inertia. Their study has been a vibrant and active research field for theoreriticians for a long time [102, 140, 93, 178, 50, 92, 160]. Such microorganisms have relatively slow propulsion, which determines that their dynamics are in the slow viscous flow or low Reynolds numberregime. Such micro-swimmer needs swimming mechanisms that are irreversible in time, e.g. non-reciprocal breast-strokes for the micro-algae [45]. There exist numerous models that are utilized to comprehend the hydrodynamics of micro-swimming. One such model is the squirmer model, which was initially examined by Lighthill and Blake [20] as an idealized representation of ciliary propulsion. In this model, the movement of cilia is represented by surface velocities on the spherical cell body [134]. Despite the fact that various types of micro-swimmers employ distinct propulsion mechanisms, there are certain commonalities that exist in the hydrodynamics they induce. Specifically, a micro-swimmer produces a propulsive force on the fluid in its immediate vicinity, which is countered by the drag force generated by the fluid.

Theoretically, many micro-swimmers are classified based on the disturbance fluid flow they induce as they propel, the most known of these *pullers* and *pushers*. For instance, a swimmer is considered a pusher if it generates thrust from the rear end, a puller if it generates impetus from its front end [93, 145, 92, 36], though other motility modes such as rotation also exist [137]. In addition, the experimentally observed fluid flow pattern around a swimming *Bacilus subtilis* shows that the fluid moves away from the front and back of the micro-swimmer and towards its sides. This behavior characterizes micro-swimmers typically known as pushers [44], as we can see in Figure 1.1.a. For puller micro-swimmers the propulsive mechanism is at the front; e.g., the two front flagella in micro-algae *Chlamydomonas reinhardtii* pull it towards the front in a motion similar to breaststroke [138, 55, 45]. Time-averaged over one breast-stroke, the fluid flow looks largely as in the sketch in Figure 1.1.b.
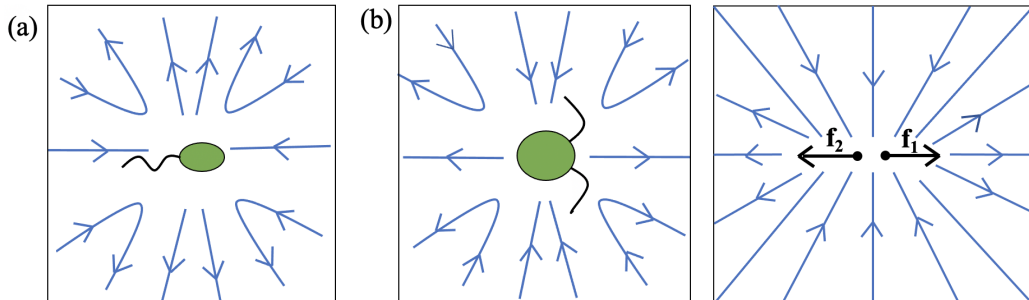
Figure 1.1 Sketch of the disturbance fluid flow by (a) pusher and (b) puller micro-swimmer in Stokes flow as observed in experiments [44, 138, 55, 45]. (c) The flow generated by an extensional Stokes force dipole resembles the pusher flow in (a).

To leading order, the forcing exerted by a micro-swimmer on the fluid can be approximated in the far-field by a force dipole, which is the flow field resulting from the action two close-point forces in opposite directions, as seen in Figure 1.1c. The disturbance flow that is created by the dipole forcing has universal characteristics in the far-field for various types of micro-swimmers or other active particles, from pushers like swimming bacteria and spermatozoa [44] to pullers like micro-algae [138, 55, 45, 118], to even artificial active micro-particles that can be manufactured to be of either or neither type [26, 25]. This feature is at the foundation of many mathematical models and simulations built to study individual and collective micro-swimmer dynamics [57, 68, 64, 65, 67, 66, 170, 146, 147, 56, 163, 164, 6, 158, 52, 107, 108, 159, 97, 174, 106, 118].

Micro-swimmers' morphology and locomotion have evolved to adapt to their environments [100, 101, 177, 53] in order to complete vital tasks such as migration or accumulation into clusters with others. These organisms can detect changes in the environment and respond to the signals they sense, be they temperature changes, nutrients, poisons, and more. In a process called *chemotaxis*, they are able to move toward the source of a beneficial chemical, for example a nutrient like oxygen, or flee from harmful toxins. A typical bacterium such as *E. coli* is observed to achieve chemotaxis though a modulation in the frequency of seemingly random tumbles or

re-orientations between a series of straight swims, or runs [15, 14]. It can execute a tumble or re-orientation by counter-rotating one or more of its flagella. As they are unable to detect spatial chemical gradients directly, bacteria rely on temporal changes in their environment along their trajectories to adjust their movement and direction[13, 14, 109]. The tumbling frequency decreases if the swimmer is moving spots with increasing attractant concentration, and remains the same if not. Overall, this random walk strategy results in a drift in the favored direction [15, 13, 87]. Other microorganisms, such as spirochetes [29], micro-algae like *Chlamydomonas reinhardtii* [138], or spermatozoa [80, 24], also achieve a chemotactic response by modulating their frequency of turning or undulation to respond to the local changes in the attractant concentration.

Microorganisms are known to use the chemotactic process to also "communicate" with each other using chemical cues [7, 142]. This occurs when individuals respond to signals from the others in the colony and will often aggregate toward them and cluster. This form of *quorum sensing* is important to the formation of biofilms in bacterial colonies[144], among other things, and it may change the behavior of the population. Bacteria *E. coli* and amoeba cell *Dictostelium discoideum* (slime mold) are known organisms that exhibit aggregation as a result of such extracellular signals.

Many experiments have studied how microorganisms or other "active" particles affect the fluid they live in, and how they interact with each-other through it. A "suspended" swimming microorganism disturbs the fluid as it moves, and this fluid can move and rotate the other microorganisms, in effect interacting with them *hydrodynamically.* In suspension of many such "active" particles interesting collective dynamics is known to emerge, with macroscopic patterns and chaotic flows in which transport and mixing properties are altered by the micro-swimmers locomotion. Colonies of swimming bacteria like *Escherichia coli* or *Bacillus Subtilis* are able to form large-scale structures with chaotic vortices and jets exhibiting speeds larger

than individuals [176, 43, 84, 169, 32, 156, 157, 179, 116]. These structures are believed to emerge as a result of hydrodynamic interactions and collisions between the micro-swimmers, which depend on the type of swimmer and its locomotion mode [146, 147, 149, 107, 108]. The structures however can be influenced by other things, for example chemical cues, temperature and other environmental changes, and these can be utilized to direct or control the collective behavior [85].

Artificial micro-swimmers, for example those that move due to surface catalytic reactions [46, 132, 133, 131, 153, 26, 25] can perform something akin to chemotaxis when put in a gradient of H_2O_2 as they swim toward its source [62, 99]. Such artificial micro-swimmers may be utilized in future technologies to perform various tasks, such as mix material in microfluidics or deliver cargo [73, 165]. It is thus of interest to the scientific community to study the collective behavior of such non-biological motile suspensions as well in order to learn how it can be controlled by use of chemical gradients, electro-magnetic forces, etc [111].

Though most theoretical or computational studies of micro-swimmers tend to focus on an individual's dynamics or a pair's interaction [93, 68, 96], there has been a significant amount of work on the micro-swimmer collective dynamics emerging due to hydrodynamic or chemotactic interactions, including continuum models [58, 5, 147, 6, 163, 61, 136, 164, 52, 48, 88, 161, 120, 181] and simulations of many interacting swimmers [41, 63, 57, 67, 146, 57, 64, 65, 67, 66, 170, 56, 150, 107, 108, 50, 174, 180, 161]. More recently there have been several studies looking at the combined effects of hydrodynamic and chemotactic interactions, continuum models [51, 78, 105, 79, 104, 106, 3, 121, 172] and particle simulations [143, 168, 115].

1.2   Micro-swimmer Motion in Porous Media

Even though in nature bacteria can be found in and navigate non-trivial environments and confinements such as tissues, soils and sediments, most experimental studies of

such microbes focus on homogeneous environments such as bulk liquid or flat surfaces. As such, we do not yet have a full understanding of how microorganisms move in such complex geometries, how their self-propulsion or "activity" impacts migration through a wet inhomogeneous medium, and thus cannot we are not yet able to devise ways to direct and control them for applications ranging from drug delivery to chemical sensing [73, 165, 111].

Swimmers's natural habitats are complex structured or random environments, which are fluid environments that have surfaces or obstacles with different sizes. We can think of these structured environments as divided into three categories depending on the confinement's relative size to the swimmer. The first one is when structure or obstacle is much bigger than the swimmer, as in Figure 1.2a, with examples being studies of confinements such a large drops or racetracks or pillar forests where the boundary curvature affects the stability and topology of collective dynamics [95, 155, 175, 108, 174, 130, 39, 40]. The second case is when the structure scale is close to the swimmer scale, as in Figure 1.2b, with examples being experimental studies with E. coli navigating porous environments consisting of hydrogel beads [18, 19] or swimmers among cylindrical pillars [110, 33, 154, 74]. The last case is when the structure scale is significantly smaller than the swimmer scale, as in Figure 1.2c, and this is the scale we will focus on in this dissertation.
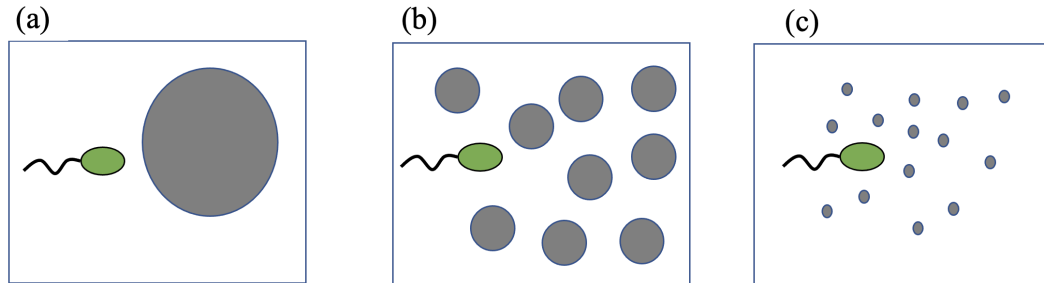
Figure 1.2   Illustration of a micro-swimmer in different structured environments: (a) structure scale is much bigger than the swimmer scale, (b) structure scale is approximately the same as the swimmer scale, and (c) structure scale is much smaller than the swimmer scale.

Studies of micro-swimmers in relatively large confinements have shown that the confinement size and geometry affects the emerging swimmer organization, for example in 2D structured environments where in size-dependent motion and transport are promoted in ordered media but hindered in disordered media such as an environment packed with obstacles [173, 39, 40, 110, 114]. Recent experiments have shown that 3D pore-scale confinement strongly affects micro-swimmer locomotion and migration [18, 19,] and it alters the dynamics and morphology of the migrating bacterial population [17, 16, 110, 113,]. Theoretical and computational studies of chemotactic motion in wet porous environments are also lagging behind, though recent work has incorporated the porosity effects by modifying the standard motility parameters substantially from their bulk liquid values [17, 1].

The difficulty with theoretical and computational modeling of active matter in such complex confinements rests with the impossible task of properly and resolving the hydrodynamical interactions as well collisions with the swimmers with each-other and any non-trivially-shaped surface or obstacle in their surrounding. Continuum models are more appropriate to model population dynamics, however one cannot faithfully include the effects of the swimmer collisions, which are crucial in determining the confined dynamics [175, 108, 174, 130]. Numerical simulations of the coupled dynamics of individually-traced micro-swimmers on the other hand are often not feasible for realistic numbers of swimmers because the difficulty and computational cost involved in resolving the non-local interactions such as hydrodynamical ones.

Approximations can be made in special cases, e.g. individual swimmers in viscoelastic or power-law flows [38, 37, 86], or collective behavior in complex or viscoelastic flows when the intra-swimmer and swimmer-boundary interactions are not included [22, 23, 97, 162, 98, 166, 89]. An extra special case is Brinkman flow which due to its linearity has made possible studies of squirmer or flagellar swimmers moving through it [94, 122, 124, 126, 123, 70].

To the best of our knowledge, there have not yet been any studies on micro-swimmer collective dynamics or on chemotactic migration in Brinkman fluid, hence we will consider these questions in this dissertation.

1.3   Viscous Flow and Its Singularities

The motion of an incompressible Newtonian fluid is described by the Navier-Stokes Equations:

$$\rho \left(\frac{\partial \mathbf{u}}{\partial t} + \mathbf{u} \cdot \nabla \mathbf{u} \right) = -\nabla p + \mu \nabla^2 \mathbf{u} + \mathbf{f}, \tag{1.1}$$

$$\nabla \cdot \mathbf{u} = 0. \tag{1.2}$$

Here ρ is the density of the fluid, $\mathbf{u}$ is the fluid velocity, p is the pressure, μ is the viscosity of the fluid, and $\mathbf{f}$ is a force applied to the fluid. In Equation (1.1), the first term is the unsteady inertial component, which is the acceleration of the flow. The second term is the non-linear inertial term. On the right-hand side, the first term is the pressure gradient, the second term describes viscous dissipation, and the final term is the force applied to the fluid by an immersed body. Equation (1.2) is the incompressibility condition. Non-dimensionalizing Equations (1.1) and (1.2), we get

$$Re \left(\frac{\partial \mathbf{u}}{\partial t} + \mathbf{u} \cdot \nabla \mathbf{u} \right) = -\nabla p + \nabla^2 \mathbf{u} + \mathbf{f}, \qquad \nabla \cdot \mathbf{u} = 0,$$

where $Re = \frac{\rho U L}{\mu}$ is the dimensionless Reynolds number, and where U denotes a typical flow speed and L is the characteristic length scale of the flow. The Reynolds number is the ratio of inertial forces to viscous forces.

Viscous dissipation dictates the fluid flow generated by the activity of microorganisms [140], for which $Re \ll 1$ [93, 92]. Equations (1.1) and (1.2) in the case of

$Re = 0$ are known as the *Stokes Equations*:

$$-\nabla p + \mu \nabla^2 \mathbf{u} + \mathbf{f} = 0, \qquad \nabla \cdot \mathbf{u} = 0. \qquad (1.3)$$

In Equation (1.3), pressure, viscosity, and body force balance instantaneously. Note that Stokes Equations are linear, which allows superposition solutions [139].

Let us consider a point force applied at $\mathbf{x}_0$ i.e., $\delta(\mathbf{x} - \mathbf{x}_0)\mathbf{f}$, in a Stokes flow. The fluid flow satisfies

$$-\nabla p + \mu \nabla^2 \mathbf{u} + \delta(\mathbf{x} - \mathbf{x}_0)\mathbf{f} = 0, \qquad \nabla \cdot \mathbf{u} = 0. \qquad (1.4)$$

We can write the solution for this scenario as:

$$\mathbf{u}(\mathbf{x}) = \mathbf{G}(\mathbf{r})\mathbf{f}, \qquad (1.5)$$

where $\mathbf{x}_0$ is the point where $\mathbf{f}$ is applied, and $\mathbf{x}$ is the field point, and $\mathbf{r} = \mathbf{x} - \mathbf{x}_0$. Physically, this solution represents the velocity field due to a concentrated point force of constant strength $\mathbf{f}$ at the point $\mathbf{x}_0$ [139]. The free-space Green function, known as the *Stokeslet* or Oseen's tensor [21, 139, 93, 158, 92], is

$$\mathbf{G}(\mathbf{r}) = \frac{1}{8\pi\mu}(\frac{\mathbf{I}}{r} + \frac{\mathbf{r}\mathbf{r}^{\mathbf{T}}}{r^3}), \qquad (1.6)$$

where $r = |\mathbf{x} - \mathbf{x}_0|$. The Stokeslet is the fundamental singularity of translational motion at zero Reynolds number [21]. From the fundamental solution of Equation

(1.5), the higher order singularities for viscous flow can be obtained by differentiation of the Stokeslet [59].

1.4   Brinkman Equations and its Singularities

In Section (1.2), we mentioned structured environments where the scale of the structure is smaller than that of the swimmer. This is particularly important because microorganisms often encounter viscous environments that are heterogeneous and contain stationary obstacles or inert impurities within the fluid medium. For instance, certain spirochetes are capable of swimming through heterogeneous media and crossing the blood-brain barrier to infect the brain. Another example is bacteria living in saturated soil in nature [72]. In such scenarios, to depict the flow of a viscous fluid through spherical particles that are smaller than the flow's characteristic length scale [34], one can utilize the *Brinkman approximation*, which can be viewed as the incorporation of a lower-order resistance term into the Stokes equations [124, 126]. The Brinkman Equations to describe viscous flow in a such porous medium are:

$$\mu \nabla^2 \mathbf{u} - \nabla p - \frac{\mu}{K_D} \mathbf{u} = 0, \qquad \nabla \cdot \mathbf{u} = 0 \qquad (1.7)$$

where μ is the viscosity, $\mathbf{u}$ is the fluid velocity, p is the fluid pressure, and $K_D > 0$ is the constant Darcy permeability. After non-dimensionalization with lengthscale L as the particle length scale, U the velocity scale and $\frac{\mu U}{L}$ is the pressure scale, we obtain

$$\nabla^2 \mathbf{u} - \nabla p - \nu^2 \mathbf{u} = 0, \qquad \nabla \cdot \mathbf{u} = 0 \qquad (1.8)$$

where $\nu = \frac{L}{\sqrt{k}}$ is the ratio of the particle dimension to the permeability length of the medium [34]. We will refer to ν as the resistance parameter.

Let's consider a Brinkman Flow with a force applied at a sole point $\mathbf{x}_0$ i.e. $\delta(\mathbf{x} - \mathbf{x}_0)\mathbf{f}$. The fluid flow generated by this point-force satisfies Equations (1.8)

$$\nabla^2\mathbf{u} - \nabla p - \nu^2\mathbf{u} + \delta(\mathbf{x} - \mathbf{x}_0)\mathbf{f} = 0, \qquad \nabla \cdot \mathbf{u} = 0 \tag{1.9}$$

whose solution is given by

$$\mathbf{u}(\mathbf{x}) = \mathbf{B}(\mathbf{r})\mathbf{f}. \tag{1.10}$$

Here $\mathbf{B}$ is the Green's function for the Brinkman Equations (1.9), commonly referred to as the *Brinkmanlet* [34]:

$$\mathbf{B}(\mathbf{r}) = H_1(r)\mathbf{I} + H_2(r)\mathbf{r}\mathbf{r}^T \tag{1.11}$$

with $\mathbf{I}$ the identity matrix, $r = |\mathbf{x} - \mathbf{x}_0|$ and

$$H_1(r) = \frac{e^{-\nu r}}{4\pi r}\left(\frac{1}{\nu^2 r^2} + \frac{1}{\nu r} + 1\right) - \frac{1}{4\pi\nu^2 r^3},$$
$$H_2(r) = -\frac{e^{-\nu r}}{4\pi r^3}\left(\frac{3}{\nu^2 r^2} + \frac{3}{\nu r} + 1\right) + \frac{3}{4\pi\nu^2 r^5}.$$

The formula given in Equations (1.10, 1.11) can be used in free-space domains for a point-force, though modifications can be sometimes achieved for half-space domains [126, 35]. A regularized Brinkmanlet solution can be derived for a "blob" or regularized force [34, 94] In periodic domains it is possible to solve the Brinkman

Equations with a more general force [125], and we outline how to do so in Appendix A as we will make use of this formula in our analysis and simulations.
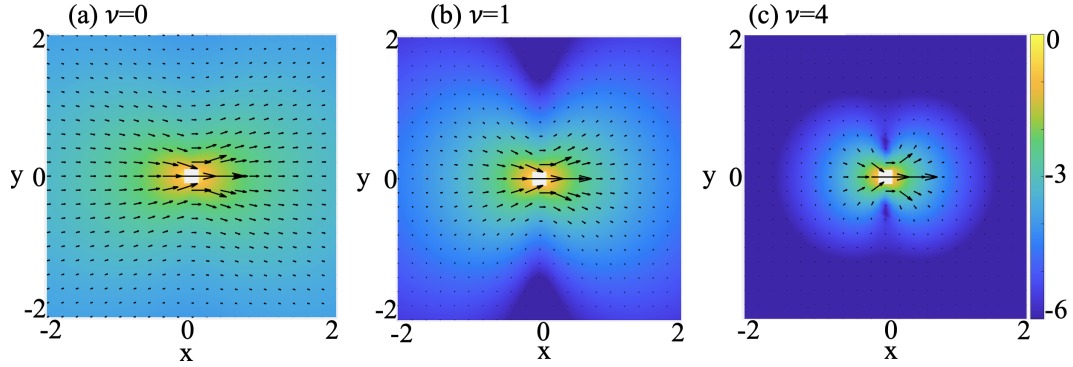
Figure 1.3 Fluid velocity generated when the force $\mathbf{f} = (1, 0, 0)$ is applied at point $\mathbf{x_0} = (0, 0, 0)$ in a Brinkman flow with different hydrodynamic resistances: $\nu = 0, 1, 4$. The vector field indicates $\mathbf{u}$, whereas the field color represents $log|\mathbf{u}|$.

When a point force is applied to a viscous fluid or Stokes flow, the velocity disturbance that follows it decays as $1/r$ with distance r, as seen in the formula for the Stokeslet in Equation (1.6). However in a Brinkman medium the decay of the velocity disturbance is significantly altered at large distances and decays much faster, at a rate of $1/r^3$ [49] because a new length-scale has been introduced into the problem. The effects of the resistance on the fluid flow generated from a single force are visible in the plots shown in Figure 1.3: the disturbance fluid flow is not as long-ranged as in the Stokes case.

Figure 1.4 Fluid velocity generated by two closely-applied opposite forces in Brinkman flow with different hydrodynamic resistances: $\nu = 0, 1, 4$. The vector field indicates $\mathbf{u}$, whereas the field color represents $log|\mathbf{u}|$.

When a point force is applied to a viscous fluid or Stokes flow, the velocity disturbance that follows it decays as $1/r$ with distance r, as seen in the formula for the Stokeslet in Equation (1.6). However in a Brinkman medium the decay of the velocity disturbance is significantly altered at large distances and decays much faster, at a rate of $1/r^3$ [49] because a new length-scale has been introduced into the problem. The effects of the resistance on the fluid flow generated from a single force are visible in the plots shown in Figure 1.3: the disturbance fluid flow is not as long-ranged as in the Stokes case.

In Figure 1.4 we plot the fluid flow generated by a force dipole (two opposite direction forces applied at an offset distance) in Brinkman flow of various resistance. We notice that the fluid flow generated by this force dipole, representative of disturbance fluid flow generated by a micro-swimmer moving through it, is also visibly affected by the medium resistance. Notably, the fluid flow becomes more localized and its effects are not felt as far as in a pure viscous flows.

1.5 Questions Motivating this Study

The fluid flows generated by each micro-swimmer can advect and rotate neighboring and further swimmers in a suspension, and this hydrodynamic interaction is known to be a crucial factor in the emergence of the self-organization and collective dynamics of pusher micro-swimmers like motile bacteria [108, 174]. Thus the differences in the fluid flow fields seen in Figure 1.4 motivate the questions behind this research project:

- *How does the environment heterogeneity, and in particular the resistance resulting from the present impurities, alter the collective motion of microswimmers?*

- *Does this resistance affect chemotactic dynamics and aggregation?*

- *Can we gain some insight into the phenomena observed in experiments by modeling the environment resistance through the Brinkman approximation?*

- *Can we provide a framework to predict and control the dynamics and migration of bacteria specifically, and active matter generally, in porous and inhomogeneous environments?*

1.6 Overview of the Dissertation

Here we provide a brief overview of the contents of the dissertation and highlight its key findings on micro-swimmers collective motion in porous media. environments.

In Chapter 1, we introduce the concept of slow viscous environments, which are commonly found in nature and are inhabited by microorganisms such as bacteria and algae. We also discuss low Reynolds number flow singularities, which are important physical phenomena that arise in these environments due to the high viscosity and low fluid velocity. The chapter provides a brief introduction to the topic and sets the stage for the subsequent chapters, which delve deeper into the mechanics and dynamics of micro-swimmers and their interactions with their environment.

In Chapter 2, we delve into the details of a continuum model of swimmers in Brinkman flow. To lay the foundation, we start by deriving some important concepts that form the basis of the model. We then present the continuum model in Stokes-Brinkman flow, the non-dimensionalization of the system. We perform analyses of the entropy and the linearized system to understand its stability characteristics. These analysis provide valuable insights into the behavior of the model for particular parameters. We present computer simulation of the full nonlinear model for a variety of resistance strength values and analyze them through measurements of quantities like active power, maximal fluid flow speed and swimmer concentration. We summarize and discuss our findings from the continuum model, stability analysis, and nonlinear simulations to conclude that resistance hinders the emergence of collective dynamics in pusher swimmer suspensions. Overall, this chapter is an essential piece of the dissertation, as it establishes the foundation necessary for the subsequent chapters.

Chapter 3 of the dissertation focuses on auto-chemotaxis and the effect that hydrodynamic resistance has on chemotactic aggregation and clustering. The chapter starts by introducing the concept of chemotaxis, which is the ability of bacteria to move towards or away from chemical gradients. We then present a continuum model of chemotaxis with tumbling and describe how it can be used to study micro-swimmers spread. Analysis of the The model is then used to perform numerical simulations, which allow us to investigate the behavior of swimmers in different porous environments. The results of the simulations are discussed, providing insights into how micro-swimmers spread can be affected by the properties of the porous material. Overall, this chapter provides an examination of the role of hydrodynamic resistance in the chemotactic dynamics and clustering of swimmers.

Chapter 4 of the dissertation provides an exploration of swimmers' spread in inhomogeneous or porous environments from an initially accumulated state. By systematically varying various factors such as auto-chemotaxis, hydrodynamics, resistance, and externally-supplied nutrients, we get a better understanding how all these factors interact and give rise to the complex emerging dynamics. This chapter also elucidates the role of the initial conditions, and in this case we find that hydrodynamic resistance hinders micro-swimmer spread and diffusion into the surrounding area.

Lastly, in Chapter 5 we summarize our findings in this dissertation and discuss possible future projects that can stem from it.

CHAPTER 2

CONTINUUM MODEL OF SWIMMERS IN BRINKMAN FLOW

2.1 Derivation of Continuum Theory

2.1.1 Propulsive rod in linear background flow

We focus now on deriving kinematic equations that pertain to a slender swimmer immersed in a Brinkman fluid, adapting from similar derivations for a slender object or swimmer immersed in Stokes flows [8, 83, 71, 60]. The swimmer here is characterized by its centerline $\mathbf{Y}(s,t)$ [8, 83, 71]. Using the local slender-body-theory approximation [60] to the centerline velocity $\mathbf{V}(s,t)$, we obtain:

$$\eta[\mathbf{V}(s,t) - \mathbf{U}(\mathbf{Y},t)] = (\mathbf{I} + \mathbf{Y}_s \mathbf{Y}_s^T)\mathbf{f}, \tag{2.1}$$

where $\mathbf{U}(\mathbf{Y},t)$ is the background fluid flow, $c = \ln(l\epsilon^2)$ with $\epsilon \ll 1$ being the swimmer aspect ratio and we defined $\eta = \frac{8\pi\mu}{-c}$. In Equation (2.1), $\mathbf{f}$ is the force per unit length exerted by the rod upon the fluid.
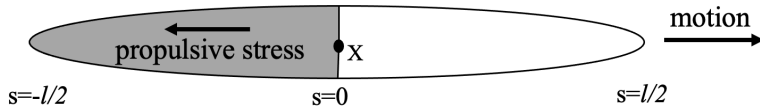
Figure 2.1 An ellipsoidal rod with propulsive stress on its body's posterior half.

Figure (2.1) depicts a basic model of a motile slender rod where the propulsive stress is applied to half of the rod's length and a no-slip condition applied to the front half. The model represents a pusher micro-swimmer, for which the thrust is generated at the rear end through the rotary motion of its flagellar bundle.

Now, we are going to add the fluid background and derive the kinematic equations. Note that $\mathbf{V}(s,t) = \mathbf{Y}_t(s,t) = \dot{\mathbf{Y}}(s,t)$. Now, for simplicity, consider a

rod of fixed length l described by its center of mass and orientation. Then,

$$\mathbf{Y}(s,t) = \mathbf{X}_c(t) + s\mathbf{p}(t),$$

where $-\frac{l}{2} \leq s \leq \frac{l}{2}$ and $|\mathbf{p}| = 1$. Note that, $\mathbf{Y}_s = \mathbf{p}$. Taking the background flow as linear: $\mathbf{U}(\mathbf{Y}) = \mathbf{A}\mathbf{Y} = \mathbf{A}(\mathbf{X}_c + s\mathbf{p})$ with $tr(\mathbf{A}) = 0$, then the velocity will be

$$\mathbf{V}(s,t) = \dot{\mathbf{Y}}(s,t) = \dot{\mathbf{X}}_c + s\dot{\mathbf{p}},$$

Plugging the above equations in Equation (2.1), we obtain

$$\eta[\dot{\mathbf{X}}_c + \mathbf{u}_s\mathbf{p} + s\dot{\mathbf{p}} - \mathbf{A}(\mathbf{X}_c + s\mathbf{p})] = (\mathbf{I} + \mathbf{p}\mathbf{p}^T)\mathbf{f}_1(s), \quad -\frac{l}{2} \leq s \leq 0 \qquad (2.2)$$

$$\eta[\dot{\mathbf{X}}_c + s\dot{\mathbf{p}} - \mathbf{A}(\mathbf{X}_c + s\mathbf{p})] = (\mathbf{I} + \mathbf{p}\mathbf{p}^T)\mathbf{f}_2(s), \quad 0 \leq s \leq -\frac{l}{2}. \qquad (2.3)$$

Note that, we need to determine $\dot{\mathbf{X}}_c$, which is the center of mass change, $\dot{\mathbf{p}}$, which is the direction change, and $\mathbf{f}(s)$, which is the force per unit length. In order to do that, we have to use the zero total force i.e. $\left(\int_{-\frac{l}{2}}^{\frac{l}{2}} \mathbf{f}(s)ds = \mathbf{0} \right)$ and zero torque $\left(\int_{-\frac{l}{2}}^{\frac{l}{2}} \mathbf{f}(s) \times \mathbf{p}ds = \mathbf{0} \right)$.

So we integrate Equations (2.2) and (2.3) with respect to s, we get

$$\eta \int_{-\frac{l}{2}}^{0} [\dot{\mathbf{X}}_c + \mathbf{u}_s\mathbf{p} + s\dot{\mathbf{p}} - \mathbf{A}(\mathbf{X}_c + s\mathbf{p})]ds = \int_{-\frac{l}{2}}^{0} (\mathbf{I} + \mathbf{p}\mathbf{p}^T)\mathbf{f}_1(s)ds. \qquad (2.4)$$

$$\eta \int_{0}^{\frac{l}{2}} [\dot{\mathbf{X}}_c + s\dot{\mathbf{p}} - \mathbf{A}(\mathbf{X}_c + s\mathbf{p})]ds = \int_{0}^{\frac{l}{2}} (\mathbf{I} + \mathbf{p}\mathbf{p}^T)\mathbf{f}_2(s). \qquad (2.5)$$

Recall that $\dot{\mathbf{X}}$, $\dot{\mathbf{p}}$, $\mathbf{X}$, $\mathbf{p}$, and $\mathbf{A}$ are not dependent on s. Therefore, From the zero-torque condition, both $\mathbf{f}_1$ and $\mathbf{f}_2$ are in the $\mathbf{p}$-direction. Therefore, we set $\mathbf{f}_1 = (f_0 + f_1 s)\mathbf{p}$ and $\mathbf{f}_2 = (f_2 + f_3 s)\mathbf{p}$ [60].Upon integration of Equations (2.2) and (2.3) with respect to arc length, we obtain the kinematic equation of the center of mass,

$$\dot{\mathbf{X}}_c = \mathbf{A}\mathbf{X}_c - \frac{u_s}{2}\mathbf{p}. \tag{2.6}$$

The zero torque condition gets satisfied if $\mathbf{f}_1 = \alpha\mathbf{p}$. Therefore,

$$\eta[\dot{\mathbf{p}} - \mathbf{A}\mathbf{p}] = 2\alpha\mathbf{p} \tag{2.7}$$

Now, by taking the dot product of the last equation with $\mathbf{p}$, (pre-multipliying by $\mathbf{p}^T$) and using the fact that $|\mathbf{p}|^2 = 1$, or $\mathbf{p}^T\mathbf{p} = 1$ and $\frac{\partial}{\partial t}|\mathbf{p}|^2 = 0$. We can find $\alpha = -\frac{\eta}{2}(\mathbf{p}^T\mathbf{A}\mathbf{p})$. Plug this back into Equation (2.7), we obtain

$$\dot{\mathbf{p}} = (\mathbf{I} - \mathbf{p}\mathbf{p}^T)\mathbf{A}\mathbf{p}.$$

The kinematic equations for a propulsive rod in linear Brinkman flow then are:

$$\dot{\mathbf{X}}_c = \mathbf{A}\mathbf{X}_c - \frac{u_s}{2}\mathbf{p}. \tag{2.8}$$
$$\dot{\mathbf{p}} = (\mathbf{I} - \mathbf{p}\mathbf{p}^T)\mathbf{A}\mathbf{p}$$
$$\mathbf{f} = -\frac{\eta}{2}s(\mathbf{p}^T\mathbf{A}\mathbf{p}).$$

2.1.2 Extra stress created by rods

The Kirkwood formula enables us to calculate the extra stress produced by particles, such as micro-swimmers or rods, that are suspended in a Newtonian fluid [42, 91]. We assume σ is the microscopic stress evaluated on the surfaces ∂B_m of N bodies. Then in a volume V, the extra stress in a suspension[9] is

$$\sigma^{(p)} = \frac{1}{V} \sum_{m=1}^{N} \int_{\partial B_m} dA[-\mathbf{f}\mathbf{X}^T - \mu(\mathbf{u}\hat{\mathbf{n}}^T + \hat{\mathbf{n}}\mathbf{u}^T)]. \tag{2.9}$$

We denote by $\mathbf{f} = -\sigma\hat{\mathbf{n}}$ the force that the particle exerts on the fluid. Here, $\hat{\mathbf{n}}$ is the unit outward normal to the surface, and $\mathbf{u}$ is the velocity on the surface. The surface integral containing $\mathbf{u} = \mathbf{u}(s)$ vanishes since, for slender bodies, the surface velocity is only a function of the arc length along the centerline. As a result, Equation (2.9) will become the following:

$$\sigma^{(p)} = -\frac{1}{V} \sum_{m=1}^{N} \int_{\partial B_m} ds \mathbf{f}\mathbf{X}^T. \tag{2.10}$$

The Kirkwood formula given by Equation (2.10) leads to the calculation of the extra stress generated by a single rod and then by a suspension of such rods. Applying Equation (2.9) to Equation (2.10) for a propulsive rod gives the contribution to the stress from a single swimmer

$$\mathbf{S} = -k_1 l^3 g \mathbf{p}\mathbf{p}^T = -\sigma_0 \mathbf{p}\mathbf{p}^T, \tag{2.11}$$

where $k_1 = \frac{\pi\epsilon}{2}$ is another geometric constant and the units of $\sigma_0 = k_1 l^3 g$ are force times length; note these are the units of the strength of a stresslet, or force dipole.

Next, we combine Equations (2.10) and (2.11) to find the volume-averaged extra stress in a box of volume L^3 containing N such swimmers. We assume that there are M swimmers in a smaller control volume L_M^3 and that the rate-of-strain tensor is constant over this smaller volume. Furthermore, we suppose a separation of scales $(l \leq L_M \leq L)$. After some manipulation, we find

$$\sigma^{(p)} = -n\Phi\sigma_0 \frac{1}{M} \sum_{m=1}^{M} \mathbf{p}\mathbf{p}^T, \tag{2.12}$$

where $n = N/L^3$ is the number density and $\Phi = (M/L_M^3)/(N/L^3)$ is the local concentration.

As explained by [60], for large M, the weighted sum converges to the configurational average with respect to Ψ_M, the probability density function for finding a rod with a given center-of-mass position and orientation in the small volume. Going from the local distribution function and concentration to the macroscopic distribution function, we write $\Psi_M = \Psi/\Phi$ and the extra stress becomes $\sigma(\mathbf{p}) = -n\sigma_0 < \mathbf{p}\mathbf{p}^T >$. Redefining Ψ as $n\Psi$, we obtain the extra stress generated by a suspension of rear-activated swimmers

$$\sigma(\mathbf{p}) = -\sigma_0 < \mathbf{p}\mathbf{p}^T >= -\sigma_0 \int\int d\mathbf{x}d\mathbf{p}\Psi\mathbf{p}\mathbf{p}^T. \tag{2.13}$$

Applying the kinematic equations (2.12) to a general disturbance flow whose rate-of-strain tensor is constant, namely $\mathbf{u}$ is a linearized velocity field around the swimmer's body, and taking the limit for a large number of swimmers M, we arrive

at the following equations for the particle fluxes for the center-of-mass and direction:

$$\dot{\mathbf{X}}_C = U\mathbf{p} + \mathbf{u} - d_x\nabla_x(\ln\Psi) \tag{2.14}$$

$$\dot{\mathbf{p}} = (\mathbf{I} - \mathbf{p}\mathbf{p}^T)\left[(\gamma\mathbf{E} + \mathbf{W})\mathbf{p}\right] - d_r\nabla_{\mathbf{p}}(\ln\Psi), \tag{2.15}$$

Here we introduced translational and rotational diffusion processes with phase space (not particle) diffusion coefficients d_x and d_p, respectively [42, 60].

The Equations (2.13, 2.14, 2.15) lie at the heart of many continuum descriptions of active suspensions [147], including the one presented next.

2.2 Continuum Model of Micro-swimmers in Stokes-Brinkman Flow

The probability distribution function $\Psi(\mathbf{x}, \mathbf{p}, t)$ represents the configuration of micro-swimmers modeled as ellipsoidal particles, where $\mathbf{x}$ denotes the swimmer center of mass and $\mathbf{p}$ denotes the direction with ($|\mathbf{p}| = 1$). The dynamic behavior of swimmers in suspension is described by a conservation equation that takes into account fluid advection and rotation as well as the diffusion of particles:

$$\frac{\partial\Psi}{\partial t} = -\nabla_x \cdot [\Psi(U_0\mathbf{p} + \mathbf{u})] - \nabla_p \cdot \left[\Psi(\mathbf{I} - \mathbf{p}\mathbf{p}^T(\gamma\mathbf{E} + \mathbf{W})\mathbf{p}\right] + D\nabla_x^2\Psi + d_r\nabla_p^2\Psi. \tag{2.16}$$

The conservation Equation (2.16) involves flux velocities in the center of mass $\mathbf{x}$ and orientation $\mathbf{p}$ that have to be specified:

$$\dot{\mathbf{x}} = U_0\mathbf{p} + \mathbf{u} - D\nabla_x(\ln\Psi) \tag{2.17}$$

$$\dot{\mathbf{p}} = (\mathbf{I} - \mathbf{p}\mathbf{p}^T)\left[(\gamma\mathbf{E} + \mathbf{W})\mathbf{p}\right] - d_r\nabla_{\mathbf{p}}(\ln\Psi). \tag{2.18}$$

In Equation (2.17), the translational velocity of a particle is expressed as the sum of the background fluid velocity $\mathbf{x}$ and the swimming speed U_0 with orientation $\mathbf{p}$. We model isotropic translational diffusion with a constant D. Here $\nabla_{\mathbf{p}}$ is the gradient operator on the sphere. Equation (2.18) is Jeffery's equation[69] and models the angular velocity $\dot{\mathbf{p}}$ in terms of the fluid rate-of-strain $\mathbf{E} = (\nabla\mathbf{u}+\nabla^T\mathbf{u})/2$ and vorticity tensor $\mathbf{W} = (\nabla\mathbf{u}-\nabla^T\mathbf{u})/2$ and of a shape parameter $-1 \leq \gamma \leq 1$. The term $(\mathbf{I}-\mathbf{p}\mathbf{p}^T)$ captures the rotation of an anisotropic particle in the local flow. Angular diffusion is included through a rotational diffusion coefficient d_r[147, 145, 106].

Microscopic organisms encounter varying fluid environments that contain networks of stationary obstacles suspended within them. The flow of viscous fluid through these porous materials can be modeled by adding an additional hydrodynamic resistance or friction term, $\frac{\mu}{K_D}\mathbf{u}$, to the Stokes-Brinkman equations. The Brinkman equation was developed specifically to model the flow through a porous material containing scattered spherical particles [31, 49, 94].

When micro-swimmers are present, the fluid velocity $\mathbf{u}(\mathbf{x}, t)$ satisfies the Stokes-Brinkman equations with an extra active stress due to the swimmers' motion in it.

$$-\mu\nabla_x^2\mathbf{u} + \nabla_x q + \frac{\mu}{K_D}\mathbf{u} = \nabla_x \cdot \Sigma^p, \tag{2.19}$$

$$\nabla_x \cdot \mathbf{u} = 0. \tag{2.20}$$

Here μ is the viscosity, q is the fluid pressure, and $K_D > 0$ the constant Darcy permeability, and Σ^p is the active stress, as derived in Equation (2.13)

$$\Sigma^p(\mathbf{x}, t) = \sigma_0 \int \Psi(\mathbf{x}, \mathbf{p}, t)(\mathbf{p}\mathbf{p}^T - \mathbf{I}/3)d\mathbf{p}. \tag{2.21}$$

The active stress Σ^p is the average configuration of the active stress $\sigma_0(\mathbf{pp}^T - \mathbf{I}/3)$ that exerted on the fluid by the particles over all possible orientations $\mathbf{p}$[148, 145, 9, 178]. If we ignore particle interactions and only consider the contribution from single-particle swimming, we can estimate the initial strength of the stresslet σ_0 by focusing on the first moment of the force distribution on the particle surface [145, 146]. Various studies have demonstrated that this approach is valid from a micro-mechanical perspective on swimming [148, 145, 146]. Lastly,

$$\sigma_0 = U_0 \mu l^2 \alpha, \tag{2.22}$$

where l is the characteristic length of the particles and α is an $O(1)$ dimensionless constant whose value depends on the mechanism of swimming and swimmer geometry. One way to classify swimmers is based on their propulsion mechanism. Swimmers that use a force around their tail, like sperm, are called pushers, and have a negative initial stresslet strength σ_0, which in turn implies a negative value for α. In contrast, swimmers that use their heads to pull themselves forward, like C. reinhardtii, are called pullers, and have a positive σ_0, indicating a positive value for α [147, 145, 106].

We define a local swimmer concentration $\Phi(\mathbf{x}, t)$ and the mean swimmer director director $< \mathbf{p}(\mathbf{x}, t) >$

$$\Phi(\mathbf{x}, t) = \int \Psi(\mathbf{x}, \mathbf{p}, t) d\mathbf{p}, \qquad < \mathbf{p}(\mathbf{x}, t) > = \int \mathbf{p} \Psi(\mathbf{x}, \mathbf{p}, t) d\mathbf{p}. \tag{2.23}$$

2.2.1 Non-dimensionalization of the system

We non-dimensionalize Equation (2.16) using the distribution-, velocity-, length- and time-scales $\Psi_c = n$, $u_c = U_0$, $l_c = (nl^2)^{-1}$, $t_c = l_c/u_c$, with $l_c = (V/V_p)l$ and $V_p = Nl^3$ the effective volume taken by N swimming particles in the fluid volume V of a cube

with length L [147]. n is the mean number density of the micro-swimmers in the volume V. This choice of non-dimensionalization normalizes the distribution function

$$\frac{1}{V} \int_V d\mathbf{x} \int d\mathbf{p} \Psi(\mathbf{x}, \mathbf{p}, t) = 1$$

with $\Psi_0 = 1/4\pi$ the probability density for the uniform isotropic state.

We also non-dimensionalize the diffusions as $D' = Dt_c/l_c^2$, $d_r' = d_r t_c$. The non-dimensionalized swimmer distribution equation becomes:

$$\frac{\partial \Psi}{\partial t} = -\nabla_x \cdot [\Psi(\mathbf{p} + \mathbf{u})] - \nabla_p \cdot [\Psi(\mathbf{I} - \mathbf{pp})(\gamma \mathbf{E} + \mathbf{W})\mathbf{p}] + D\nabla_x^2 \Psi + d_r \nabla_p^2 \Psi. \quad (2.24)$$

The fluid equations are non-dimensionalized using $\alpha = \sigma_0/(U_0 \mu l_c^2)$ for α a non-dimensional $O(1)$ constant whose sign tells whether the micro-swimmers are pushers ($\alpha < 0$), pullers ($\alpha > 0$)[147, 106]. The non-dimensional permeability parameter is $\nu = l_c/\sqrt{K_D}$, and we will refer to is as the hydrodynamic resistance. The non-dimensional Stokes-Brinkman fluid equations are

$$-\nabla_x^2 \mathbf{u} + \nabla_x q + \nu^2 \mathbf{u} = \alpha \nabla_x \cdot \int \Psi(\mathbf{x}, \mathbf{p}, t)(\mathbf{pp}^T - \mathbf{I}/3)d\mathbf{p}, \quad (2.25)$$

$$\nabla_x \cdot \mathbf{u} = 0. \quad (2.26)$$

2.2.2 The system in two dimensions

Since the numerical simulations that will be presented later are performed for a two-dimensional (2D) system, we briefly discuss how the equations in this system are different from those in a three-dimensional (3D) system.

In 2D, we have only one orientation angle, $\theta \in [0, 2\pi]$ with $\mathbf{p} = (\cos\theta, \sin\theta)$. The 2D

model does not differ much in appearance from the 3D one in Equation (2.16) except that in 2D, we have the isotropic state $\Psi_0 = 1/2\pi$.

$$\frac{\partial \Psi}{\partial t} = -\nabla_x \cdot (\Psi \dot{\mathbf{x}}) - \partial_\theta (\Psi \dot{\theta}) \tag{2.27}$$

$$\dot{\theta} = \mathbf{p}_\perp \cdot (\gamma \mathbf{E} + \mathbf{W})\mathbf{p} - d_r \partial_\theta (\ln \Psi)$$

$$\dot{\mathbf{x}} = \mathbf{p} + \mathbf{u} - D\nabla_x (\ln \Psi)$$

$$\Sigma^p = \alpha \int_0^{2\pi} \Psi(\mathbf{x}, \theta, t)(\mathbf{pp} - \mathbf{I}/2)d\theta.$$

Here $\mathbf{p}_\perp = (-\sin\theta, \cos\theta)$ is the unit vector perpendicular to the particle orientation. These are coupled to the fluid equations with active particle stress and additional hydrodynamic resistance or friction in the Stokes-Brinkman equations,

$$-\nabla_x^2 \mathbf{u} + \nabla_x q + \nu^2 \mathbf{u} = \nabla_x \cdot \Sigma^p, \tag{2.28}$$

$$\nabla_x \cdot \mathbf{u} = 0. \tag{2.29}$$

2.3 The System Entropy

The total entropy S, defined as

$$S = \int d\mathbf{x} s = \int d\mathbf{x} \int d\mathbf{p} \frac{\Psi}{\Psi_0} \ln(\frac{\Psi}{\Psi_0}), \tag{2.30}$$

with $\Psi_0 = \frac{1}{4\pi}$. Note that $S = \int d\mathbf{x} s(\mathbf{x}, t) \geq 0$ and S realizes its minimum value of zero only for $\Psi = \Psi_0$, the homogeneous and isotropic state.

Differentiating the equation for $s = \int d\mathbf{p}(\Psi/\Psi_0)\ln(\Psi/\Psi_0)$ with respect to time and assuming $f = \frac{\Psi}{\Psi_0}$ yields,

$$
\begin{aligned}
s_t &= \int d\mathbf{p}\, f_t(\ln f + 1) \\
&= \int d\mathbf{p}(\ln f + 1)[-\nabla_x \cdot ((\mathbf{p} + \mathbf{u})f) - \nabla_p \cdot (((\mathbf{I} - \mathbf{p}\mathbf{p}^T)\nabla_x\mathbf{u}\,\mathbf{p})f) \\
&\quad + D\nabla_x^2 f + \nabla_p \cdot (d_r \nabla_p f)] \\
&= -\mathbf{u}\cdot\nabla_x s + \int d\mathbf{p}[-\mathbf{p}\cdot\nabla_x(f\ln f) - f\nabla_p\cdot((\mathbf{I}-\mathbf{p}\mathbf{p}^T)\nabla_x\mathbf{u}\,\mathbf{p}) \\
&\quad + D(\ln f + 1)\nabla_x^2 f - d_r|\nabla_p \ln f|^2 f].
\end{aligned}
$$

Using $\nabla_p \cdot ((\mathbf{I} - \mathbf{p}\mathbf{p}^T)\nabla_x\mathbf{u}\,\mathbf{p}) = -3\mathbf{p}^T\nabla_x\mathbf{u}\,\mathbf{p} = -3\mathbf{p}\mathbf{p}^T : \mathbf{E}$, we obtain

$$
\begin{aligned}
s_t + \mathbf{u}\cdot\nabla_x s + \nabla_x \cdot \int d\mathbf{p}\,\mathbf{p}\, f \ln f &= D\nabla_x^2 s + 3\left(\int d\mathbf{p} f \mathbf{p}\mathbf{p}^T\right) : \mathbf{E} \\
&\quad - \int d\mathbf{p}\left(D|\nabla_x \ln f|^2 + d_r|\nabla_p \ln f|^2\right)\, f.
\end{aligned}
$$
(2.31)

The momentum equation can be integrated over the fluid domain to obtain:

$$
2\int d\mathbf{x}\,\mathbf{E} : \mathbf{E} + \nu^2\int d\mathbf{x}|\mathbf{u}|^2 = -\int d\mathbf{x}\,\mathbf{E} : \Sigma^p.
$$
(2.32)

Integrating Equation (2.31) in $\mathbf{x}$ and using the above Equation (2.32) results in:

$$
\begin{aligned}
\mathcal{D}_t S &= 3\int d\mathbf{x}\,\mathbf{E} : \int d\mathbf{p} f \mathbf{p}\mathbf{p}^T - \nu^2\int d\mathbf{x}|\mathbf{u}|^2 - \int d\mathbf{x}\int d\mathbf{p} f[D|\nabla_x \ln f|^2 + d_r|\nabla_p \ln f|^2] \\
&= \frac{-6}{\alpha}\int d\mathbf{x}\,\mathbf{E} : \mathbf{E} - \nu^2\int d\mathbf{x}|\mathbf{u}|^2 - \int d\mathbf{x}\int d\mathbf{p} f[D|\nabla_x \ln f|^2 + d_r|\nabla_p \ln f|^2].
\end{aligned}
$$

Therefore we obtain an exact equation for the evolution of the entropy:

$$4\pi\mathcal{D}_t S = \frac{-6}{\alpha}\int d\mathbf{x}\mathbf{E}:\mathbf{E} - \nu^2\int d\mathbf{x}|\mathbf{u}|^2 - \int d\mathbf{x}\int d\mathbf{p}\Psi[D|\nabla_x \ln\Psi|^2 + d_r|\nabla_p \ln\Psi|^2].$$

(2.33)

We note the three distinctive contributions in Equation(2.33) from the hydro-dynamics, resistance, and diffusive processes.

The first term in the right hand side of Equation(2.33) contains the rate of viscous dissipation $\int d\mathbf{x}\mathbf{E}:\mathbf{E}$ which is positive definite, hence, in the absence of any external forcing or boundaries, for suspensions of pullers ($\alpha > 0$) any fluctuations from the isotropic state as measured by the entropy are expected to monotonically dissipate, whereas for suspensions of pushers ($\alpha < 0$) there is a feedback loop where fluctuations create velocity gradients which further increase fluctuations [147]. These are eventually balanced by the diffusive processes in the system, seen here in the third term in the right hand side of Equation (2.33).

Last, but not least, the hydrodynamic resistance makes an appearance in the second term of Equation (2.33). As $\int d\mathbf{x}|\mathbf{u}|^2$ is positive definite and $\nu^2 \geq 0$, it is clear that the resistance is expected to dampen any fluctuations from the isotropic state, thus having a stabilizing effect on the system. This expectation is supported out by the results of our linear stability analysis of the isotropic state, as well as by the results of our nonlinear simulations, both presented in subsequent sections.

2.4 Linear Stability Analysis

2.4.1 The eigenvalue problem

We now consider the stability of a nearly uniform and isotropic suspension. Let the swimmer's suspension be a perturbation about the uniform isotropic state $\Psi = \Psi_0 =$

$1/4\pi$ and zero fluid flow $\mathbf{u_0} = \mathbf{0}$, $|\epsilon| << 1$

$$\Psi(\mathbf{x}, \mathbf{p}, t) = 1/4\pi + \epsilon\Psi'(\mathbf{x}, \mathbf{p}, t), \qquad \mathbf{u}(\mathbf{x}, \mathbf{p}, t) = \mathbf{0} + \epsilon\mathbf{u}'(\mathbf{x}, \mathbf{p}, t).$$

For simplicity, we neglect angular diffusion $d_r = 0$ but we retain translational diffusion D. Substituting these into Equation (2.16) and keeping only $O(\epsilon)$ terms, we get the linearized equations for the distribution and the fluid

$$\frac{\partial\Psi'}{\partial t} = -\mathbf{p} \cdot \nabla_x\Psi' + 3\gamma\Psi_0\mathbf{p^T}E'\mathbf{p} + D\nabla_x^2\Psi' + d_r\nabla_p^2\Psi'. \tag{2.34}$$

$$-\nabla^2\mathbf{u}' + \nabla q' + \nu^2\mathbf{u}' = \alpha\nabla \cdot \int \Psi'(\mathbf{x}, \mathbf{p}, t)(\mathbf{pp}^T - \mathbf{I}/3)d\mathbf{p}, \tag{2.35}$$

$$\nabla \cdot \mathbf{u}' = 0. \tag{2.36}$$

We consider plane wave perturbations for the distribution function and for all the other perturbation variables:

$$\Psi(\mathbf{x}, \mathbf{p}, t) = 1/4\pi + \epsilon\Psi'(\mathbf{x}, \mathbf{p}, t) = 1/4\pi + \epsilon\tilde{\Psi}(\mathbf{p}, \mathbf{k})\exp(i\mathbf{k} \cdot \mathbf{x} + \sigma t)$$

$$\mathbf{u}(\mathbf{x}, \mathbf{p}, t) = \mathbf{0} + \epsilon\mathbf{u}'(\mathbf{x}, \mathbf{p}, t) = \mathbf{0} + \epsilon\tilde{\mathbf{u}}(\mathbf{p}, \mathbf{k})\exp(i\mathbf{k} \cdot \mathbf{x} + \sigma t),$$

with $|\epsilon| << 1$, $\mathbf{k}$ the wavenumber and $\sigma(k)$ the growth rate. Substituting these into Equation (2.34), we get an equation that is linear in $\tilde{\Psi}$:

$$(\sigma + i\mathbf{p} \cdot \mathbf{k} + Dk^2)\tilde{\Psi} = \frac{3}{2}i\gamma\Psi_0\mathbf{p^T}(\tilde{\mathbf{u}}\mathbf{k^T} + \mathbf{k}\tilde{\mathbf{u}}^T)\mathbf{p}.$$

Let $\mathbf{k} = k\hat{\mathbf{k}}$. We solve the fluid equations for the fluid velocity

$$\tilde{\mathbf{u}} = \frac{ik}{k^2 + \nu^2}(\mathbf{I} - \hat{\mathbf{k}}\hat{\mathbf{k}}^T)\tilde{\Sigma}^p\hat{\mathbf{k}}, \qquad (2.37)$$

$$\tilde{\Sigma}^p = \alpha \int \tilde{\Psi}'\mathbf{p}'\mathbf{p}'^T d\mathbf{p}'. \qquad (2.38)$$

We plug this into the $\tilde{\Psi}$ equation and simplify, to obtain

$$(\sigma + i\mathbf{p} \cdot \mathbf{k} + Dk^2)\tilde{\Psi} = -\frac{3\gamma k^2}{4\pi(k^2 + \nu^2)}\mathbf{p}^T(\mathbf{I} - \hat{\mathbf{k}}\hat{\mathbf{k}}^T)\tilde{\Sigma}^p\hat{\mathbf{k}}\hat{\mathbf{k}}^T\mathbf{p}. \qquad (2.39)$$

Without loss of generality, we let $\hat{\mathbf{k}} = \hat{\mathbf{z}}$, $\mathbf{p} = [\sin\theta\cos\phi, \sin\theta\sin\phi, \cos\theta]$ and $d\mathbf{p} = \sin\theta d\theta d\phi$ for $\theta \in [0, \pi]$, $\phi \in [0, 2\pi)$. Then, we can write

$$(\sigma + ik\cos\theta + Dk^2)\tilde{\Psi} = -\frac{3\gamma\alpha k^2}{4\pi(k^2 + \nu^2)}\cos\theta\sin\theta[\cos\phi F_1 + \sin\phi F_2],$$

where for simplicity we have defined the following integral operators of $\tilde{\Psi}$

$$F_1(\tilde{\Psi}) = \int_0^{2\pi}\cos\phi'\int_0^\pi \sin^2\theta'\cos\theta'\tilde{\Psi}(\theta', \phi')d\theta'd\phi'$$

$$F_2(\tilde{\Psi}) = \int_0^{2\pi}\sin\phi'\int_0^\pi \sin^2\theta'\cos\theta'\tilde{\Psi}(\theta', \phi')d\theta'd\phi'$$

Equation (2.39) constitutes a linear eigenvalue problem for the perturbation mode $\tilde{\Psi}$ and the growth rate σ. Applying the operator F_1 to $\tilde{\Psi}$ in Equation (2.39) we obtain:

$$F_1 = -\frac{3\gamma\alpha k^2}{4\pi(k^2 + \nu^2)}\int_0^\pi \frac{\sin^3\theta\cos^2\theta}{(\sigma + \lambda_0 + ik\cos\theta + Dk^2)}d\theta F_1.$$

with the same equation for F_2. Canceling F_1 gives an integral equation for σ:

$$1 = -\frac{3\gamma\alpha k^2}{4\pi(k^2 + \nu^2)} \int_0^\pi \frac{\sin^3\theta\cos^2\theta}{(\sigma + \lambda_0 + ik\cos\theta + Dk^2)}\,d\theta. \tag{2.40}$$

Letting $a = (\sigma + Dk^2)/ik$, we can evaluate the integral and obtain

$$1 = -\frac{3\alpha\gamma k^2}{4(k^2 + \nu^2)}\frac{1}{ik}\left[2a^3 - \frac{4}{3}a + (a^4 - a^2)\log\left(\frac{a-1}{a+1}\right)\right], \tag{2.41}$$

which we rewrite as

$$0 = \mathcal{F}(\sigma, k) := \frac{-4ik}{3(-\alpha\gamma)}\frac{k^2 + \nu^2}{k^2} + \left[2a^3 - \frac{4}{3}a + (a^4 - a^2)\log\left(\frac{a-1}{a+1}\right)\right]. \tag{2.42}$$

Equation (2.42) is the dispersion relation for the growth rate $\sigma(k)$ in terms of wave-numbers k. If $\mathrm{Re}(\sigma(k)) \geq 0$ for a particular k indicates some perturbation from the uniform isotropic state will grow in time.

Note that for the case of no resistance, $\nu = 0$, the dispersion relation reduces to that found by many groups studying collective dynamics of micro-swimmer suspensions, e.g. [147, 163, 164]

2.4.2 Small-wavenumber asymptotic approximation

The dispersion relation shown in Equation (2.42), $\mathcal{F}(\sigma, k) = 0$ cannot be solved exactly for the growth rate $\sigma(k)$. To gain insight into the behavior of the system, we look for long-wave (small wave-number k) asymptotic solutions. For this calculation, we assume the resistance is on the same order as the small wave-number, $\nu = \tau k$.

We assume a power series expansion $\sigma = \sigma_0 + \sigma_1 k + \sigma 2 k^2 + ...$ for small k. The coefficients $\sigma_0, \sigma_1, \sigma_2, ...,$ can be determined from systematically solving the equations $\mathcal{F}_0(\sigma) = 0, \mathcal{F}_1(\sigma) = 0, \mathcal{F}_2(\sigma) = 0, ...,$ where these equations arise from a power series expansion in k of the dispersion relation Equation (2.42) as in $\mathcal{F}(\sigma, k) = \mathcal{F}_0(\sigma) + \mathcal{F}_1(\sigma)k + \mathcal{F}_2(\sigma)k^2 + ...$ The *Maple* calculations are shown in the Appendix B.1.

We obtain two distinct asymptotic solutions, or branches, for the growth rate:

$$\sigma_{H_1} = \frac{(-\alpha\gamma)}{5(1+\tau^2)} + \left[\frac{-15(1+\tau^2)}{7(-\alpha\gamma)} - D\right] k^2 + \frac{17875(1+\tau^2)^3}{147(-\alpha\gamma)^3} k^4 + O(k^5), \qquad (2.43)$$

$$\sigma_{H_2} = \left[\frac{(1+\tau^2)}{(-\alpha\gamma)} - D\right] k^2 - \frac{3(1+\tau^2)^2\pi}{4(-\alpha\gamma)^2} k^3 + \frac{3(1+\tau^2)^3(3\pi^2-8)}{8(-\alpha\gamma)^3} k^5 + O(k^6). \quad (2.44)$$

We observe that both branches of $\sigma_H(k)$ are negative for pullers $(\alpha > 0)$ for any swimmer shape γ, which means the puller suspension is stable under perturbations. Translational diffusion with rate D also has an unsurprising stabilizing effect for any type of suspension.

For pushers $(\alpha < 0)$ however, $\sigma_H(k)$ term may be positive for non-spherical swimmers $(\gamma > 0$ and has its maximum of $-\alpha/5$ at $k = 0$ for elongated pusher swimmers $\gamma = 1$ in flows with no resistance $\tau = 0 = \nu$; for increasing ν or τ, the value of $\sigma_{H1}(k = 0)$ decreases. The next term in the σ_{H_1} series shows a decrease from this maximum, with the decrease being higher for non-zero resistance τ. For a given wave-number k that is very small, we see that overall non-zero resistance lowers the value of $\sigma_{H1}(k)$, so resistance has an overall stabilizing effect on this branch of the growth rate for perturbations of pusher suspensions.

2.4.3 Numerical solution of the dispersion relation

We numerically solve the dispersion relation Equation (2.42), $\mathcal{F}(\sigma(k, \nu), k) = 0$ for the growth rate $\sigma(k, \nu)$ for each ν and then each wavenumber k by using an iterative

quasi-Newton solver (e.g., Matlab's *fsolve* with a trust-region search). We start with $\nu = 0$ and then advance for small ν increments $d\nu$, and for each ν we advance in small k increments dk. For small small k and small ν, we use as initial guess the asymptotic expansions from Equation (2.42). More generally, when solving for $\sigma(k + dk, \nu + d\nu)$ we use as an initial guess the average of $\sigma(k, \nu + d\nu)$ and $\sigma(k + dk, \nu)$.

The solution to the hydrodynamics dispersion relation for elongated $(\gamma = 1)$ swimmers with various ν is shown in Figures (2.2) and (2.3).

We start the description of the solutions with the result for homogeneous flow i.e. $\nu = 0$, and $D = 0$ in Figure 2.2. We see $\sigma_{H_1}(k = 0) = 0.2$ and $\sigma_{H_2}(k = 0) = 0$. At $k_m(\nu = 0) \approx 0.18$, (subscript m is for merge), the real parts of the two branches of σ_H merge, then decrease together until they cease to be positive for $k_+(\nu = 0) \approx 0.57$. The imaginary parts of σ_H branches are zero for $k < k_m(\nu = 0)$ and for $k > k_m(\nu = 0)$, they are non-zero and increase in magnitude for increasing wavenumber k.

For simplicity, we define the variables k_- and k_+ and the wavenumbers where $Re(\sigma_H(k)) > 0$ for $k_- < k < k_+$. We define $k_b(\nu)$ and $k_m(\nu)$ as the wavenumber where the two branches of $Re(\sigma_H)$ separate and merge respectively.

The real parts of the two σ_H branches become positive for $k > k_-(\nu)$, then separate at $k_b(\nu)$ (subscript b for bifurcation) and merge again at $k_m(\nu)$, then decrease together for increasing k until they cease to be positive for $k > k_+(\nu)$. The imaginary parts of the two σ_H branches are nonzero for $k_-(\nu) < k < k_b(\nu)$ and merge to zero for $k_b(\nu) < k < k_m(\nu)$, then separate into conjugate parts for $k > k_m(\nu)$. In Figure 2.4 we show a plot of critical wavenumbers k_-, k_b, k_m, k_+ with varying ν.

For $\nu \neq 0$ but small, both branches of σ_H start at 0, hence $\sigma_{H_1}(k = 0, \nu \neq 0) = 0$ and $\sigma_{H_2}(k = 0, \nu \neq 0) = 0$.

At $\nu_c \approx 0.075$, we have $k_b(\nu) = k_m(\nu)$ and the real parts of the two σ_H branches merge and stay merged for $\nu > \nu_c$, whereas their imaginary parts are nonzero and conjugates.
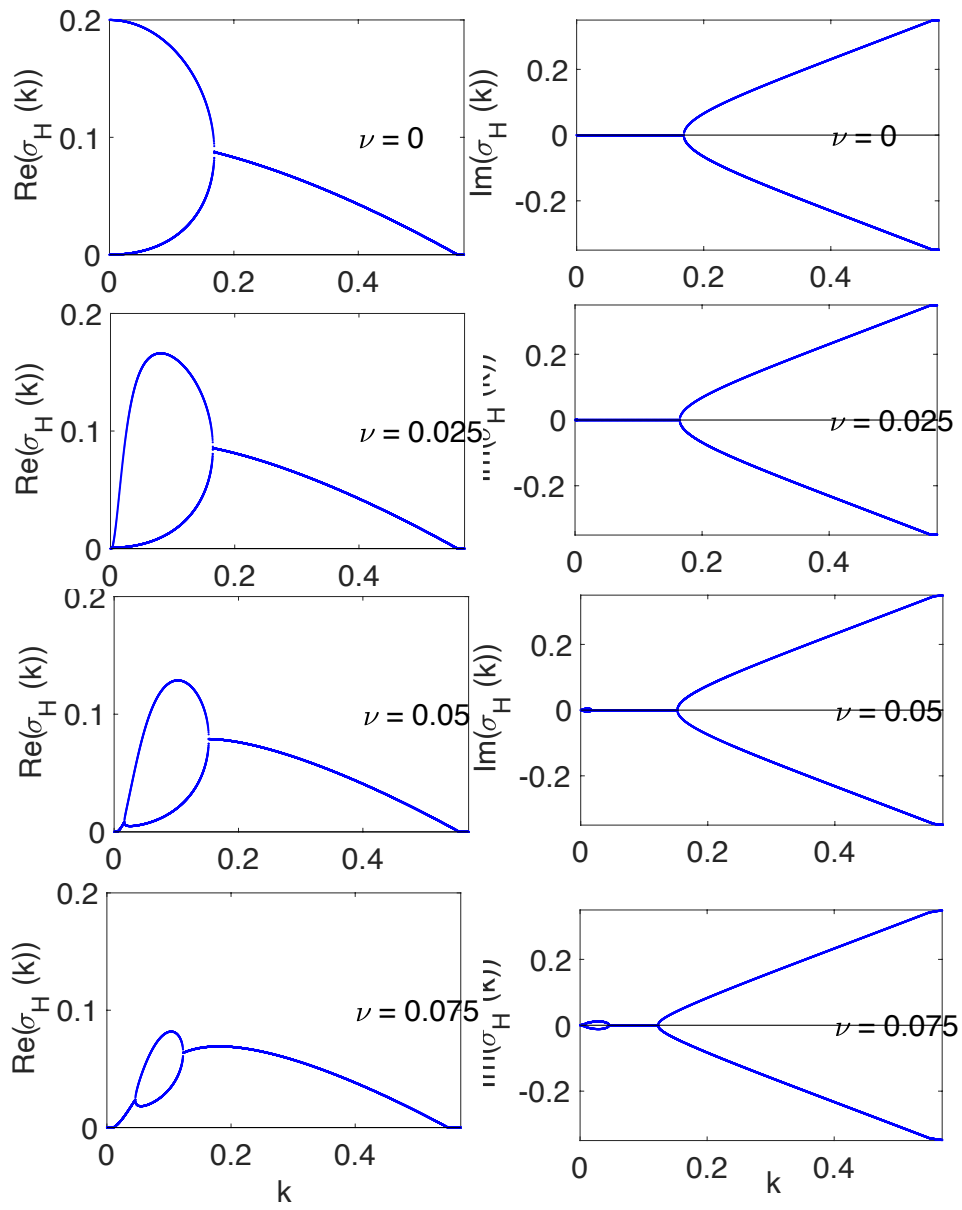
Figure 2.2 Real and imaginary parts of the numerical solution of the relation (2.42) for the growth rate $\sigma_H(k)$, $\nu = 0, 0.025, 0.05, 0.075$.
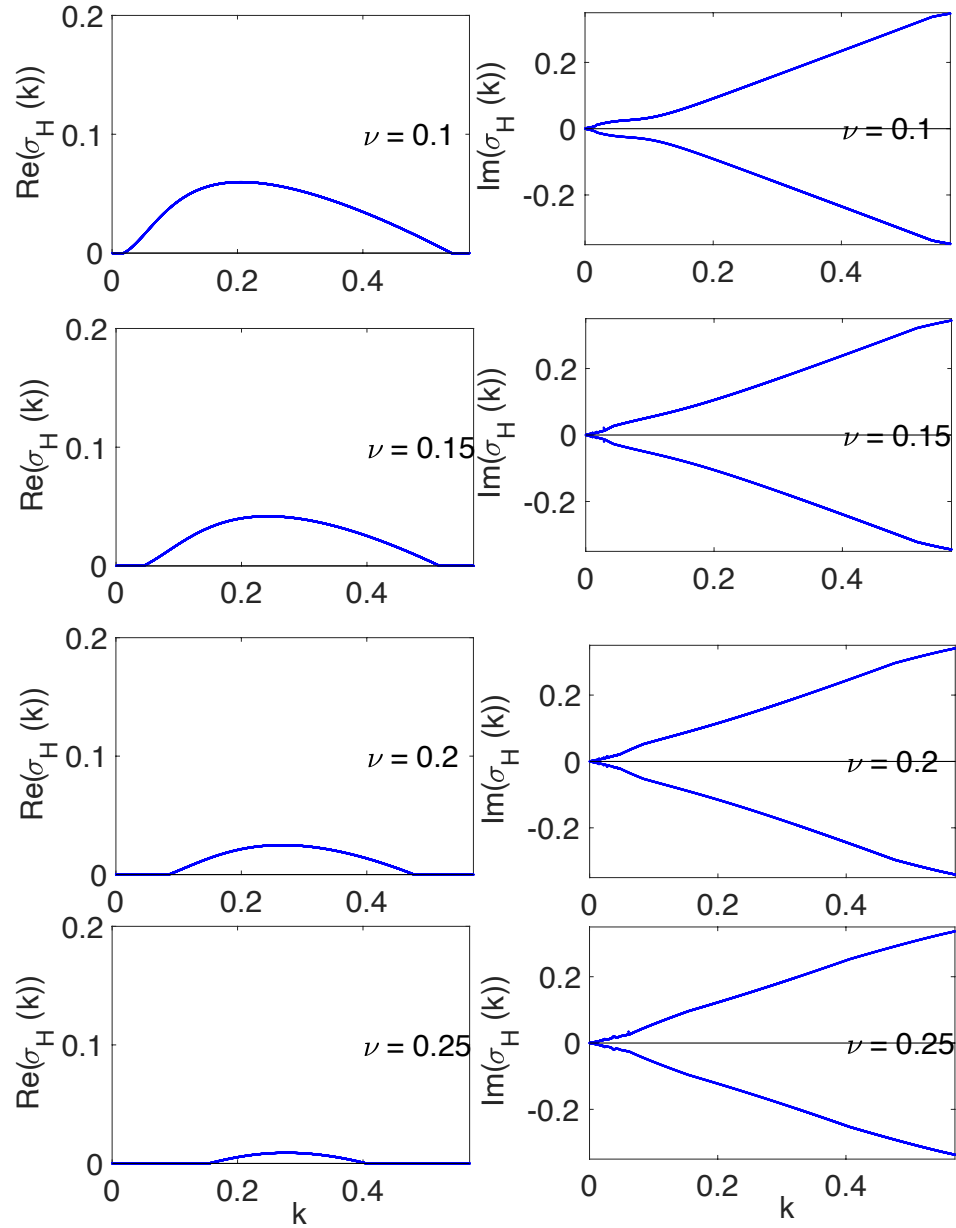
Figure 2.3 Real and imaginary parts of the numerical solution of the relation (2.42) for the growth rate $\sigma_H(k)$, $\nu = 0.1, 0.15, 0.2$.
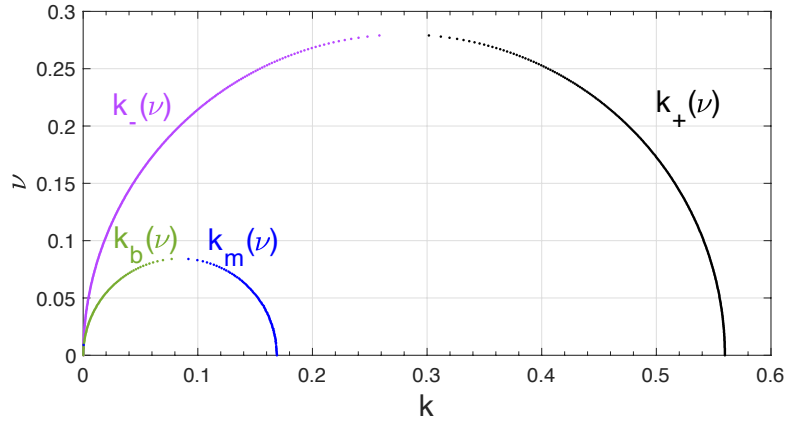
Figure 2.4 Plots of the critical wavenumbers k_-, k_b, k_m, k_+ with varying ν.

At $\nu_z \approx 0.275$ we have $k_-(\nu) = k_+(\nu)$ and the real parts of the two σ_H branches no longer have any positive parts for any wavenumber k. Hence linear theory tells us that $\nu > \nu_z$ turns off the hydrodynamic instability for pusher suspensions for *any* wavenumber k, thus any system size.

Lastly, in Figure 2.5, we plot the maximum of $Re(\sigma(k))$ for varying ν. We will later use the plot's information to determine parameters for which we can stabilize this system or a similar one.
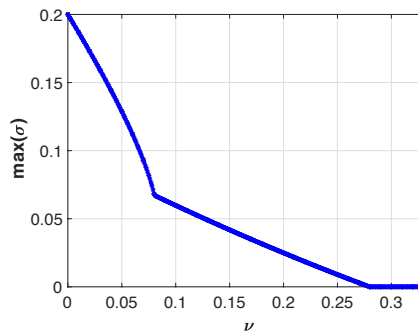
Figure 2.5 Maximum of $Re(\sigma(k))$ with varying ν.

2.4.4 Linear analysis and dispersion relation in 2D

We now consider the system in two-dimensions, as in Equations (2.27), where we have only one orientation angle $\theta \in [0, 2\pi)$ and $\mathbf{p} = [\cos\theta, \sin\theta]$. Similar to the 3D case in the previous sections, we can analyze the stability of nearly-uniform and isotropic

35

suspension in 2D where $\Psi_0 = 1/2\pi$. For simplicity, we consider zero diffusions, $D = 0 = d_r$. The linearized distribution equation is

$$\frac{\partial \Psi'}{\partial t} = -\mathbf{p} \cdot \nabla \Psi' + 2\gamma\psi_0 \mathbf{p}^T \mathbf{E}'\mathbf{p}. \tag{2.45}$$

We consider plane-wave perturbations for the distribution

$$\Psi(\mathbf{x}, \mathbf{p}, t) = 1/2\pi + \epsilon\tilde{\Psi}(\mathbf{p}, \mathbf{k})\exp(i\mathbf{k} \cdot \mathbf{x} + \sigma t), \tag{2.46}$$

with $|\epsilon| << 1$, $\mathbf{k}$ the wavenumber and σ the growth rate.

Substituting the solution for $\tilde{\Sigma}^p$ and the fluid velocity, we obtain

$$(\sigma + ik\sin\theta)\tilde{\Psi} = \frac{-\alpha\gamma k^2}{\pi ik(k^2 + \nu^2)}\sin\theta\cos\theta \int_0^{2\pi} \tilde{\Psi}' \sin\theta'\cos\theta' d\theta', \tag{2.47}$$

where $\mathbf{k} = k\hat{\mathbf{k}}$. This is a linear equation for $\tilde{\Psi}$:

$$\tilde{\Psi} = \frac{-\alpha\gamma}{\pi ik}\frac{k^2}{(k^2 + \nu^2)}\frac{\sin\theta\cos\theta}{(\sigma + ik\sin\theta)}\int_0^{2\pi} \tilde{\Psi}' \sin\theta'\cos\theta' d\theta'. \tag{2.48}$$

Multiplying both sides by $\sin\theta\cos\theta$ and then integrating in θ, we obtain:

$$1 = \frac{-\alpha\gamma}{ik\pi}\frac{k^2}{(k^2 + \nu^2)}\int_0^{2\pi} \frac{\sin^2\theta\cos^2\theta}{(\sigma + \lambda_0 + ik\sin\theta)}d\theta \tag{2.49}$$

which is an implicit integral equation for σ.

Letting $a = \sigma/ik$, we can evaluate the integral and the result is

$$1 = \frac{-\alpha\gamma}{ik} \frac{k^2}{(k^2 + \nu^2)} \left[2a^3 - a \pm 2a^2\sqrt{a^2 - 1} \right] \qquad (2.50)$$

which can be re-arranged as

$$0 = \mathcal{F}(\sigma, k) := \frac{-ik}{-\alpha\gamma} \frac{(k^2 + \nu^2)}{k^2} + \left[2a^3 - a \pm 2a^2\sqrt{a^2 - 1} \right] \qquad (2.51)$$

This is the hydrodynamic dispersion relation in 2D. It is a cubic equation for a and can be solved exactly for a and thus for σ, though we have to take care that the solution satisfies the integral relation in Equation (2.49). From the two cases arising from the $\pm$, only the minus case is feasible [61, 103]. We obtain these roots

$$
\begin{aligned}
\sigma_{H1} &= -\frac{A}{\Delta} + \frac{B\Delta}{A} + \frac{\Delta}{12} \\
\sigma_{H2} &= \frac{A}{2\Delta} - \frac{2B\Delta}{A} + \frac{\Delta}{12} \pm \frac{i\sqrt{3}}{2} \left(-\frac{A}{2\Delta} - \frac{B\Delta}{A} \right)
\end{aligned}
\qquad (2.52)
$$

where for simplicity of the formula we have let $\Delta = (-\alpha\gamma)/(1 + \tau^2)$ and

$$
\begin{aligned}
A &= \frac{1}{12} \left[-\Delta^4 + 36\Delta^2 k^2 - 216k^4 + 24\Delta^2 k^3\sqrt{-3\Delta^2 + 81k^2} \right]^{1/3} \\
B &= \frac{1}{6} \left[k^2 - \frac{\Delta^2}{24} \right].
\end{aligned}
$$

For small wavenumber k and $\nu = \tau k$, these branches become

$$\sigma_{H1} \approx \frac{-\alpha\gamma}{4(1+\tau^2)} - \frac{2(1+\tau^2)}{-\alpha\gamma}k^2 + O(k^3)$$

$$\sigma_{H2} \approx -\frac{(1+\tau^2)}{\alpha\gamma}k^2 + O(k^3) \qquad (2.53)$$

Note that for these bear many similarities to the asymptotic solutions in 3D. The first branch however is slightly different in magnitude: here $\sigma_{H1}(k = 0, \tau = 0) = 1/4$ for elongated pushers with $-\alpha\gamma = 1$, whereas in 3D we would get $\sigma_{H1}(k = 0, \tau = 0) = 1/5$ because $\sigma_{H1} \approx (-\alpha\gamma)/5 + O(k^2)$.
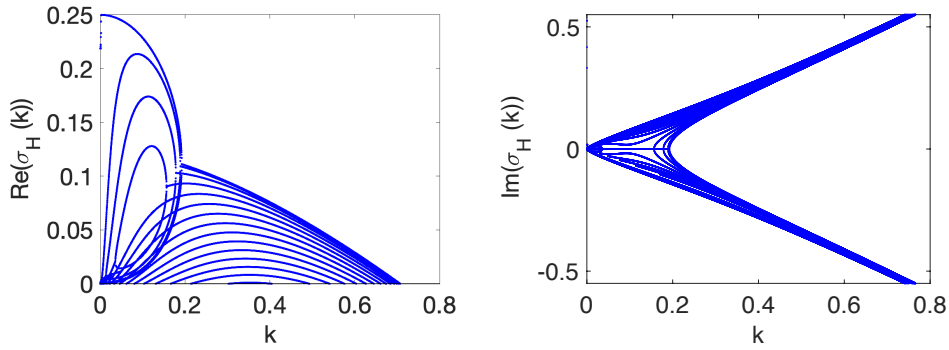
Figure 2.6   Real and imaginary parts of the numerical solution of the 2D dispersion relation Equation (2.51) for the growth rate $\sigma_H(k)$, $\nu = 0 : 0.025 : 0.35$.

The solutions to the dispersion relation for various resistance values ν are shown in Figure 2.6. We notice that the real and imaginary parts of $\sigma(k)$ in the 2D problem bear significant qualitative similarities, e.g. in overall shape, to those from the 3D problem, except that the magnitudes and the critical values k_-, k_b, k_m, k_+ are slightly different. For example, here $Re(\sigma_{H1}(0) = 1/4)$, whereas in 3D it was $1/5$. Here $Re(\sigma_{H1} > 0$ for $\nu \leq 0.36$, whereas in 3D it was $\nu \leq 0.27$.

2.5   Nonlinear Simulations and Results

2.5.1   Numerical method

Linear stability analysis suggested parameters for which perturbations from the uniform isotropic state will grow for given domain sizes, but it does not tell us what the dynamics will look like. To investigate the dynamics of the motile suspensions, we perform numerical simulations of the full nonlinear system, Equations (2.24) and (2.25).

Since a full 3D system is computationally heavy due to three space variables and two orientation variables, we focus instead a periodic 2D system in which the particles are constrained to move and rotate in the (x, y)-plane with orientation parameterized by one angle $\theta \in [0, 2\pi)$, so that the direction is $\mathbf{p} = (\cos\theta, \sin\theta, 0)$. The domain is discretized uniformly with typically $M = 128 - 256$ points in the x and y directions and $M_\theta = 32$ points in the angle direction. We use second-order accurate finite differences to calculate the flux terms in the conservation equation. The trapezoidal rule is used to compute the integrals in orientation θ, e.g. for the active particle stresses Σ^p, swimmer density Φ.

As the computational domain is periodic, we can employ spectral methods, specifically Fast Fourier Transforms, to solve the fluid equations (2.25) by using the Hasimoto solutions as shown in Equations (A.4) and (2.37).

Once the fluid velocity is known, we integrate the conservation Equation (2.24) using a second order Adams-Bashforth scheme with sufficiently small time-step to keep the calculations stable.

The initial condition is chosen to be a random perturbation around the uniform isotropic state, as also used in forerunner studies [147, 105, 106]:

$$\Psi(\mathbf{x}, \theta, 0) = \frac{1}{2\pi} \left[1 + \sum_i \epsilon_i \, cos(\mathbf{k}_0 \cdot \mathbf{x} + \xi_i) P_i(\theta) \right], \qquad (2.54)$$

where $\epsilon_i \in [-0.01, 0.01]$) are randomly-chosen small coefficients, ξ_i is a random phase, and $P_i(\theta)$ is a third order polynomial of $sin(\theta)$ and $cos(\theta)$ with random $O(1)$ coefficients.

The results presented here are for elongated pusher swimmers with $\gamma = 1$ and $\alpha = -1$. We choose a periodic square box with side $L = 25$, a size which allows for enough unstable modes according to our linear stability analysis results. Translational and rotational diffusions are included with coefficients $D = d_r = 0.01$ to ensure that the distribution function remains bounded in time.

2.5.2 The effect of the Brinkman resistance

Figures 2.7 to 2.12 present simulations of the dynamics of an initially isotropic suspension for various values of the hydrodynamic resistance parameter, $\nu \in 0..0.25$, suggested from the linear stability analysis. The simulations consider pushers that are initially uniformly distributed and pointing in random directions, resulting in an initial fluid flow perturbation around zero.

For small ν at short times we obtain the dynamics observed for Stokesian swimmer suspensions [147]. The fluctuations decay and the concentration field becomes smoother. The mean director field and the velocity field also change and quickly become smooth and correlated on scales on the order of the box size. At longer times the concentration field begins to develop strong fluctuations at wavelengths on the order of the box size, whereas the director and velocity fields remain correlated over large scales. The strong fluctuations are not steady in time: their magnitude stabilizes due to diffusion but their shape and position keep evolving, with dense concentration bands regions constantly merging, breaking up, and reorganizing.

As we increase the hydrodynamic resistance parameter ν, we notice a visible delay in the onset of the instability and a decrease in the magnitude of the concentration bands. Specifically, at $(\nu = 0.1)$, we observe that the onset of the

instability is delayed, and the concentration band magnitudes are lower compared to the case with lower resistance ($\nu = 0$). At ($\nu = 0.15$), the onset of the instability is further delayed and the concentration bands are lower, indicating a dampening effect of the hydrodynamic resistance on the fluctuations. Finally, at high hydrodynamic resistance ($\nu = 0.25$ and further), the instability is considerably suppressed, and the perturbations decay to zero. This result suggests that pushers have difficulties accumulating and moving collectively due to the higher frictional resistance.

The observed effects can be explained by considering the competition between the tendency of pushers to accumulate and form concentration bands and the damping effect of the fluid flow resistance. As the resistance parameter ν is increased, the frictional forces acting on the fluid and bacteria become stronger, leading to a decrease in the amplitude of the concentration bands and a delay in the onset of the instability. Moreover, at higher values of ν, the damping effect dominates over the tendency of bacteria to form concentration bands, resulting in the suppression of the hydrodynamic instability and a decrease in the collective motion of bacteria.
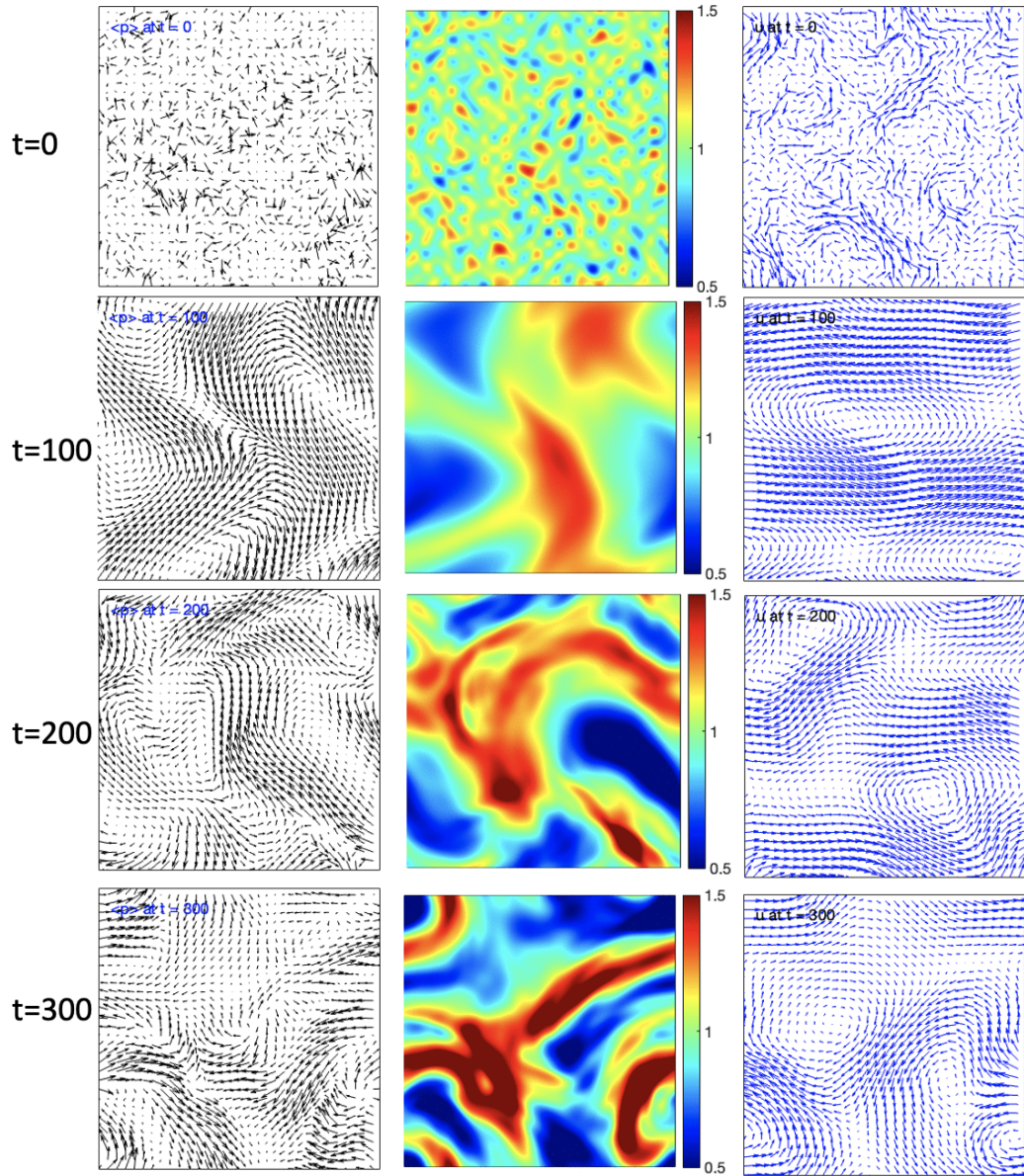
Figure 2.7 The swimmer director $< \mathbf{p} >$, concentration Φ and fluid velocity $\mathbf{u}$ at times $t = 0, 100, 200, 300$ for $\nu = 0$.
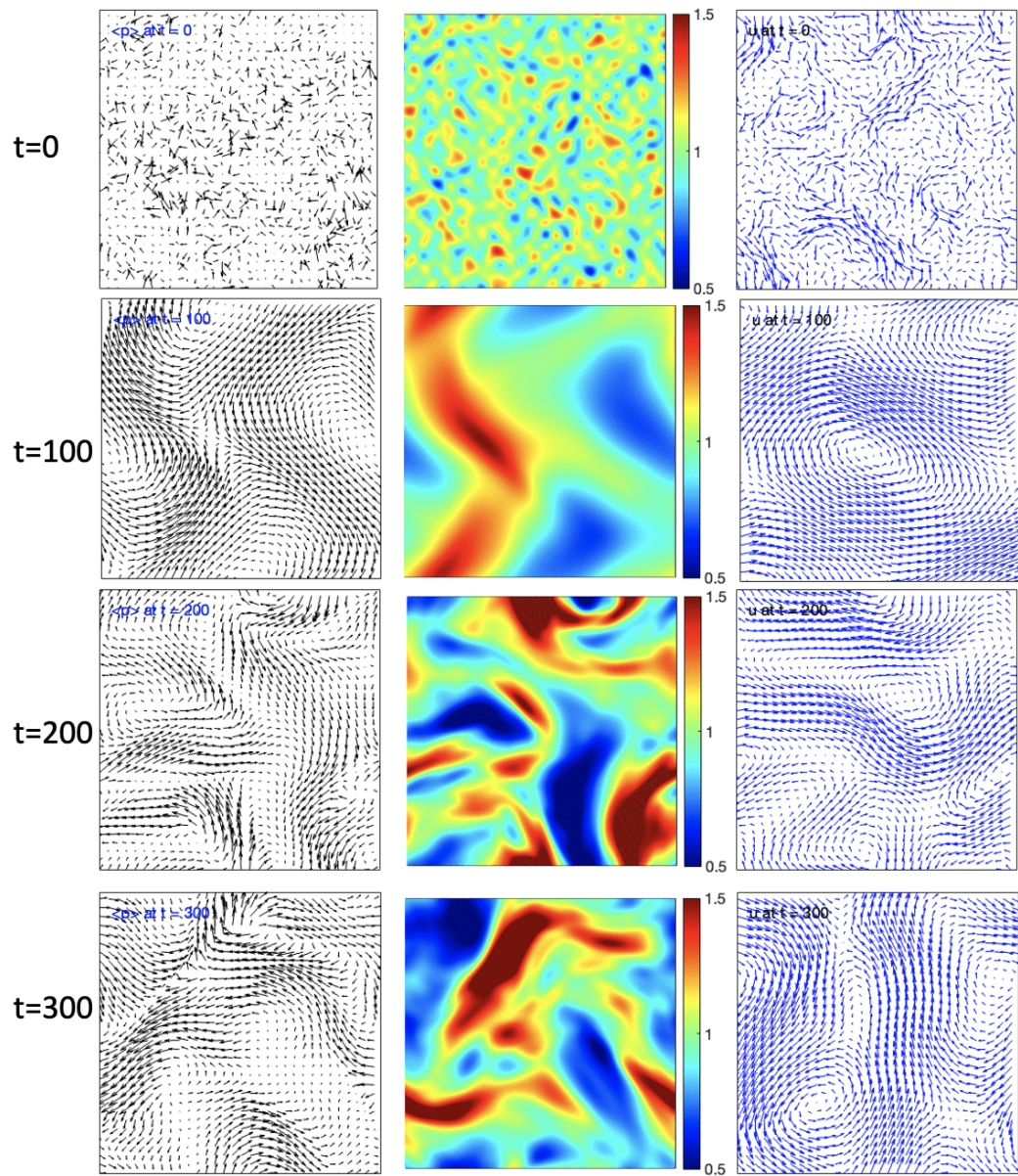
Figure 2.8 The swimmer director $< \mathbf{p} >$, concentration Φ and fluid velocity $\mathbf{u}$ at times $t = 0, 100, 200, 300$ for $\nu = 0.05$.
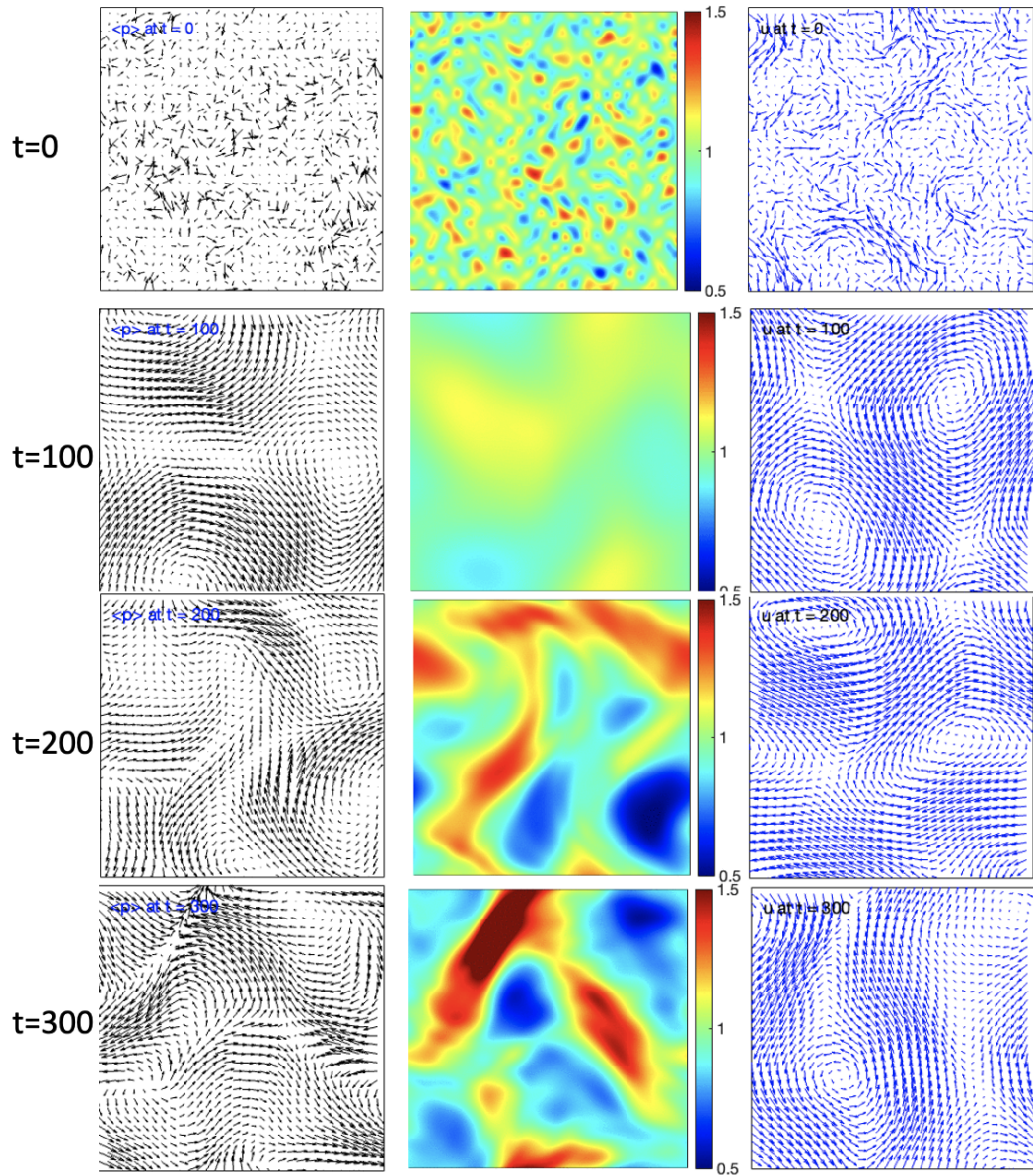
Figure 2.9 The swimmer director $< \mathbf{p} >$, concentration Φ and fluid velocity $\mathbf{u}$ at times $t = 0, 100, 200, 300$ for $\nu = 0.1$.
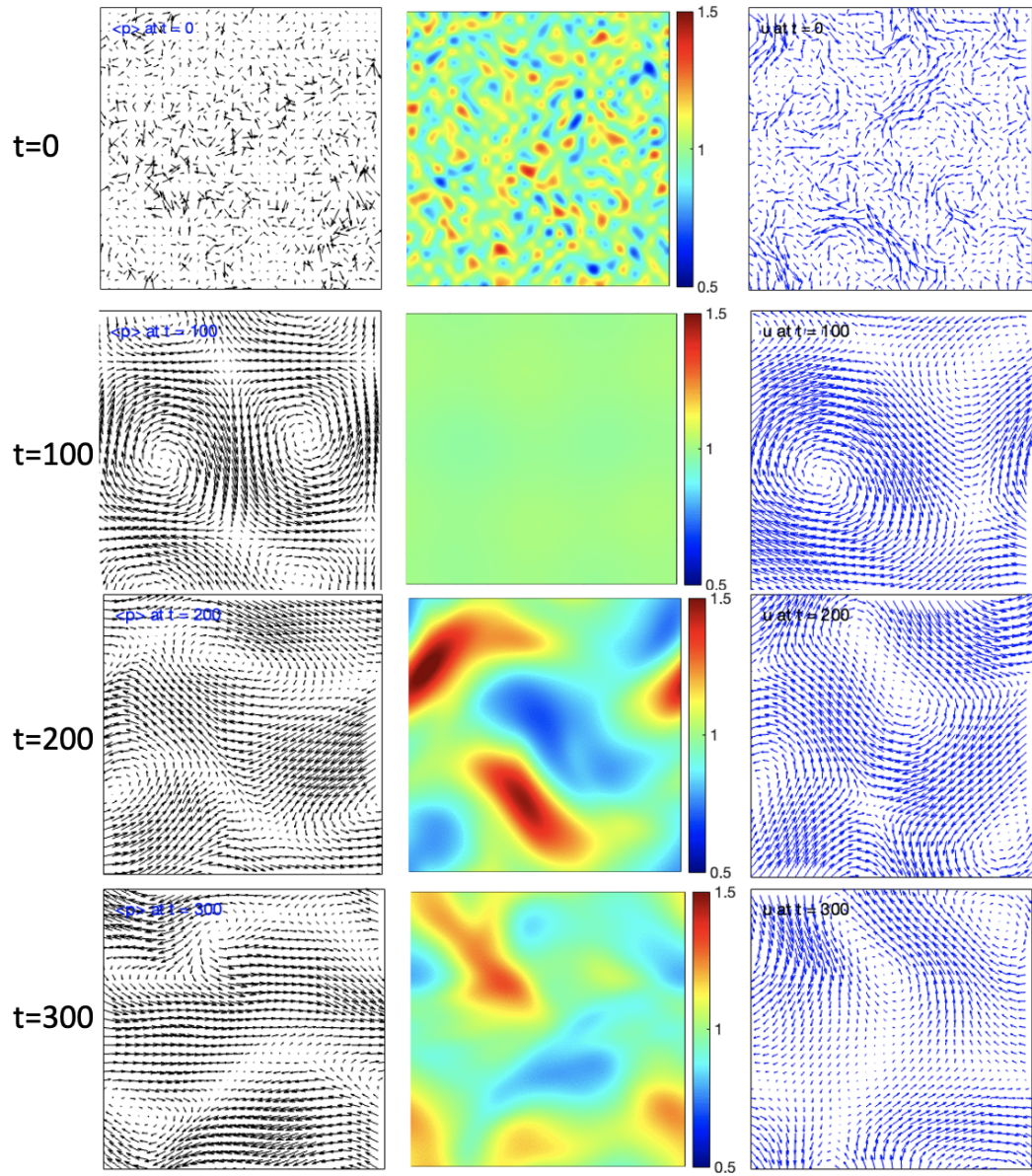
Figure 2.10 The swimmer director $< \mathbf{p} >$, concentration Φ and fluid velocity $\mathbf{u}$ at times $t = 0, 100, 200, 300$ for $\nu = 0.15$.
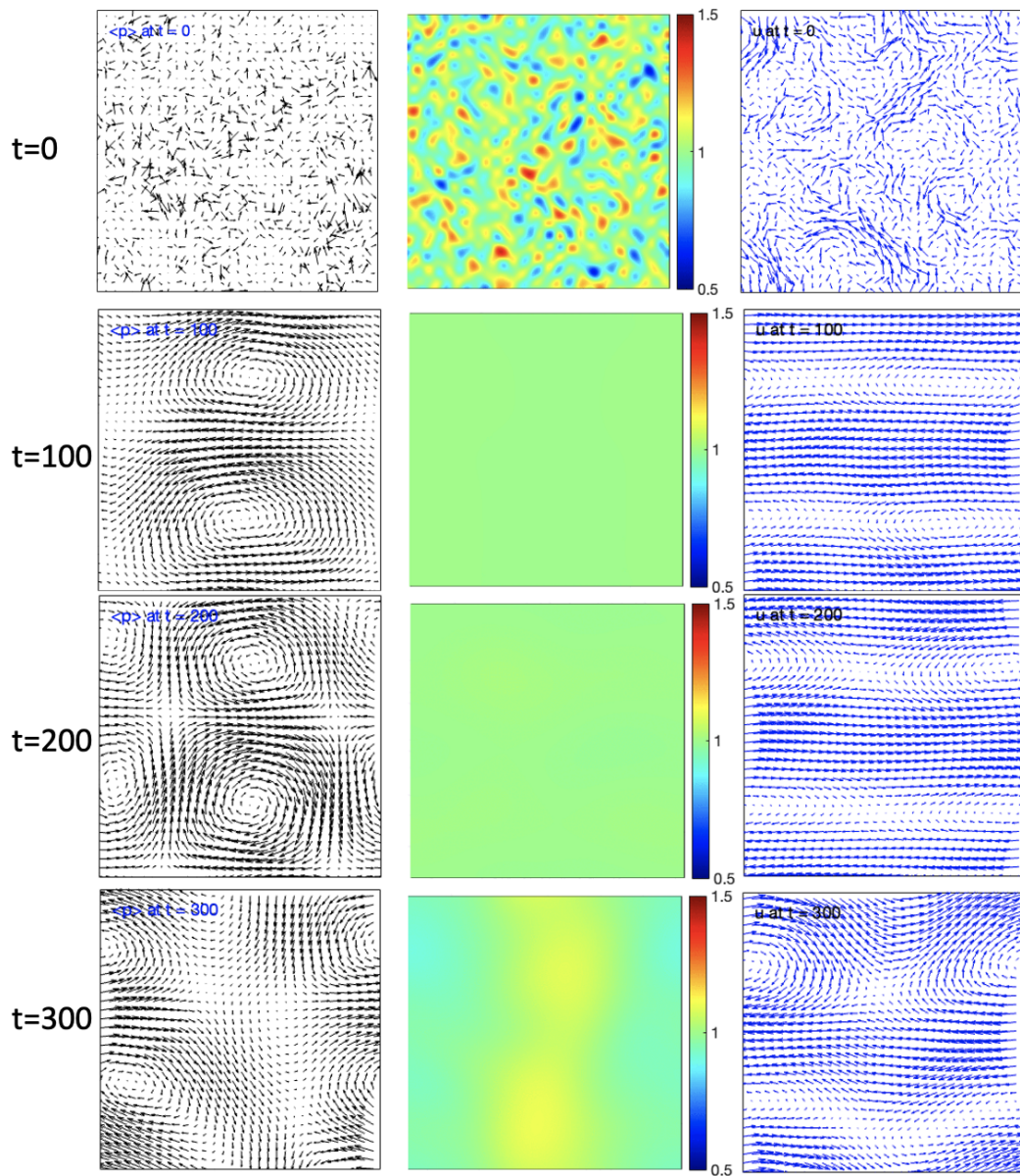
Figure 2.11 The swimmer director $< \mathbf{p} >$, concentration Φ and fluid velocity $\mathbf{u}$ at times $t = 0, 100, 200, 300$ for $\nu = 0.2$.
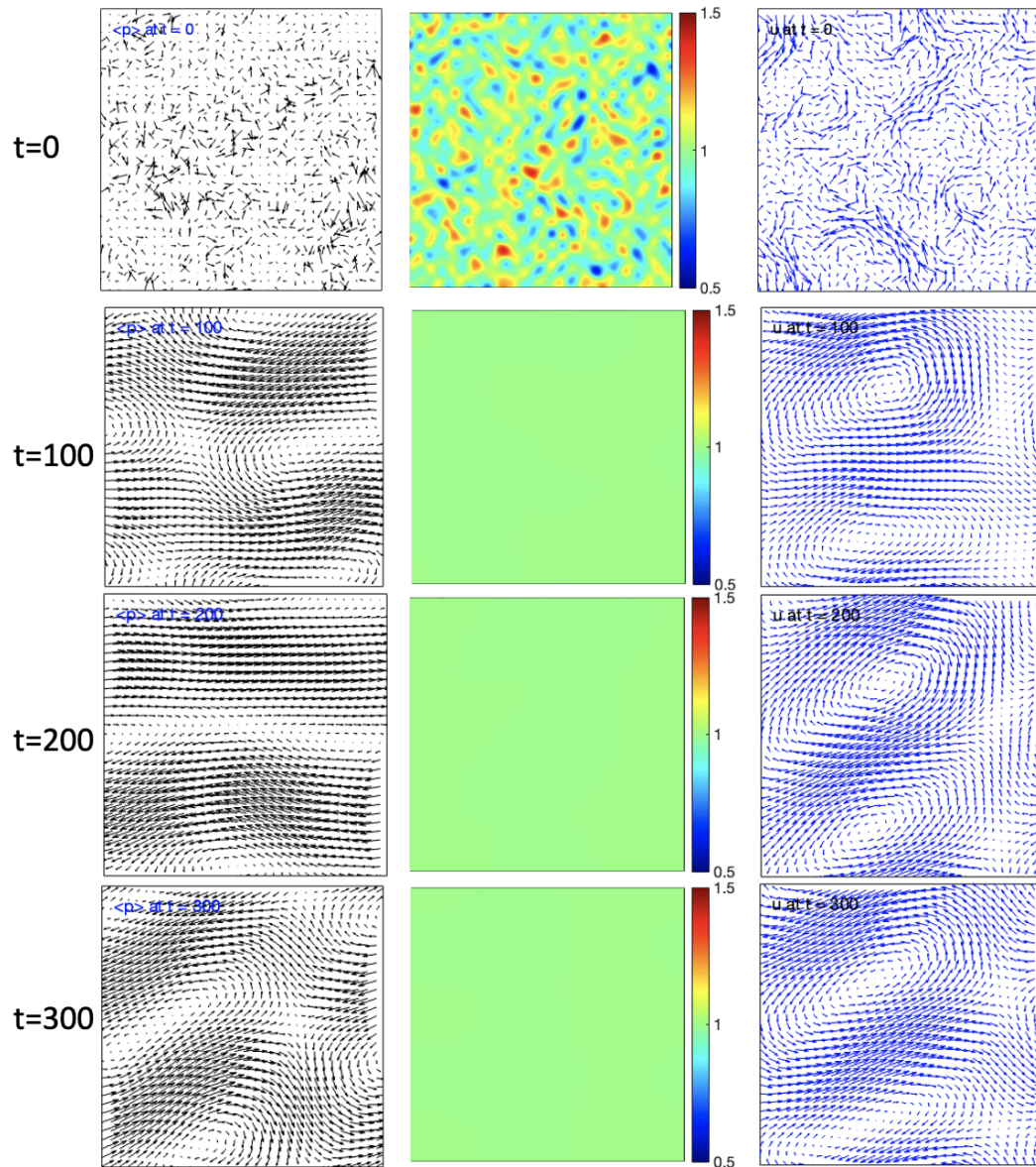
Figure 2.12 The swimmer director $< \mathbf{p} >$, concentration Φ and fluid velocity $\mathbf{u}$ at times $t = 0, 100, 200, 300$ for $\nu = 0.25$.

2.5.3 Quantifying the effect of the Brinkman resistance

In last section, we noted the impact of the Brinkman resistance on an initially isotropic pusher suspension. We will now quantify this effect in more detail.

To quantify the effect of the resistance, in Figure 2.13 we present the evolution of three metrics in time, namely $max(\mathbf{\Phi})$, $mean(|\mathbf{u}|)$, and $max(|\mathbf{u}|)$, which give information about the magnitude of the concentration bands, local fluids flows and overall averaged fluid flows. Analysis of the data presented in Figure 2.13 reveals a clear trend: as the resistance is increased, the values of these metrics decrease. This trend continues until reaching a resistance value of $\nu = 0.25$, beyond which $max(\mathbf{\Phi})$, $mean(|\mathbf{u}|)$, and $max(|\mathbf{u}|)$ approach nearly zero values. It is evident that resistance has a dampening effect on the measured quantities, indicating its inhibitory influence.
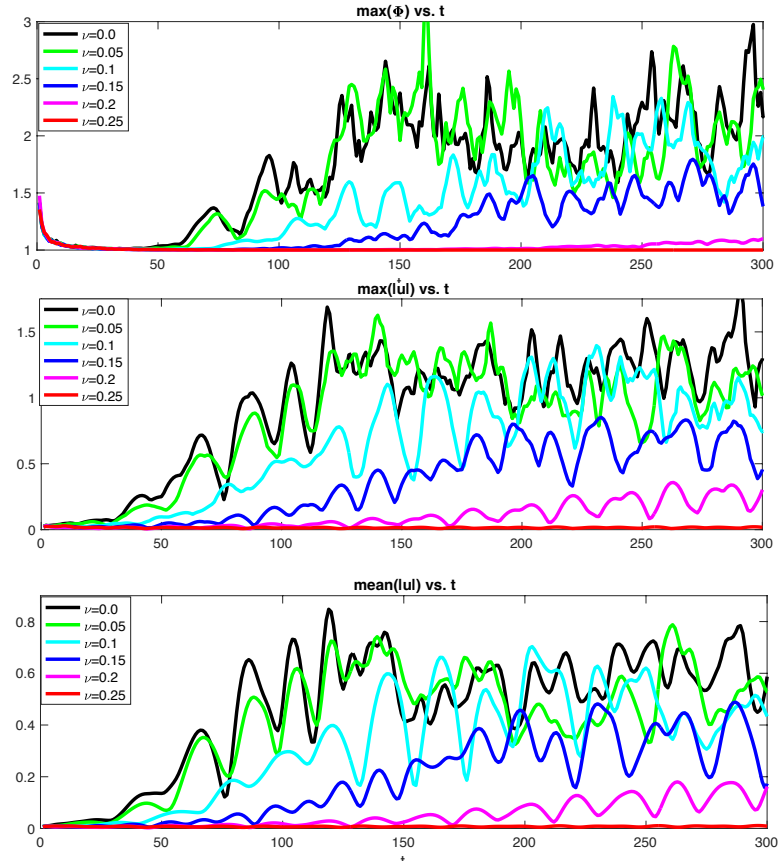
Figure 2.13 Comparisons of $max(\mathbf{\Phi})$, $mean(|\mathbf{u}|)$, and $max(|\mathbf{u}|)$ for different ν.

Next, in Figure 2.14, we use three other quantities, namely $< \mathbf{u} \cdot \mathbf{n} >$, the entropy $S(t)$ as introduced in Equation (2.30), and the global input power $P(t)$, to investigate the impact of resistance on the system dynamics. Here we also observe a consistent pattern: as the resistance parameter increases, there is a noticeable decrease in the values of these metrics, persisting until resistance value at $\nu = 0.25$, beyond which the metrics exhibit a substantial reduction, approaching almost zero values. Resistance has a pronounced dampening effect on these measured quantities, indicating its ability to hinder the dynamics of the system.
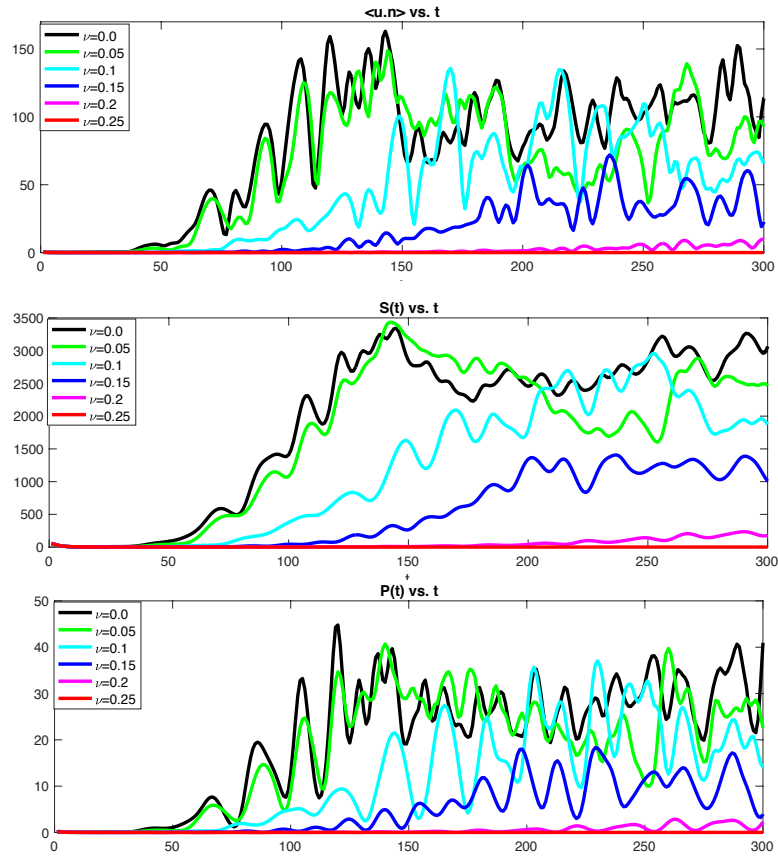
Figure 2.14 Comparisons of $< \mathbf{u} \cdot \mathbf{n} >$, entropy $S(t)$, power $P(t)$ for different ν.

As we noticed in Figures 2.7 to 2.12 a correlation between the fluid velocity $\mathbf{u}$ and the swimmer director $< \mathbf{p} >$ fields, we look at the spatially-averaged contraction:

$$\langle \mathbf{u} \cdot \mathbf{n} \rangle(t) = \int d\mathbf{x} \Psi(\mathbf{x}, t) \mathbf{u}(\mathbf{x}, t) \cdot \mathbf{n}(\mathbf{x}, t), \tag{2.55}$$

with $\mathbf{n}$ defined by $\Phi(\mathbf{x}, t)\mathbf{n}(\mathbf{x}, t) =< \mathbf{p} >$. It has been known [147] that that for pushers, the initially small $< \mathbf{u} \cdot \mathbf{n} > (t)$, grows to reach a plateau, suggesting that pushers tend to align in the local disturbance flow and swim in the direction of the flow. Alignment with the flow was anticipated since the particles align in the local shear according to Jeffery's Equation (2.18), but here we see they on average tend to swim in the direction of the local fluid velocity. This preferred alignment and orientation result in an increase in the effective swimming velocity for pusher swimmers.

Comparisons of this spatially-averaged contraction $< \mathbf{u} \cdot \mathbf{n} >$ over time for different values of ν show that the hydrodynamic resistance decreases it, with the effect being more pronounced with increased value of ν.

Recall the system entropy $S(t)$, as defined in Equation (2.30), for which we obtained the exact evolution dynamics encapsulated in Equation (2.33). Entropy is a thermodynamic quantity that measures the degree of disorder or randomness in a system. It is related to the availability of energy to do work and is a fundamental concept in thermodynamics, and can be used to study the behavior of fluids, such as in the context of turbulence and mixing, and is important in the study of fluid flow in complex systems [90, 12, 28].

Comparisons of the entropy $S(t)$ for different values of resistance ν also reveal interesting trends as we can see in Figure 2.14. In the absence of hydrodynamic resistance, the system experiences instability, and as a result, the entropy grows

rapidly. However, as time progresses, the entropy growth rate eventually saturates, and the system enters a state of statistical equilibrium. As we introduce hydrodynamic resistance by increasing the value of ν, we observe a decrease in the system entropy. This is due to the damping effect that the resistance has on the system, which reduces the degree of disorder and randomness of the particles. When $\nu = 0.25$, the effect of hydrodynamic resistance is significant enough to prevent any instability from taking place, and the entropy decays over time as we can see in Figure 2.14.

Swimmers convert their consumed energy into motion, and this can be quantified in terms of the input power into the system. By examining the input power generated by the swimming particles, we can gain a better understanding of how they contribute to the system dynamics. Recalling Section (2.3), we rewrite Equation (2.32) as

$$2 \int d\mathbf{x} \mathbf{E} : \mathbf{E} + \nu^2 \int d\mathbf{x} |\mathbf{u}|^2 = - \int d\mathbf{x} \int d\mathbf{p} (\alpha \mathbf{p} \cdot \mathbf{E} \cdot \mathbf{p}) \Psi. \qquad (2.56)$$

The left-hand side of the equation represents the rate of viscous dissipation in the fluid, while the right-hand side represents the active input power generated by the particles. The global input power $P(t)$ is then deduced from this equation:

$$P(t) = -\alpha \int \int d\mathbf{x} d\mathbf{p} (\mathbf{p} \cdot \mathbf{E} \cdot \mathbf{p}) \Psi. \qquad (2.57)$$

A consequence of Equation (2.56) is that for pushers ($\alpha < 0$) the input power is largest when the particles are aligned with the axes of extension of the rate-of-strain tensor. This alignment occurs any particle whose orientation dynamics is governed by Jeffery's Equation (2.18), thus we can expect the input power to grow in time in agreement with the existence of an instability [].

It is clear in Figure 2.14 that when there is no Brinkman resistance, $P(t)$ is initially small and increases with time as the hydrodynamic instability takes place, eventually reaching a plateau indicating that the system has entered a state of statistical equilibrium. When Brinkman resistance is introduced, we observe that the global input power decreases, indicating that the system requires less power to maintain the fluid flow and dynamics. The Brinkman resistance to the flow of the fluid reduces the velocity and, hence, the kinetic energy of the fluid. As the value of ν increases, the effect of the hydrodynamic resistance becomes more pronounced, and the global input power quickly decays to zero.

2.6 Summary and Discussion

We investigated through mathematical modeling, analysis, and numerical simulations, the collective motion of micro-swimmers in a fluid with resistance.

We derive and use a continuum model to describes the collective dynamics of micro-swimmers. The swimmers' motion is coupled to the dynamics of the fluid which is modeled through a Stokes-Brinkman equation with an added active stress.

We analyzed the entropy equations of the full system, as well as the stability of the linearized system to see that the Brinkman hydrodynamic resistance has a dampening effect on the dynamics of a pusher micro-swimmer suspension. The linear stability of the uniform isotropic state reveals that the suspension transitions from a long-wave instability to a finite range one one where the collective swimmer chaotic motion is weakened. The linear analysis also suggested parameter ranges for which we could expect to see the growth of fluctuations in a system of a particular size.

Numerical simulations of the full nonlinear system of equations were performed to observe the emergent dynamics in an initially uniform isotropic pusher suspension. As expected from the analyses, for low resistance the simulations reveal the emergence of swimmer concentration bands that dynamically form, merge and break up in

quasi-periodic fashion, and are accompanied by a mixing fluid flow. Resistance tends to inhibit the motion of the swimmers and the formation of these concentration bands. As resistance increases, the emergence of hydrodynamic instability in the pusher suspension is suppressed. In fact, for sufficiently large resistance values, the dynamics can be completely suppressed to the uniform state. The resistance acts as a hindering factor in the movement of the swimmers, inhibiting the development of coherent structures and organized behavior. It disrupts the fluid flow patterns and the hydrodynamic interactions between swimmers, impending the emergence of macroscopic collective motion.

CHAPTER 3

CHEMOTAXIS IN POROUS WET MEDIA

Chemotaxis, defined as a sensing and directed motion of organisms in response to signaling molecules or chemical stimuli in their surrounding, is a fundamental biological process exhibited by many organisms, including bacteria, in which they move in response to chemical gradients in their environment. Micro-organisms utilize chemotaxis not only to navigate towards nutrient-rich regions and away from toxins [13, 14, 15], but also to communicate with each other through chemical cues and aggregate into clusters [142, 7, 117, 128]. Chemotaxis plays a crucial role in various biological phenomena, such as immune response, wound healing, and microbial colonization.

Many continuum theories have been developed to study chemotactic motion, most notably the Keller-Segel one [81, 82], though there are an increasing number of mean-field theories modeling the run-and-tumble behavior have also have also been popular to study bacterial aggregation, e.g in [2, 10, 30, 127, 129, 152, 151]. These latter studies include a conservation equation for the swimmer configurations. On the other hand, there has been a significant amount of work studying the emerging collective dynamics in micro-swimmer suspensions, e.g. [163, 6, 164, 48, 149, 161, 181]. Many of these theories couple the conservation equation of the swimmer configurations to the fluid dynamics using a force dipole exerted by the swimming particles on the surrounding fluid. Historically chemotactic behavior was studied mostly and in the absence of fluid or chemo-attractant dynamics, but recent work has coupled these two schools of thought and studied their compound effects on the swimmer suspensions [105, 51, 78, 79, 104, 106].

Despite many of the biological micro-swimmers living and having evolved porous habitats like soils, sediments and tissues, our understanding of micro-swimmer chemotactic migration in inhomogeneous environments is still in its infancy because many experimental studies of chemotactic behavior have been performed in bulk liquid [17]. Recent experiments have shown that pore-scale confinement is a strong regulator of migration [18, 19], and it markedly alters the dynamics and morphology of the migrating bacterial population [17, 16, 113]. Theoretical and computational studies of chemotactic motion in wet porous environments are also lagging behind, though recent work has incorporated the porosity effects by modifying the standard motility parameters substantially from their bulk liquid values [17, 1]. But as the environment affects the hydrodynamic interactions among swimmers and the strength of the collectively-generated fluid flows, it stands to reason that it would affect the transport and diffusion of the chemo-attractants in it, thus impacting chemotactic motion and migration.

In this chapter then we will study the effects of the environment inhomogeneity, specifically resistance, in the emerging collective dynamics of micro-swimmer suspension that is able to respond to chemical cues generated by the other swimmers. We modify our prior model to include chemotactic responses of micro-swimmers to the collectively-generated chemo-attractant, as well as the dynamics of the chemo-attractant by coupling the aforementioned run-and-tumble and hydrodynamic continuum theories [105, 106]. We model the inhomogeneous wet porous environment through a hydrodynamic resistance term in fluid flow equations, as done in the previous chapter. Analysis of the linearized system and simulations of the full nonlinear system will be presented.

3.1 Model of Chemotaxis in Wet Porous media

Following the previous chapter, we represent the configuration of ellipsoidal micro-swimmers by a distribution function $\Psi(\mathbf{x}, \mathbf{p}, t)$ of the center of mass position $\mathbf{x}$ and orientation vector $\mathbf{p}$ ($|\mathbf{p}| = 1$). The suspension dynamics is described by a conservation equation that includes a run-and-tumble chemotactic response as well fluid advection, rotation and diffusion of swimmers:

$$
\begin{aligned}
\frac{\partial \Psi}{\partial t} = &-\nabla_x \cdot [\Psi(\mathbf{p} + \mathbf{u})] - \nabla_p \cdot [\Psi(I - \mathbf{p}\mathbf{p}^T)(\gamma \mathbf{E} + \mathbf{W})\mathbf{p}] \\
&+ \left[\Psi\lambda(\mathbf{p}) - \frac{1}{4\pi} \int \Psi(\mathbf{p}')\lambda(\mathbf{p}')d\mathbf{p}' \right] + D\nabla_x^2\Psi + d_r\nabla_p^2\Psi.
\end{aligned}
$$

The third term on the right hand side of the above equation (inside square brackets) is new and describes run-and-tumble chemotaxis for bacteria micro-swimmers. Here $\lambda(\mathbf{p})$ represents a chemical gradient-dependent tumbling rate, indicating the probability of a bacterium undergoing a tumbling event within a given time interval. This tumbling rate is influenced by the local chemical concentration experienced by the bacterium, thereby modulating the frequency of tumbling behaviors exhibited by the microorganism. We employed a linearized biphasic form for the tumbling response in our model [30, 105].

$$
\lambda(\mathbf{p}) = \begin{cases} \lambda_0 \left(1 - \chi\mathcal{D}_tC\right) & \text{if } \mathcal{D}_tC > 1/\chi \\ \lambda_0 & otherwise, \end{cases} \tag{3.1}
$$

where

$$
\mathcal{D}_tC = \frac{\partial C}{\partial t} + \mathbf{u} \cdot \nabla C + U_0\mathbf{p} \cdot \nabla \tag{3.2}
$$

represents the rate of change of the chemo-attractant along the path of the micro-swimmer. It quantifies how the chemo-attractant concentration varies as the swimmer moves through its environment. λ_0 is a non-dimensionalized parameter that represents the basic tumbling rate, which determines the rate at which the bacterium undergoes tumbling in the absence of chemotaxis. The dimensionalized chemotactic strength is denoted by χ and influences the responsiveness of the bacterium to the chemo-attractant gradient. $C(\mathbf{x}, t)$ represents the chemo-attractant concentration [104].

The translational and angular velocities are included here the same way as in Chapter 2. The local swimmer concentration $\Phi(\mathbf{x}, t)$ and the mean swimmer director director $< \mathbf{p}(\mathbf{x}, t) >$ are defined as before in Equations (2.23).

The chemo-attractant has its own dynamic behavior and is influenced by both fluid advection and molecular diffusion. It evolves as

$$\frac{\partial C}{\partial t} + \mathbf{u} \cdot \nabla C = D_c \nabla^2 C - \beta_1 C + \beta_2 \Phi. \tag{3.3}$$

In Equation (3.3), D_c is the non-dimensional diffusion constant. This equation has two essential terms that govern the behavior of the chemo-attractant field in the presence of micro-swimmers. The first term, $-\beta_1 C$, accounts for the degradation of chemo-attractant occurring at a constant rate β_1. This term represents the gradual reduction of chemo-attractant concentration over time. The second term, $\beta_2 \Phi$, captures the localized consumption or production of the chemo-attractant by the swimmers. When $\beta_2 < 0$ the swimmers are consuming chemo-attractant from the surrounding, thereby lowering its concentration. Conversely, when $\beta_2 > 0$ is positive, the term indicates the production of chemo-attractant by the swimmers, leading to an increase in its concentration nearby [103, 105, 106].

Lastly, the fluid dynamics is governed by the Stokes-Brinkman Equations with an additional active stress due to the swimmers moving in it and remains unchanged from Equation 2.25 presented in the previous Chapter.

3.2   Linear Stability Analysis

3.2.1   The eigenvalue problem

Similar to Section (2.4.1), we study the stability of the suspension around the uniform and isotropic state $\Psi_0 = \frac{1}{4\pi}$. We assume that there is no swimmer diffusion ($D = d_r = 0$) and that the chemo-attractant field is quasi-static:

$$D_c \nabla^2 C - \beta_1 C + \beta_2 \Phi = 0. \tag{3.4}$$

We focus on auto-chemotactic suspensions described by Equation (3.3), where β_1 and β_2 are both positive, specifically the swimmer produce the chemo-attractant. By studying the linear stability of the system, we can identify the parameter regimes and conditions for which perturbations in the system will either grow or decay over time. To analyze the dynamics of the system, we study the perturbations of the system around the uniform isotropic state $\Psi_0 = 1/4\pi$ for the swimmer distribution and steady-state for the chemo-attractant concentration $\bar{C} = \beta_2/\beta_1 \bar{\Phi} = \beta_2/\beta_1$.

$$\Psi(\mathbf{x}, \mathbf{p}, t) = 1/4\pi + \epsilon \Psi'(\mathbf{x}, \mathbf{p}, t), \qquad C(\mathbf{x}, t) = \frac{\beta_2}{\beta_1} + \epsilon C'(\mathbf{x}, t),$$

with $|\epsilon| << 1$. By making this choice, the tumbling rate is simplified to

$$\lambda(\mathcal{D}_t C) = \lambda_0 (1 - \chi \mathbf{p} \cdot \nabla C).$$

The linearized distribution equation then is

$$\frac{\partial \Psi'}{\partial t} = -\mathbf{p}^T \nabla \Psi' + \frac{3\gamma}{4\pi} \mathbf{p}^{\mathbf{T}} E' \mathbf{p} - \lambda_0 \Psi' + \frac{\lambda_0 \chi}{4\pi} \mathbf{p}^T \nabla C' + \frac{\lambda_0}{4\pi} \int \Psi' d\mathbf{p}'. \qquad (3.5)$$

We proceed by examining a perturbation in the form of a plane wave for the distribution function, where $\Psi'(\mathbf{x}, \mathbf{p}, t) = \tilde{\Psi}(\mathbf{p}, \mathbf{k}) \exp(i\mathbf{k}^T \mathbf{x} + \sigma t)$, along with other relevant quantities. The parameter $\mathbf{k} = k\hat{\mathbf{k}}$ represents the wavenumber and $k = |\mathbf{k}|$.

By utilizing the quasi-static chemo-attractant form of Equation (3.4), we can solve for the chemo-attractant concentration in terms of the swimmer concentration Φ and thus the swimmer distribution Ψ:

$$\tilde{C} = \frac{\beta_2}{\beta_1 + k^2 D_c} \int \tilde{\Psi}' d\mathbf{p}'. \qquad (3.6)$$

The fluid velocity perturbation $\tilde{\mathbf{u}}$ found as in Chapter 2, namely Equation (2.37). Substituting the expressions for $\nabla \tilde{\mathbf{u}}$ and $\tilde{C}$ in Equation (3.5), we obtain

$$\sigma \tilde{\Psi} = -ik\mathbf{p}^T \hat{\mathbf{k}} \tilde{\Psi} - \frac{3\gamma \alpha k^2}{4\pi(k^2 + \nu^2)} \mathbf{p}^T (\mathbf{I} - \hat{\mathbf{k}}\hat{\mathbf{k}}^T) \int \mathbf{p}' \mathbf{p}'^T \tilde{\Psi}(\mathbf{p}') d\mathbf{p}' \, \hat{\mathbf{k}}\hat{\mathbf{k}}^T \mathbf{p}$$

$$- \lambda_0 \tilde{\Psi} + \frac{\lambda_0}{4\pi} \left(1 + \frac{\beta_2 \chi \, ik \, \mathbf{p}^T \hat{\mathbf{k}}}{\beta_1 + k^2 D_c} \right) \int \tilde{\Psi}(\mathbf{p}') d\mathbf{p}'. \qquad (3.7)$$

Without loss of generality, we let $\hat{\mathbf{k}} = \hat{\mathbf{z}}$, $\mathbf{p} = [\sin\theta\cos\phi, \sin\theta\sin\phi, \cos\theta]$ and $d\mathbf{p} = \sin\theta d\theta d\phi$ for $\theta \in [0, \pi]$, $\phi \in [0, 2\pi)$. Then, we can write

$$(\sigma + \lambda_0 + ik\cos\theta)\tilde{\Psi} = -\frac{3\gamma \alpha k^2}{4\pi(k^2 + \nu^2)} \cos\theta \sin\theta[\cos\phi F_1 + \sin\phi F_2]$$

$$+ \frac{\lambda_0}{4\pi} \left[1 + \frac{\beta_2 \chi}{\beta_1 + k^2 D_c} ik\cos\theta \right] G, \qquad (3.8)$$

where for simplicity we have defined the following integral operators of $\tilde{\Psi}$

$$F_1(\tilde{\Psi}) = \int_0^{2\pi} \cos\phi' \int_0^{\pi} \sin^2\theta' \cos\theta' \tilde{\Psi}(\theta', \phi')d\theta' d\phi'$$

$$F_2(\tilde{\Psi}) = \int_0^{2\pi} \sin\phi' \int_0^{\pi} \sin^2\theta' \cos\theta' \tilde{\Psi}(\theta', \phi')d\theta' d\phi'$$

$$G(\tilde{\Psi}) = \int_0^{2\pi} \int_0^{\pi} \sin\theta' \tilde{\Psi}(\theta', \phi')d\theta' d\phi'.$$

We can derive the eigenvalue relations for the perturbation mode $\tilde{\Psi}$ and the growth rate σ by solving the linear eigenvalue problem given in Equation (3.8). To do this, we apply the operators F_1 and G to $\tilde{\Psi}$ in Eq.(3.8), obtaining for $F_1(\tilde{\Psi})$ and $G(\tilde{\Psi})$:

$$F_1 = -\frac{3\gamma\alpha k^2}{4\pi(k^2 + \nu^2)} \int_0^{\pi} \frac{\sin^3\theta \cos^2\theta}{(\sigma + \lambda_0 + ik\cos\theta)} d\theta F_1$$

$$G = -\frac{\lambda_0}{2} \int_0^{\pi} \frac{\sin\theta}{(\sigma + \lambda_0 + ik\cos\theta)} d\theta G.$$

The equation for F_2 is identical to that for F_1. Canceling F_1 and G, we obtain two separate integral dispersion relations:

$$1 = -\frac{3\alpha k^2}{4\pi(k^2 + \nu^2)} \int_0^{\pi} \frac{\sin^3\theta \cos^2\theta}{(\sigma + \lambda_0 + ik\cos\theta)} d\theta$$

$$1 = -\frac{\lambda_0}{2} \frac{\chi\beta_2 ik}{(\beta_1 + k^2 D_c)} \int_0^{\pi} \frac{\sin\theta \cos\theta}{(\sigma + \lambda_0 + ik\cos\theta)} d\theta - \frac{\lambda_0}{2} \int_0^{\pi} \frac{\sin\theta}{(\sigma + \lambda_0 + ik\cos\theta)} d\theta.$$

Letting $a = (\sigma + \lambda_0)/(ik)$, $R = \chi\beta_2/(\beta_1 + k^2 D_c)$ and evaluating the integrals give us two uncoupled dispersion relations that are implicit equations for $\sigma(k)$:

$$1 = -\frac{3\gamma\alpha k^2}{4(k^2 + \nu^2)}\frac{1}{ik}\left[2a^3 - \frac{4}{3}a + (a^4 - a^2)\log\left(\frac{a-1}{a+1}\right)\right], \tag{3.9}$$

$$1 = \frac{\lambda_0}{2}R\left[2 + a\log\left(\frac{a-1}{a+1}\right)\right] - \frac{\lambda_0}{2}\frac{1}{ik}\log\left(\frac{a-1}{a+1}\right), \tag{3.10}$$

which we re-write as

$$0 = \mathfrak{F}(\sigma, k) = \frac{-4ik}{3(-\alpha\gamma)}\frac{k^2 + \nu^2}{k^2} + \left[2a^3 - \frac{4}{3}a + (a^4 - a^2)\log\left(\frac{a-1}{a+1}\right)\right], \tag{3.11}$$

$$0 = \mathcal{G}(\sigma, k) = \frac{-2ik}{\lambda_0} + 2Rik + (aRi(k-1))\log\left(\frac{a-1}{a+1}\right). \tag{3.12}$$

We will refer to the Equation (3.11) is referred to as the *Brinkman Hydrodynamics dispersion relation* due to the presence of hydrodynamics-related variables like γ, α, and we refer to Equation (3.12) as the *Chemotaxis run-and-tumble dispersion relation* based on the presence of chemotaxis parameters like $R, \chi, \beta_1, \beta_2$.

The hydrodynamics relation is like the dispersion relation in Equation (2.42) of Chapter 2, but here it also features the basal tumbling parameter λ_0 in the definition of $a = (\sigma + \lambda_0)/(ik)$. Notice that the hydrodynamic resistance parameter ν shows up only in Equation (3.11), and, according to the linear theory, it should not be affecting the chemotaxis.

The autochemotactic dispersion is exactly that found by Lushi et al. [105, 104, 106] for auto-chemotactic micro-swimmer suspensions. This relation is unaffected by both hydrodynamics and the swimming mechanism, as noted by the absence of the dipole strength parameter α. The auto-chemotactic relation primarily relies on the

dynamics of the chemo-attractant, as indicated by the presence of the chemotactic term R.

Notably, the resistance does not appear anywhere in Equation (3.15), and at least in the linearized system, it does not impact the chemotactic instability.

3.2.2 Small-k asymptotic solutions of dispersion relations

The dispersion relations described by Equations (3.11) and (3.12) cannot be solved analytically for the growth rate $\sigma(k)$. These equations, which govern the relationship between the wavenumber and the growth rate in the given system, do not have closed-form solutions that can be obtained analytically.

Following the same steps as in Section (2.4.2), we find small k asymptotic solutions $\sigma(k) = \lambda_0 + \sigma_0 + \sigma_1 k + \sigma_2 k^2 + O(k^3)$ for both dispersion relations.

For the hydrodynamic dispersion relation Equation (3.11), we obtain:

$$\sigma_{H_1} = -\lambda_0 + \frac{(-\alpha\gamma)}{5(1+\tau^2)} + \left[\frac{-15(1+\tau^2)}{7(-\alpha\gamma)} - D\right]k^2 + \frac{17875(1+\tau^2)^3}{147(-\alpha\gamma)^3}k^4 + O(k^5),$$

(3.13)

$$\sigma_{H_2} = -\lambda_0 + \left[\frac{(1+\tau^2)}{(-\alpha\gamma)} - D\right]k^2 - \frac{3(1+\tau^2)^2\pi}{4(-\alpha\gamma)^2}k^3 + \frac{3(1+\tau^2)^3(3\pi^2-8)}{8(-\alpha\gamma)^3}k^5 + O(k^6).$$

(3.14)

The two solutions we obtain, shown in Equations (3.13, 3.14), are similar to the Equations (2.43, 2.44) that we found in Section 2.4.1, but the basal tumbling λ_0 is now present. Both of these branches are now decreased exactly by λ_0, so basal tumbling has a stabilizing effect. Translational diffusion with rate D also has an unsurprising stabilizing effect. We observe that both branches of $\sigma_H(k)$ are negative for pullers ($\alpha > 0$) for any basal tumbling value and any swimmer shape, which means the puller suspension perturbation is stable.

For pushers ($\alpha < 0$) however, the $\sigma_H(k)$ term may be positive depending on the balance of the terms: $\sigma_{H1}(k = 0) = -\lambda_0 + (-\alpha\gamma)/5(1 + \tau^2)$ and is positive only if $(-\alpha\gamma)/(1 + \tau^2) > 5\lambda_0$. The maximum of this branch is $1/5$ and is obtained at $k = 0$ for elongated $\gamma = 1$ non-tumbling λ_0 pusher swimmers $\alpha = -1$ in Stokes flow conditions $\tau = 0 = \nu$, and for increasing ν or τ, the value of $\sigma_{H1}(k = 0)$ decreases. For a given wave-number k that is very small, we see that non-zero resistance lowers the value of $\sigma_{H1}(k)$, so resistance has a stabilizing effect.

We also seek an asymptotic solution for the auto-chemotactic relation Equation (3.12), following the previous steps and those for Stokesian chemotactic suspensions in [105, 104, 106]. Note $R = \bar{\chi}/(1 + \bar{D}_c k^2) \approx \bar{\chi}(1 - \bar{D}_c k^2 + \bar{D}_c^2 k^4 + ...)$ for small k where $\bar{\chi} = (\chi \beta_2)/\beta_1$, and $\bar{D}_c = D_c/\beta_1$. As shown in the Appendix B.2, we find:

$$\sigma_C(k) = \frac{\bar{\chi}\lambda_0 - 1}{3\lambda_0}k^2 - \left[\frac{\bar{\chi}\bar{D}_c}{3} + \frac{(5\lambda_0\bar{\chi} - 1)(\bar{\chi}\lambda_0 - 1)}{45\lambda_0^3}\right]k^4 + O(k^5). \tag{3.15}$$

Equation (3.15) shows that $\sigma_C(0) = 0$, and for very small k the growth rate $\sigma_C(k)$ grows quadratically in the positive direction if $\bar{\chi}\lambda_0 - 1$. Hence Equation (3.15) also shows that to obtain $\sigma_C > 0$ and have a chemotactic instability, we need $\bar{\chi}\lambda_0 > 1$, or more specifically $\chi\beta_2\lambda_0/\beta_1 > 1$. The chemo-attractant diffusion comes in at the next order term in Equation (3.15) and has a stabilizing effect.

3.2.3 Numerical solutions of the dispersion relations

Similar to Section 2.4.3 in Chapter 2, we solve the dispersion relations Equations (3.11) and (3.12) with an iterative quasi-Newton solver.

In Figure 3.1 we show the numerical solution of the hydrodynamic dispersion relation Equation (3.13), and specifically highlight the difference from Figures 2.2 and 2.3 that results from the presence of basal tumbling λ_0. The imaginary part of the $Im(\sigma_H(k)$ is unaffected by λ_0 as they are identical to the respective plots in Chapter 2.

But the effect of basal tumbling is obvious on the branches of $Re(\sigma_H(k))$: specifically tumbling has shifted them downwards by λ_0 in comparison to the non-tumbling result in Chapter 2. This shows that tumbling per se has a stabilizing effect on the system. Moreover, as $\lambda_0 \geq 0.2$ shifts the entire $Re(\sigma_H(k))$ to non-positive values, then $\lambda_0 \geq 0.2$ suffices to turn off the hydrodynamic instability for any wavenumber k.
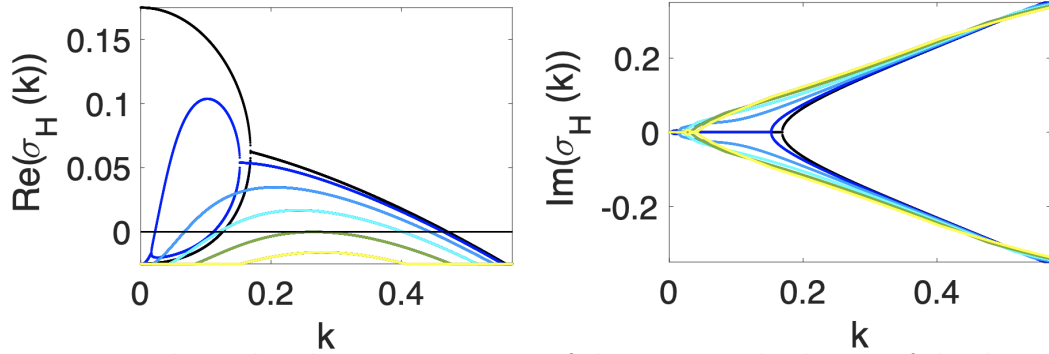
Figure 3.1 The real and imaginary parts of the numerical solution of the dispersion relation Equation (3.13) with $\lambda_0 = 0.025$, $\nu = 0, 0.05, ..., 0.3$.

Figure 3.2 shows the numerical solution for $\sigma_C(k)$ of Equation(3.12) for two different parameter sets $\lambda_0, \chi, \beta_1, \beta_2, D_c$. We notice $\sigma_C(k)$ is real-valued, $\sigma_C(0) = 0$, and, consistently with the asymptotic results of Equation (3.15), $\sigma_C(k) > 0$ for small k if $\chi\beta_2/\beta_1 - 1/\lambda_0 > 0$. The initially-upward curve of $\sigma_C(k)$ turns and comes down to zero and eventually becomes negative for some larger k-value because chemo-attractant diffusion has a stabilizing effect at $O(k^4)$. In all, for auto-chemotactic swimmer suspensions, there is a finite band of unstable modes when $\chi\beta_2/\beta_1 > 1/\lambda_0$, and its width is controlled by chemo-attractant diffusion. [105].

The linear stability analysis of chemotactic suspensions in two dimensions is included in the Appendix C. As in the 3D analysis presented above, we found two distinct dispersive relations, for the hydrodynamics and chemotaxis respectively. The hydrodynamic dispersion relation is the same as that found in Section 2.4.4 for non-chemotactic suspensions but with the addition of basal tumbling in a similar manner
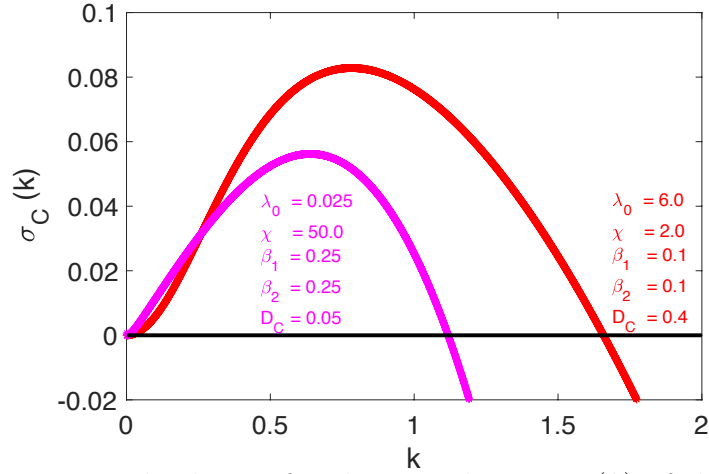
Figure 3.2 Numerical solution for the growth rate $\sigma_C(k)$ of the auto-chemotactic dispersion relation Equation (3.12) for two sets of parameters $\chi, \beta_1, \beta_2, D_c$.

to the 3D case here. The chemotaxis dispersion relation is also qualitatively similar to the 3D version here.

3.2.4   Phase diagram of complex dynamics

The asymptotic analysis and the numerical solutions to the dispersion relations provide valuable information about parameter ranges. From Equation (3.13) and Figure 3.1 we see that $\lambda_0 \geq 0.2$ turns off the hydrodynamic instability for any wavenumber, hence system size [105]. From Equation (3.15) we see that to have a chemotactic instability, i.e. $\sigma_C(k) > 0$, we need $\chi\beta_2/\beta_1 > 1/\lambda_0$. Lastly, upon examining Figures 3.1 and (2.5), along with the dispersion relation for hydrodynamics described by Equation (3.12), we see that $\lambda_0 \geq \lambda_0(\nu) := max(\sigma(k,\nu))$ from the plot effectively disables the hydrodynamic instability for any system size.

Building upon this information gathered from the linear theory, we plot the surfaces $\lambda_0 = 0.2$, $\chi\beta_2/\beta_1 = 1/\lambda_0$ and $\lambda_0 = \lambda_0(\nu)$ on a 3D plot with axis ν, λ_0, and $\chi\beta_2/\beta_1$, shown in Figure 3.3. By examining the 3D regions resulting from the surfaces' intersections and where a parameter set is situated with respect to them,

we can gain insight on which instabilities would likely arise, and thus gain insight on the combined effects of the hydrodynamics, auto-chemotaxis and resistance.
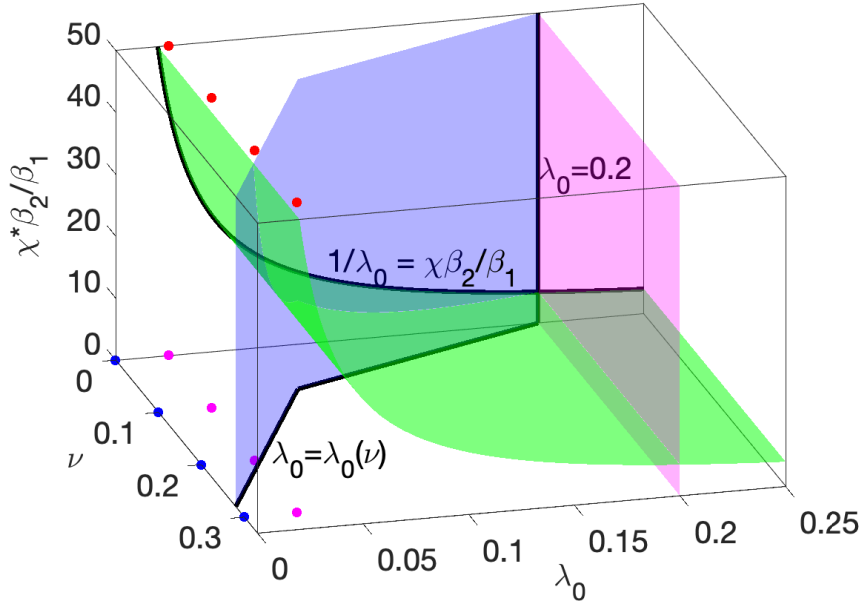
Figure 3.3 3D phase diagram of parameter regions for expected dynamics depending on the presence of resistance, hydrodynamic and auto-chemotactic instabilities. The dots note parameter values for nonlinear simulations: the blue ones for those already presented in Chapter 2, magenta and red ones for parameters from stability plots in Figures 3.1 and 3.2 and presented next in this chapter.

To better visualize these 3D regions, we show 2D slices phase diagram for various resistance parameters $\nu = 0, 0.1, 0.2, 0.3$ in Figure 3.4. These slices help us observe how the system's dynamics evolve under different resistance conditions.

The phase diagram obtained for the case where $\nu = 0.0$ and shown in Figure 3.4a is that found by Lushi et al., [105, 104, 106] for auto-chemotactic pusher suspensions in homogenous viscous fluids. This diagram reveals four distinct regions of dynamics, which we have labeled as follows: hydrodynamic collective swimming ($\lambda_0 < 0.2$, $\chi\beta_2/\beta_1 < 1/\lambda_0$), chemotactic aggregation ($\lambda_0 > 0.2$, $\chi\beta_2/\beta_1 > 1/\lambda_0$), dynamic aggregation or mixed dynamics ($\lambda_0 < 0.2$, $\chi\beta_2/\beta_1 > 1/\lambda_0$), and the uniform state without hydrodynamic or chemotactic instabilities ($\lambda_0 > 0.2$, $\chi\beta_2/\beta_1 < 1/\lambda_0$).
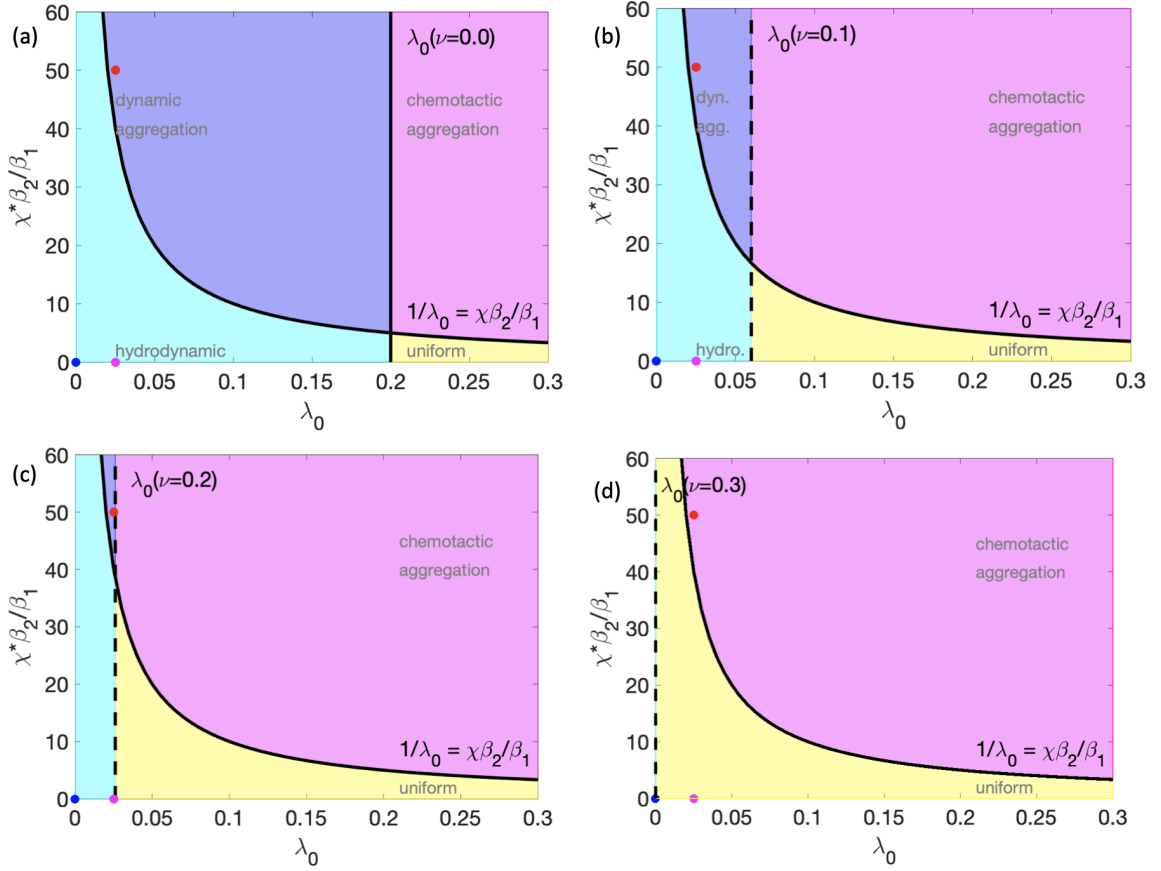
Figure 3.4 Phase diagram of parameter regions and expected dynamics for $\nu = 0, 0.1, 0.2, 0.3$. The dots note parameter values utilized in nonlinear simulations.

When resistance is introduced ($\nu > 0$), a hydrodynamic instability can still occur if $\lambda_0 < \lambda_0(\nu)$, where $\lambda_0(\nu)$ is defined as the maximum value of $\sigma(\nu)$ obtained from the curve in Figure 2.5. Essentially, as ν increases, the boundary for the hydrodynamic instability, which was initially at $\lambda_0(\nu = 0) = 0.2$, shifts to the left. This can be observed in the Figure 3.4, where the regions corresponding to hydrodynamic collective swimming and dynamic aggregation shrink with increasing ν. Eventually, these regions disappear entirely for $\nu \approx 0.27$, as indicated by $max(\sigma_H \nu \approx 0.27) = 0$. It is worth noting that the stability criterion used in constructing the phase diagram was $\lambda_0(\nu) = max(\text{Re}\,\sigma(\nu))$, which is valid for all

k. However, a more accurate criterion could be derived if the specific domain or length-scale size L was known, such as $\lambda_0(\nu) = \text{Re}(\nu = 0.2, k = 2\pi/L)$.

Finally, the dots in Figures 3.3 and 3.4 denote the parameter values employed in the nonlinear simulations. The blue dots represent the parameters used in the figures presented in Chapter 2, while the magenta and red dots correspond to the simulations to be showcased in this chapter. These dots serve as reference points, linking the theoretical analysis and the numerical simulations, and provide insights into the specific parameter combinations explored in the study.

3.3   Nonlinear Dynamics

In Chapter 2, we analyzed the effect of resistance in the absence of chemotaxis and tumbling. Here we investigate the impact of resistance on the dynamics regions identified through the linear stability analysis and depicted in Figure 3.4, namely the hydrodynamic collective swimming, the dynamic aggregation, and the auto-chemotactic aggregation states. The simulation details and the initial conditions for the distribution function Ψ are as in Chapter 2: . In addition, the initial chemo-attractant distribution is taken to be $C(\mathbf{x}, 0) = \beta_2/\beta_1$.

3.3.1   Resisting hydrodynamic collective swimming

To further explore the influence of resistance on the hydrodynamic collective swimming state, we consider tumbling but non-chemotactic pusher suspensions with basic tumbling rate $\lambda_0 = 0.025$. These parameter set is noted as magenta dots in the phase diagrams of Figures 3.3 and 3.4. From Figure 3.1, we expect a hydrodynamic instability for this parameter set.

Figures 3.5 - 3.7 show simulations of the dynamics of an initially isotropic pusher suspension with varying hydrodynamic resistance parameters ν.

$$\nu = 0.0, \qquad \lambda = 0.025, \chi = 0$$
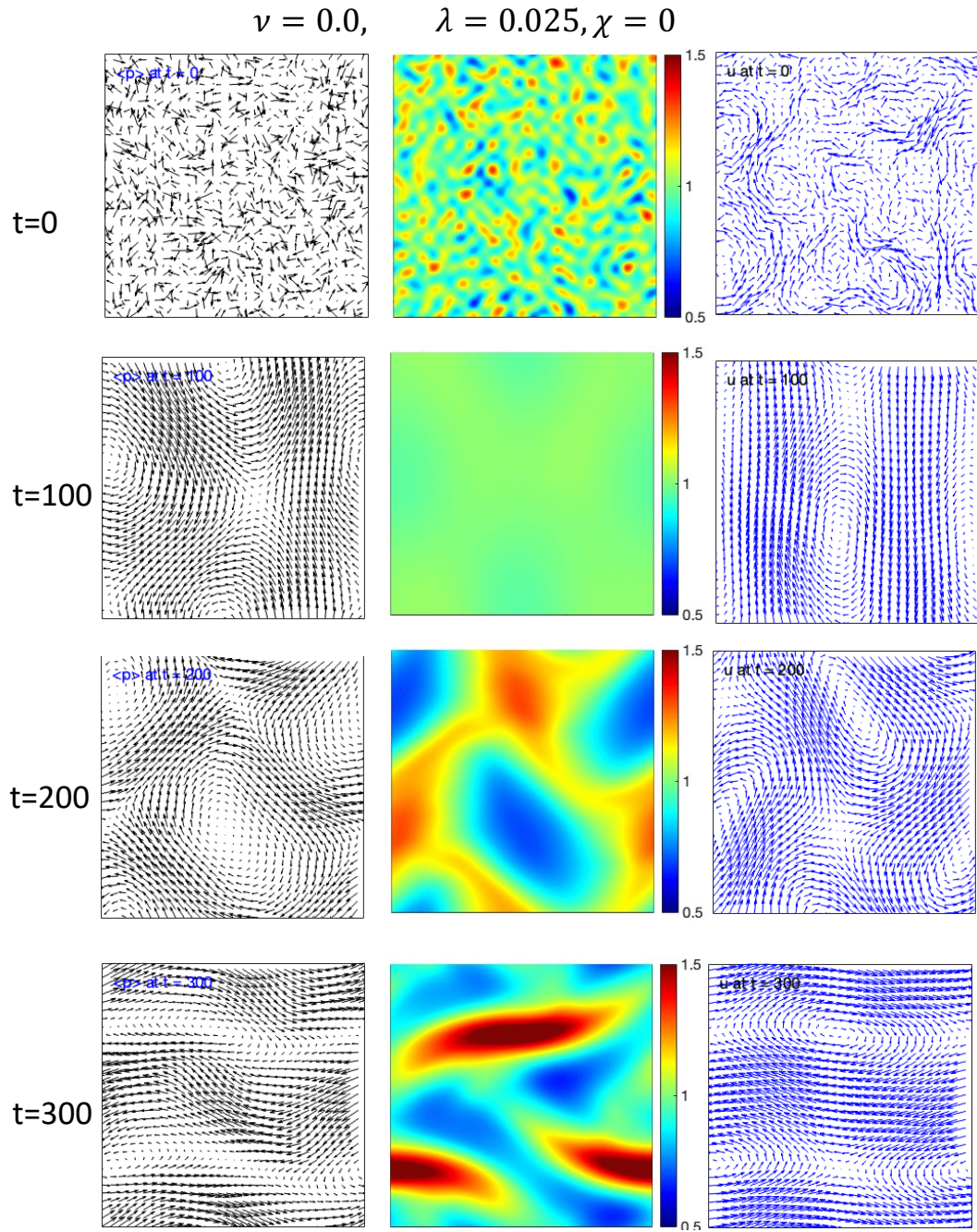
Figure 3.5 The average swimmer director $< \mathbf{p} >$, concentration Φ and fluid velocity $\mathbf{u}$ at times $t = 0, 100, 200, 300$ for $\nu = 0$.

$$\nu = 0.1, \qquad \lambda = 0.025, \chi = 0$$
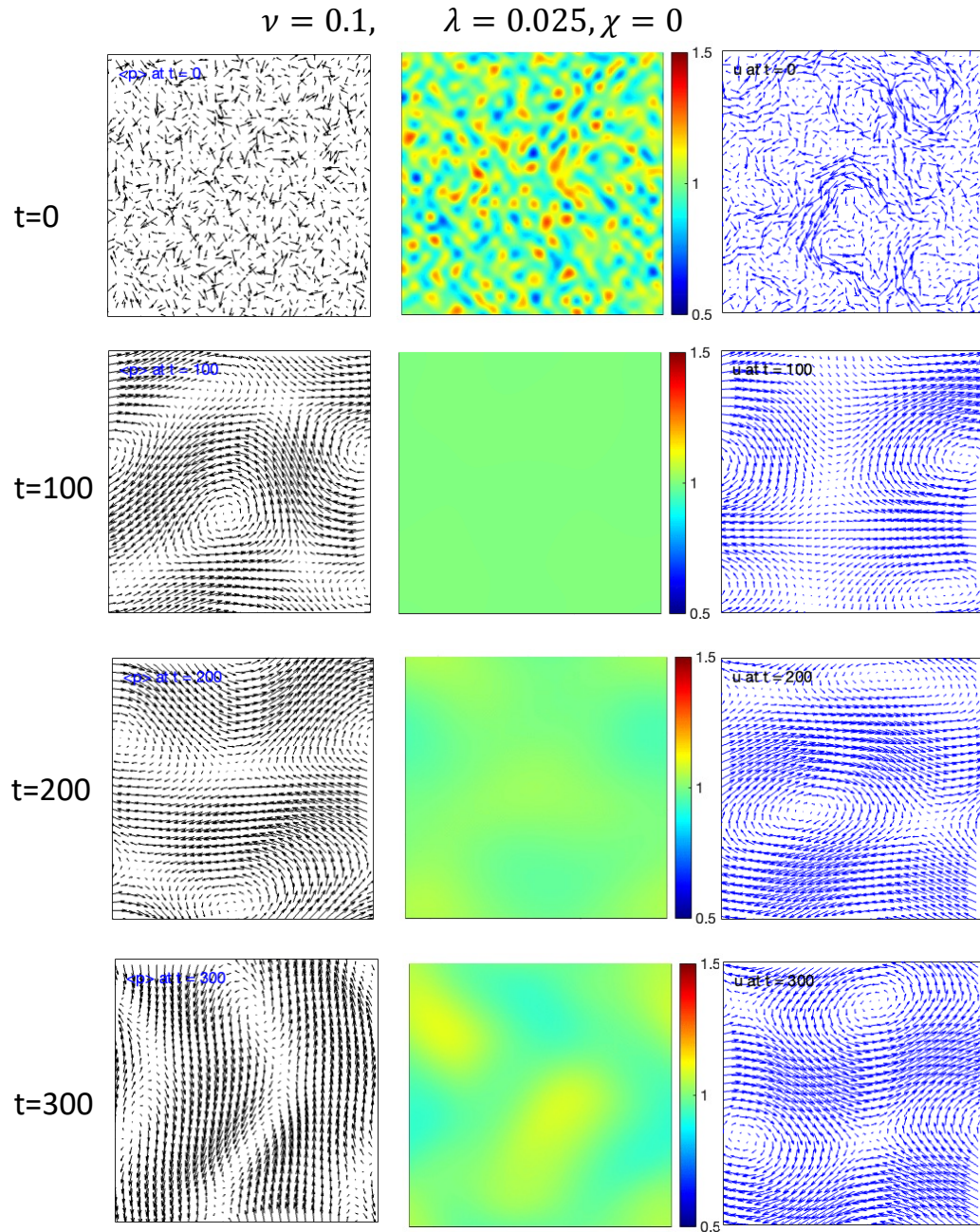
Figure 3.6 The average swimmer director $< \mathbf{p} >$, concentration Φ and fluid velocity $\mathbf{u}$ at times $t = 0, 100, 200, 300$ for $\nu = 0.1$.
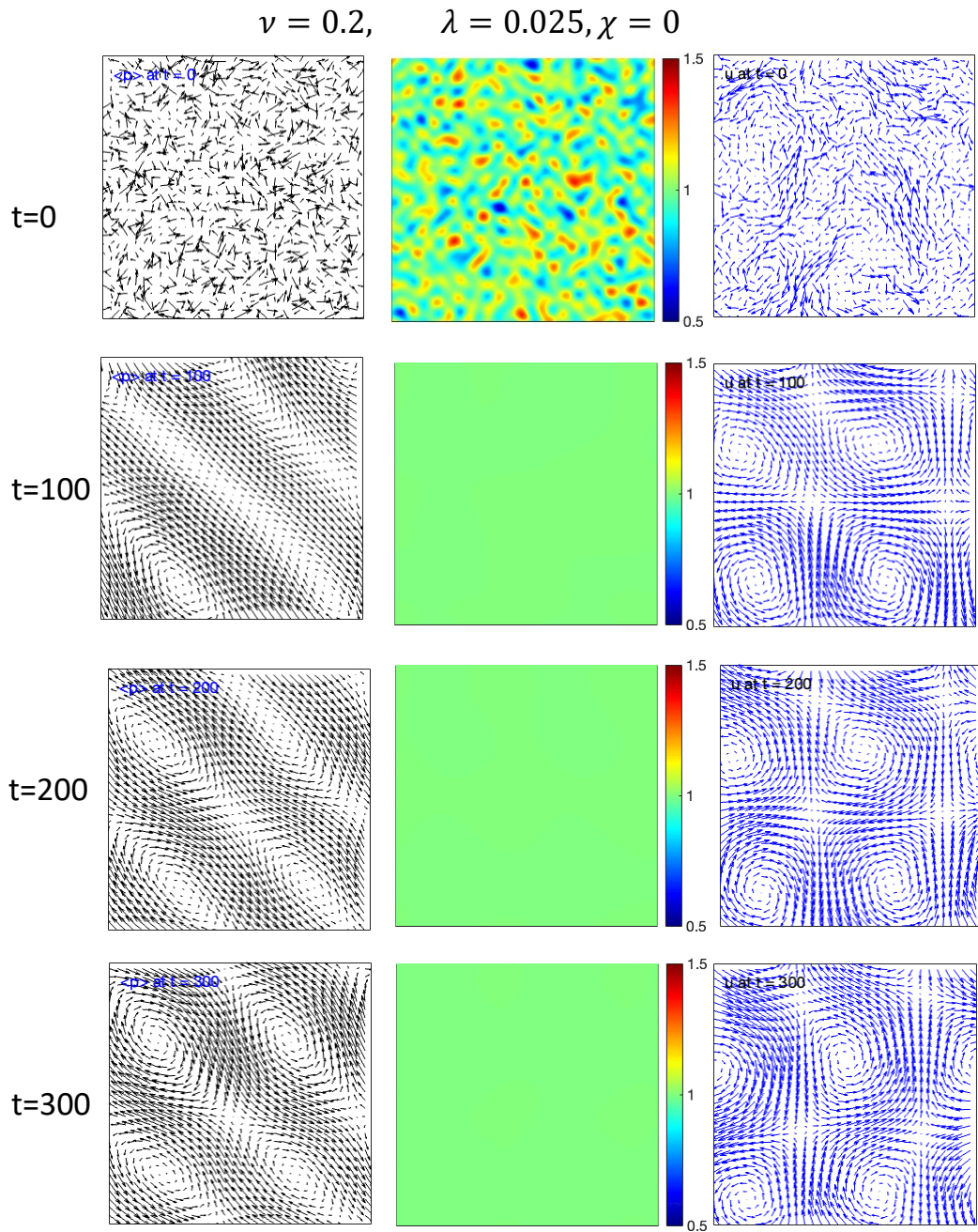
Figure 3.7 The average swimmer director $< \mathbf{p} >$, concentration Φ and fluid velocity $\mathbf{u}$ at times $t = 0, 100, 200, 300$ for $\nu = 0.2$.

For low ν, we observe the emergence of bacteria concentration bands that exhibit bending, folding, and intricate patterns, accompanied by a fluid flow that promotes mixing. For increasing ν, we observe a visible delay in the onset of the instability compared to the case with ($\nu = 0$). This delay suggests that higher resistance hinders the development of the instability, resulting in a slower evolution of the concentration bands.

For high hydrodynamic resistance reaches $\nu = 0.2$, we observe a significant suppression of the instability, with the initial perturbations decaying to zero and resulting into a stabilized and uniform dynamics. This suggests that strong hydrodynamic resistance can effectively suppress the emergence of concentration bands and the hydrodynamic collective swimming state.

Lastly, at $\nu = 0.3$ and higher (not shown), the initial perturbations are quickly and completely suppressed, resulting in a uniform distribution of the swimmers without the formation of concentration bands or any visible instabilities, which is to be expected because this particular parameter falls under the uniform dynamics region in the phase diagrams of Figures 3.3-3.4.

As in Section 2.5.3, we can quantify the impact of Brinkman resistance by employing the same metrics. Figure 3.8 the maximum concentration $max(\mathbf{\Phi})$, and maximum fluid velocity $max(|\mathbf{u}|)$ and mean fluid velocity $max(|\mathbf{u}|)$ over time, whereas Figure 3.9 presents $< \mathbf{u} \cdot \mathbf{n} >$, the entropy $S(t)$, and the global input power $P(t)$.

For easier comparisons and discernment of the effects of basic tumbling, we also include in Figures 3.8 and 3.9 these quantities for non-tumbling suspensions $\lambda_0 = 0$, whose parameters are shown as blue dots in the phase diagrams of Figures 3.3-3.4.
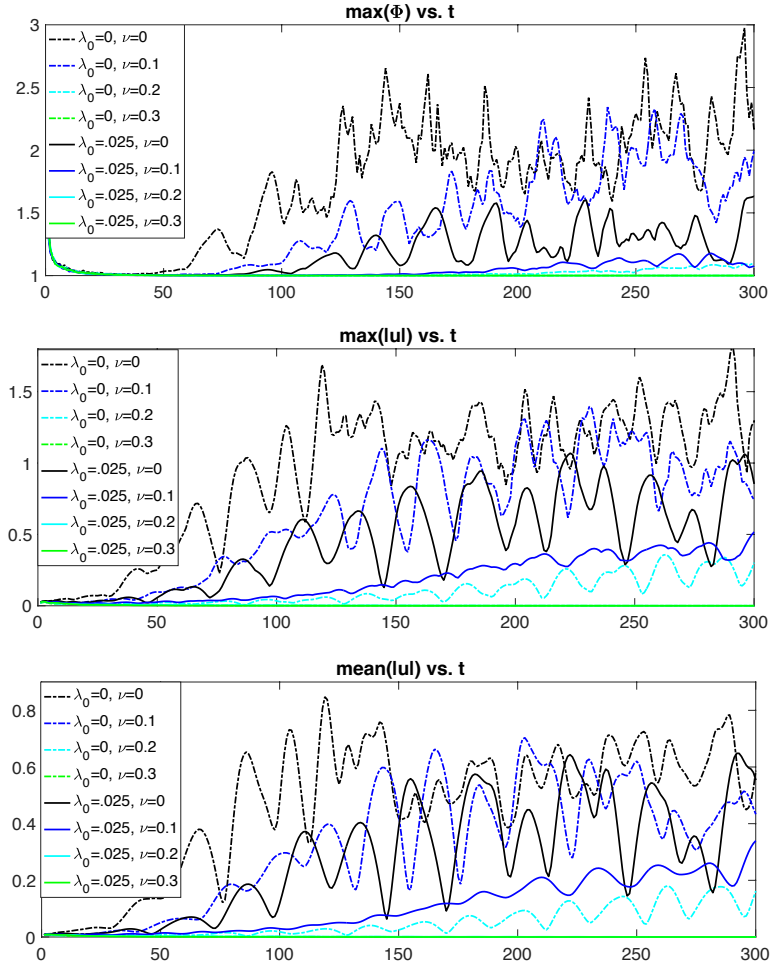
Figure 3.8 Comparisons over a long time of $max(\mathbf{\Phi})$, $max(|\mathbf{u}|)$, and $mean(|\mathbf{u}|)$ for $\lambda_0 = 0, 0.025$ and different ν.

Without tumbling, we observe a decrease in the overall magnitude of all these quantities for increasing resistance ν. Upon introducing tumbling into the system, we see a decrease in the magnitudes of all these quantities for the purely-tumbling as compared to the non-tumbling case. Basic tumbling per se, as anticipated from the linear stability analysis and Figure 3.1, acts as a stabilizer on the system and dampens the hydrodynamic instability and thus the emergence of the hydrodynamic collective swimming state. The hydrodynamic resistance further suppresses the hydrodynamic instability.
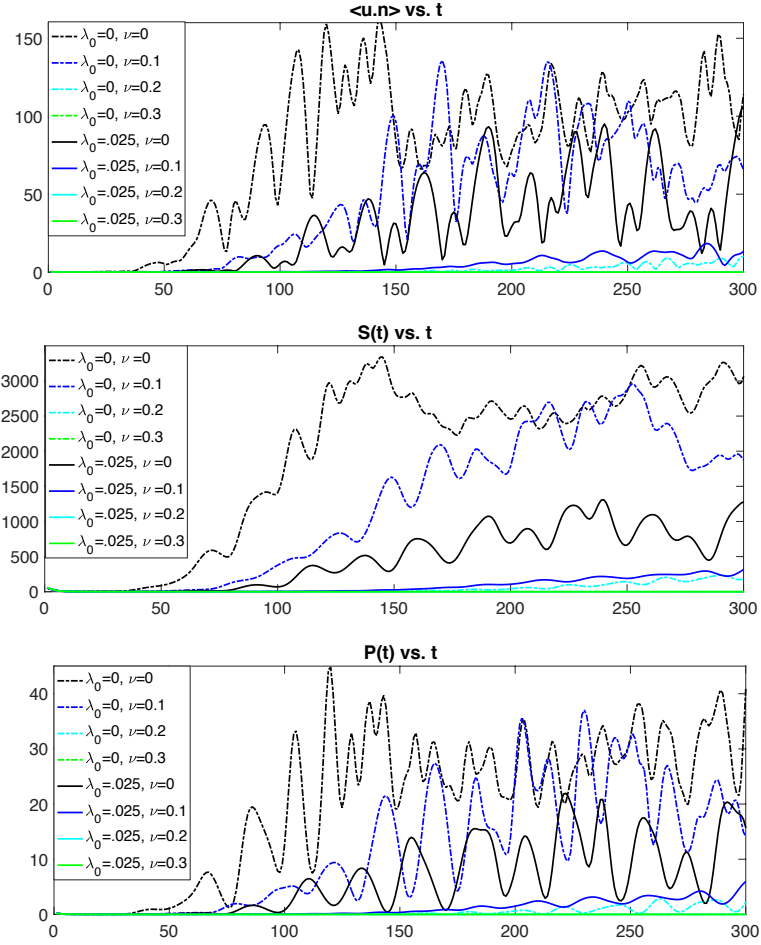
Figure 3.9 Comparisons over a long time of $< \mathbf{u} \cdot \mathbf{n} >$, $S(t)$, and $P(t)$ for $\lambda_0 = 0, 0.025$ and different ν.

3.3.2 Resisting dynamic aggregation

To see the effect of resistance on the dynamic aggregation state, we examine the dynamics of auto-chemotactic pusher suspensions with parameters $\lambda_0 = 0.025$, $\chi = 50$, $\beta_1 = 0.25$, $\beta_2 = 0.25$, and $D_c = 0.05$ for which there is both a hydrodynamic instability and an auto-chemotactic instability for the chosen domain size $L = 25$, as shown in Figures 3.2. This parameter set is denoted as red dots in the phase space diagrams, Figure 3.3, are carefully chosen to reside within the dynamic aggregation region for $\nu = 0$, $\nu = 0.1$, and $\nu = 0.2$, but not for $\nu = 0.3$.

Consistent with our linear stability analysis, we choose the initial chemo-attractant distribution to be $C(\mathbf{x}, 0) = \beta_2/\beta_1 = 1$ for all simulations.

Figures 3.10 to 3.12 present snapshots of the dynamics that allow us to observe firstly the predicted dynamic aggregation state, and secondly the changes in the suspension dynamics as we increase the hydrodynamic resistance parameter ν.

First, we describe the dynamics pertaining to the dynamic aggregation state without resistance, as also studied by [106]. The micro-swimmers produce chemo-attractant as well as aggregate towards it. A strong mixing flow emerges, and it advects both the swimmers and the chemo-attractant, resulting in dynamic aggregation of swimmers occurring due to their local auto-chemotactic tendency. This effect is seen from the sharper and narrower concentration bands in the auto-chemotactic suspension in Figure 3.10 compared to the non-chemotactic or just tumbling cases presented earlier for same $\nu = 0$.

In the rest of the figures, we can clearly see the impact of increasing resistance on the swimmer suspension dynamics. One noticeable effect is the visible delay in the onset of the instability as we move from lower resistance ($\nu = 0$) to higher resistance ($\nu > 0$). This delay indicates that the higher resistance hinders the development of the instability, resulting in a slower evolution of the concentration bands.

It is interesting to note that for $\nu = 0.2$, despite the parameter set falling within the dynamic aggregation region, we observe uniform dynamics instead of the expected aggregation behavior. This occurrence highlights the concept of marginal stability due to the proximity of the parameter set location to both the region boundary surfaces $\lambda_0 = \lambda_0(\nu = 0.2)$ and $1/\lambda_0 = \chi\beta_2/\beta_1$. It also reminds us us that linear theory alone cannot predict the nonlinear system dynamics.

Lastly, for $\nu = 0.3$ and higher (not shown), we obtain the uniform dynamics state, as expected from the results of linear analysis.
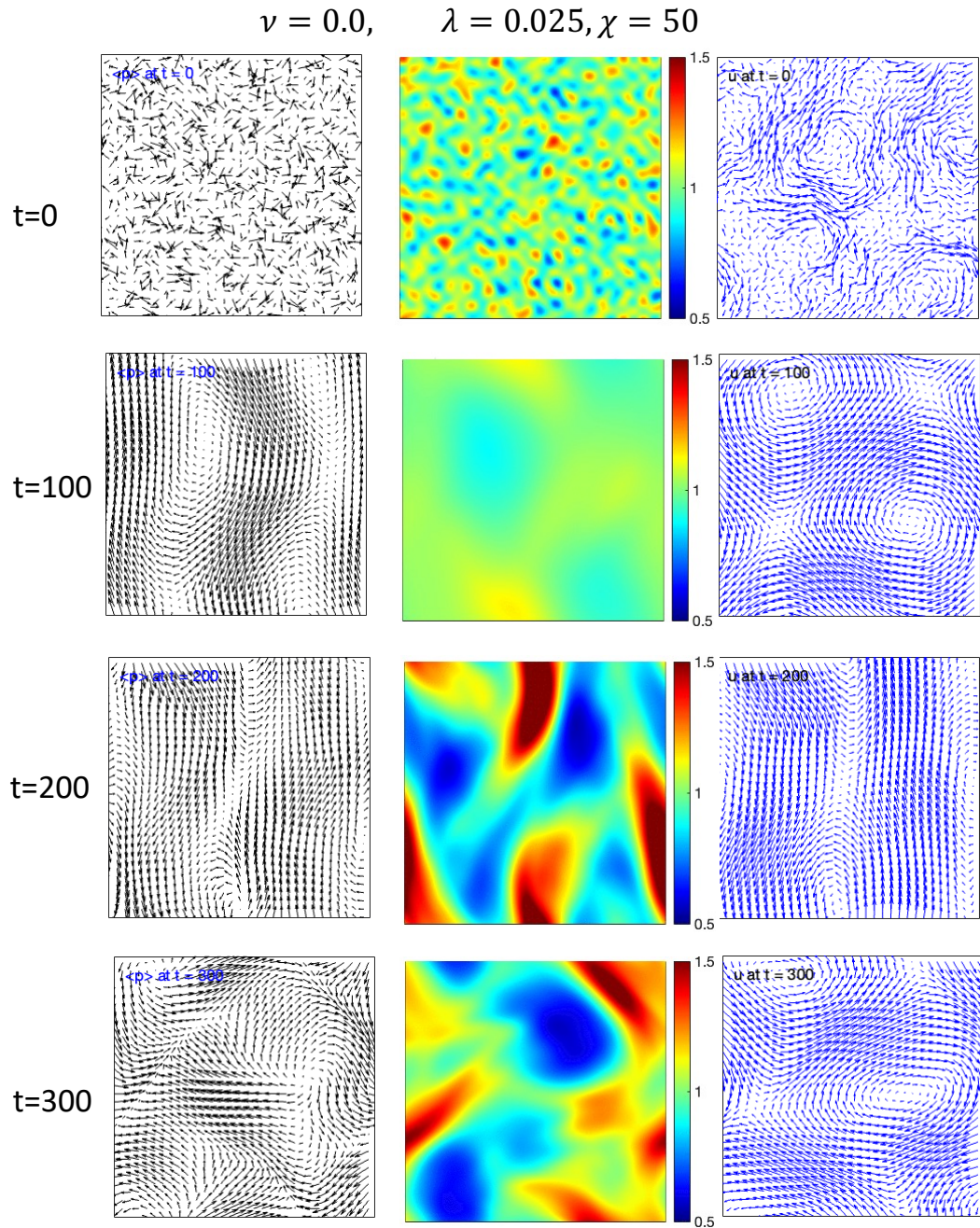
$$\nu = 0.0, \qquad \lambda = 0.025, \chi = 50$$

Figure 3.10 The average autochemotactic swimmer director $< \mathbf{p} >$, concentration Φ and fluid velocity $\mathbf{u}$ at times $t = 0, 100, 200, 300$. Parameters are $\lambda_0 = 0.025, \chi = 50, \beta_1 = 0.25 = \beta_2$, and $\nu = 0$.
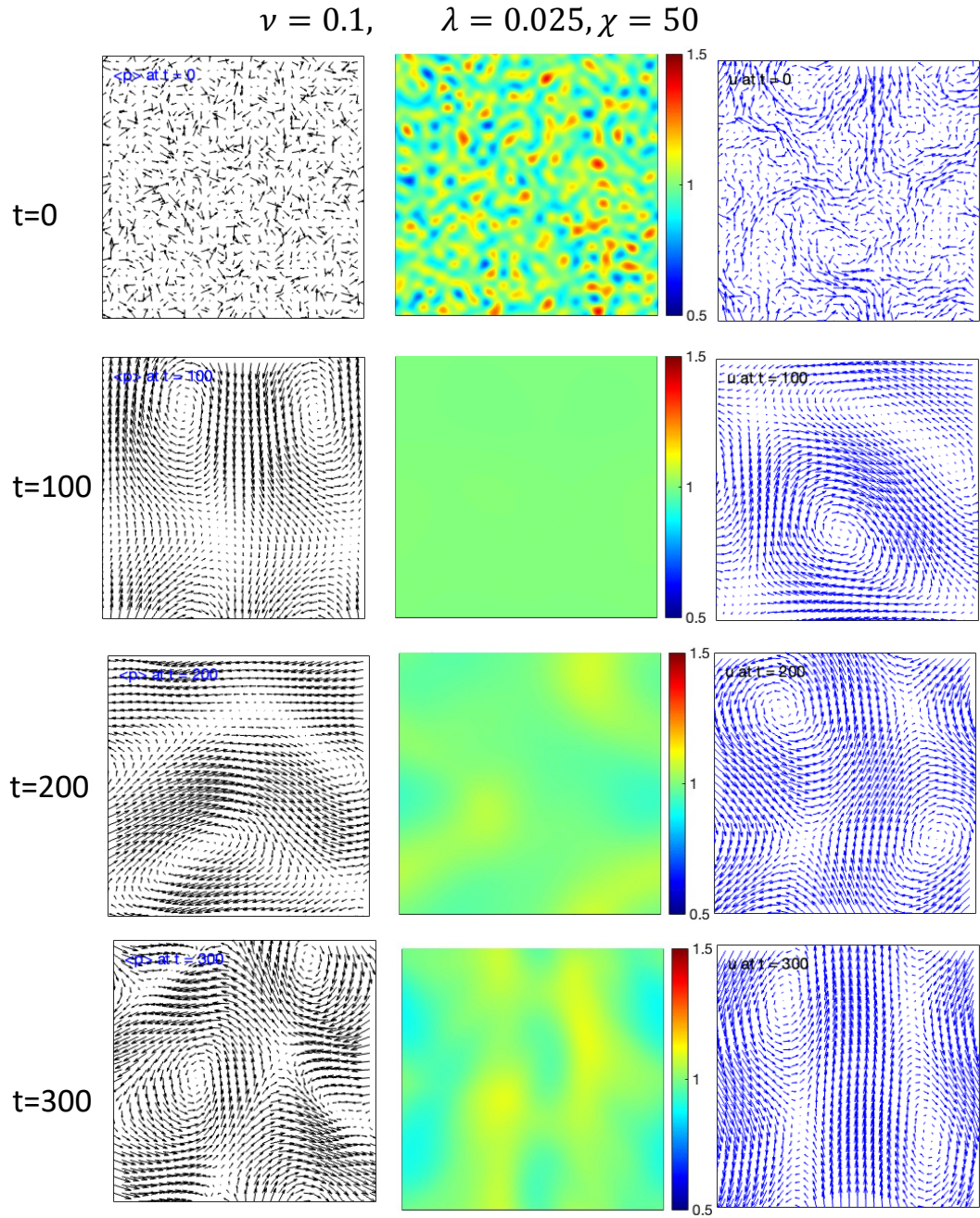
Figure 3.11 The average autochemotactic swimmer director $< \mathbf{p} >$, concentration Φ and fluid velocity $\mathbf{u}$ at times $t = 0, 100, 200, 300$. Parameters are $\lambda_0 = 0.025, \chi = 50, \beta_1 = 0.25 = \beta_2$, and $\nu = 0.1$.
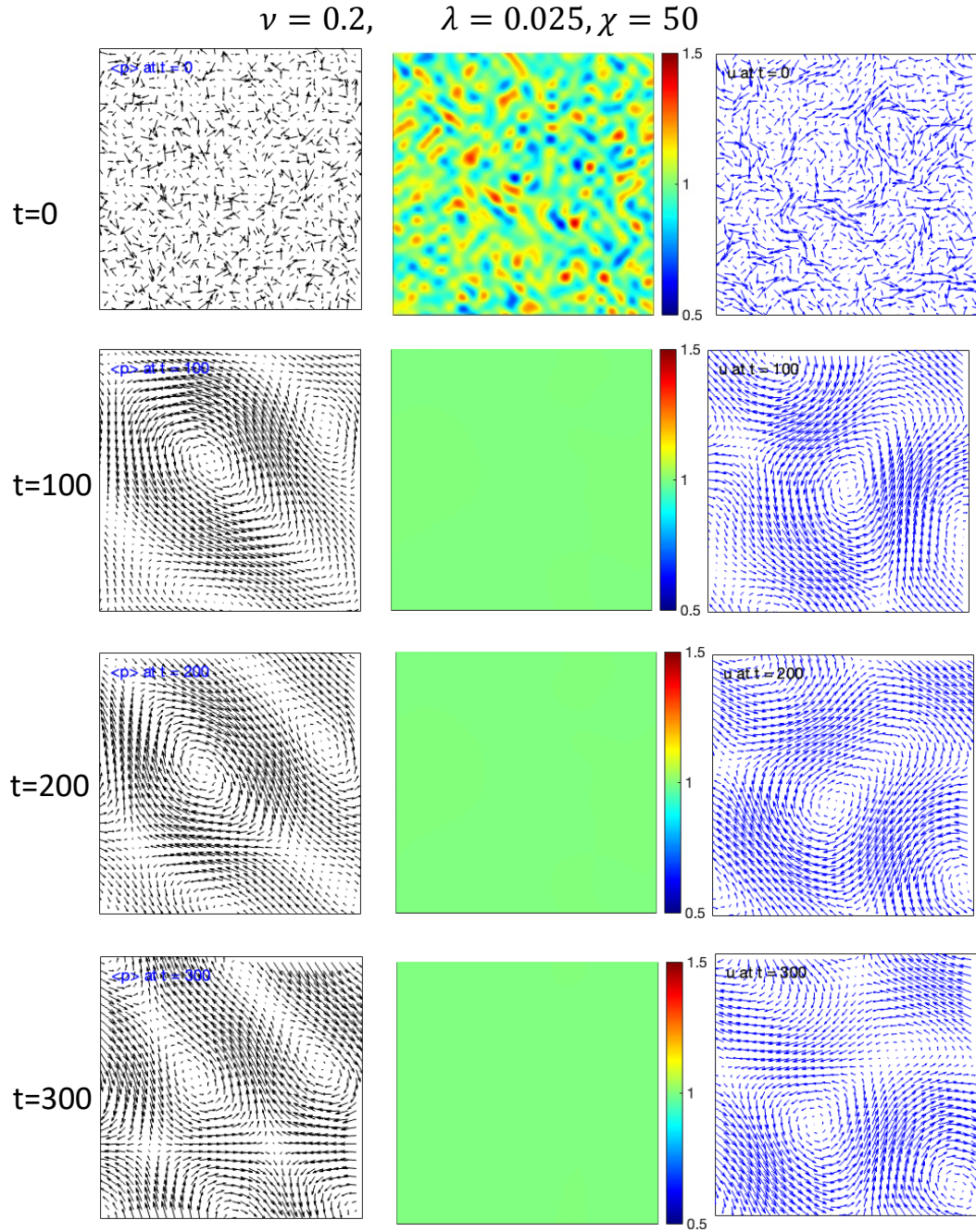
Figure 3.12 The average autochemotactic swimmer director $< \mathbf{p} >$, concentration Φ and fluid velocity $\mathbf{u}$ at times $t = 0, 100, 200, 300$. Parameters are $\lambda_0 = 0.025, \chi = 50, \beta_1 = 0.25 = \beta_2$, and $\nu = 0.2$.

As before, we can quantify these observed effects by comparing quantities like the maximum concentration, maximum and mean fluid velocity, entropy and global input power, shown in Figures 3.13 and 3.14). We also include the quantities for a non-chemotactic suspension with the same basic tumbling rate.

Comparing the chemotactic suspension to the purely tumbling ones for the same ν, we observe an overall higher magnitude of all the measured quantities. Notably, at the onset of the instability, the quantities' high's and lows seem to occur at the same time, supporting the idea that in this regime auto-chemotaxis reinforces the dynamics induced by the hydrodynamics.
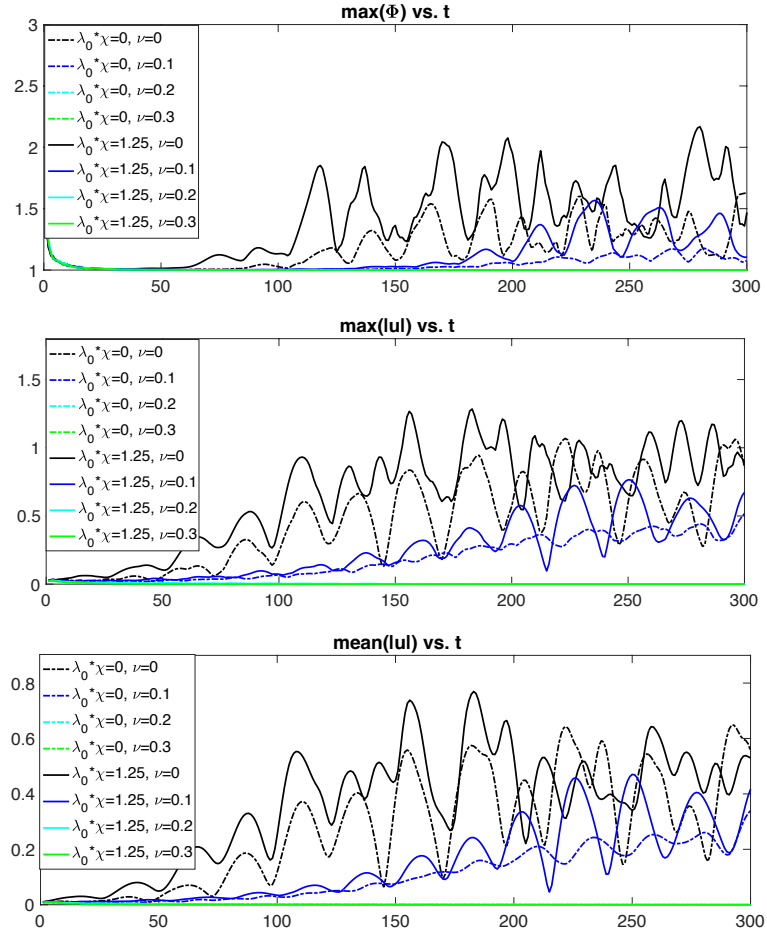
Figure 3.13 Comparisons of $max(\Phi)$, $max(|\mathbf{u}|)$, and $mean(|\mathbf{u}|)$ for swimmers in the "dynamic aggregation" regime for different ν.
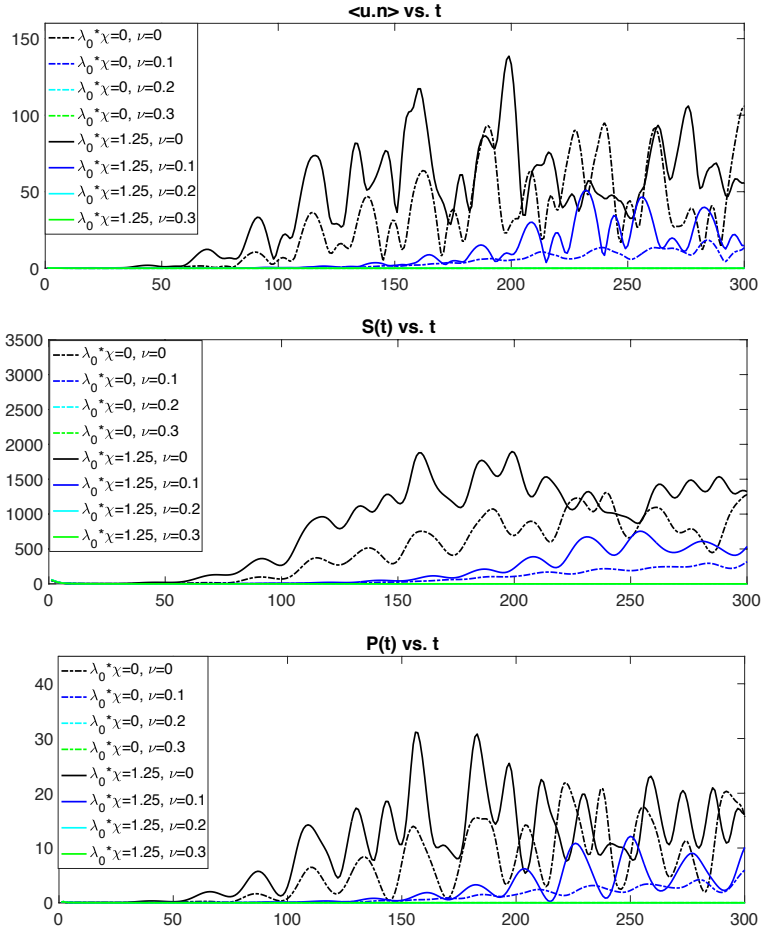
Figure 3.14 Comparisons of $max(\Phi)$, $max(|\mathbf{u}|)$, and $mean(|\mathbf{u}|)$ for swimmers in the "dynamic aggregation" regime for different ν.

As we increase the hydrodynamic resistance, ν, we notice that the aggregation instability induced by chemotaxis decreases. This can be attributed to the resistance's damping effect to the overall swimmer motion, which in turn affects aggregation due to the nonlinear coupling of the terms.

Lastly, even though linear theory gave separate hydrodynamic and chemotactic instabilities and predicted resistance to only affect the former, here we can clearly see that it affects both processes in the dynamic aggregation regime as they are nonlinearly coupled.

3.3.3 Resisting auto-chemotactic aggregation

In this section, we focus on investigating the effects of resistance on the auto-chemotactic aggregation regime of Figures 3.3, where according to the linear theory only the chemotactic instability is present. We select parameters $\lambda_0 = 6, \chi = 2, \beta_1 = 0.1 = \beta_2$, and $D_c = 0.4$. These parameter values are of particular interest as they approximate conditions from experimental studies involving E. Coli bacteria [106, 151].

The selected parameter values yield a chemotactic instability according to the linear stability analysis as shown in the plot of σ_C in Figure 3.2, hence we expect aggregation and clustering of the swimmers. Note however that $\lambda_0 = 6.0$, is considerably larger than the threshold value of $\lambda_0 = 0.2$ associated with fully suppressing the hydrodynamic collective swimming state derived from the linear stability analysis in the phase diagram, Figure 3.3.

In Figures 3.15 to 3.18 we present snapshots of the average swimmer director, concentration field, and also generated fluid flows (not to scale) for various resistance parameters ν.

First, let us explain the aggregation dynamics that emerges in the absence of resistance, Figures 3.15. The perturbations in the pusher suspension slowly merge in clusters. These clusters soon become quasi-elliptical in shape, then start to move and become dynamic clusters that continuously change shape, move around the domain, and may merge with other motile clusters [106]. Despite this parameter set being located far from the hydrodynamic instability region in the parameter phase space, the fluid flows in these aggregates are nontrivial due to the high swimmer concentration there and the nonlinear coupling. These fluid flows contribute to the deformation of the clusters as well as their motility.
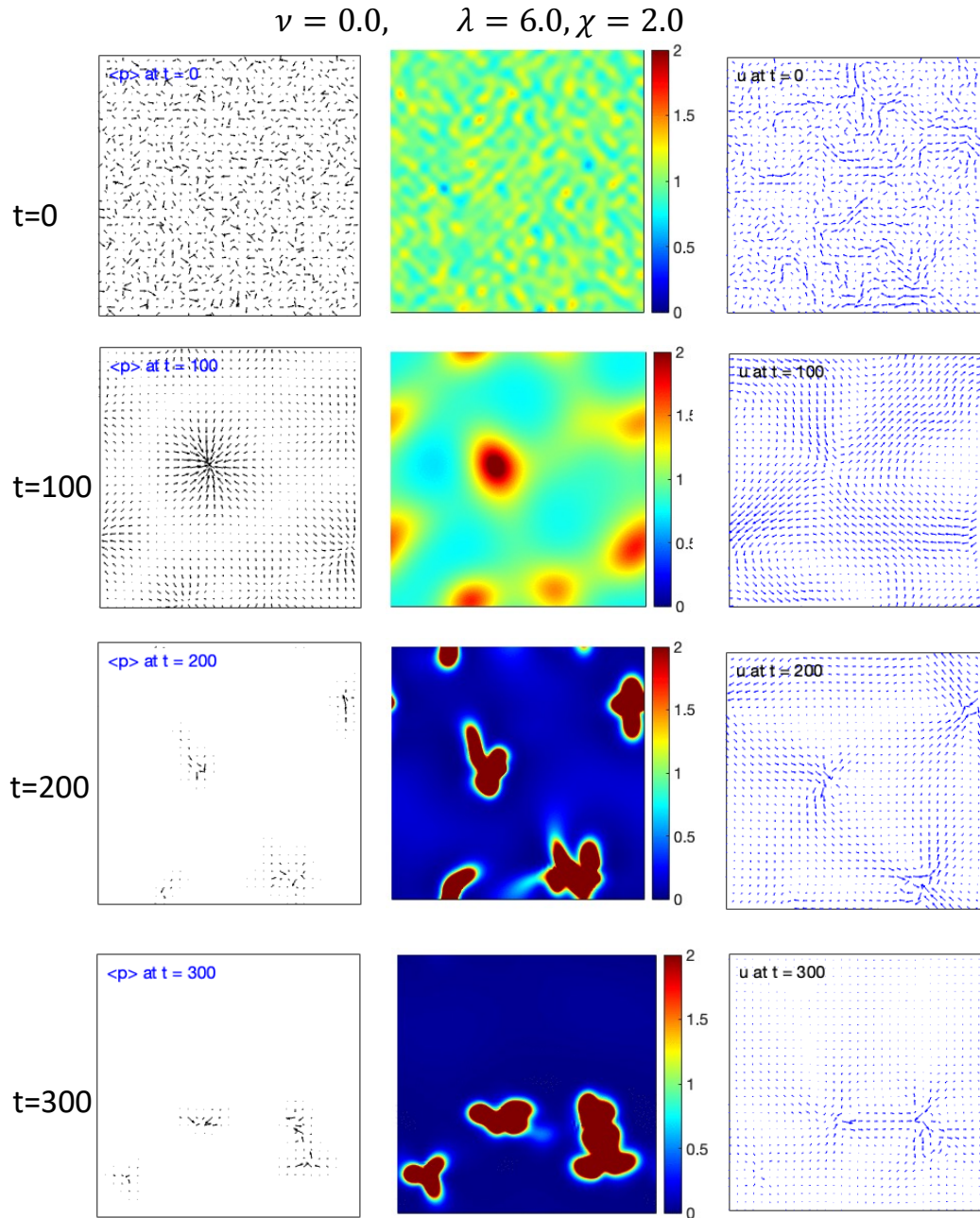
Figure 3.15 The average swimmer director $< \mathbf{p} >$, concentration Φ and fluid velocity $\mathbf{u}$ at times $t = 0, 100, 200, 300$ for autochemotactic swimmers with $\lambda_0 = 6.0, \chi = 2.0, \beta_1 = 0.1 = \beta_2$ and $\nu = 0$.

$$\nu = 0.1, \qquad \lambda = 6.0, \chi = 2.0$$
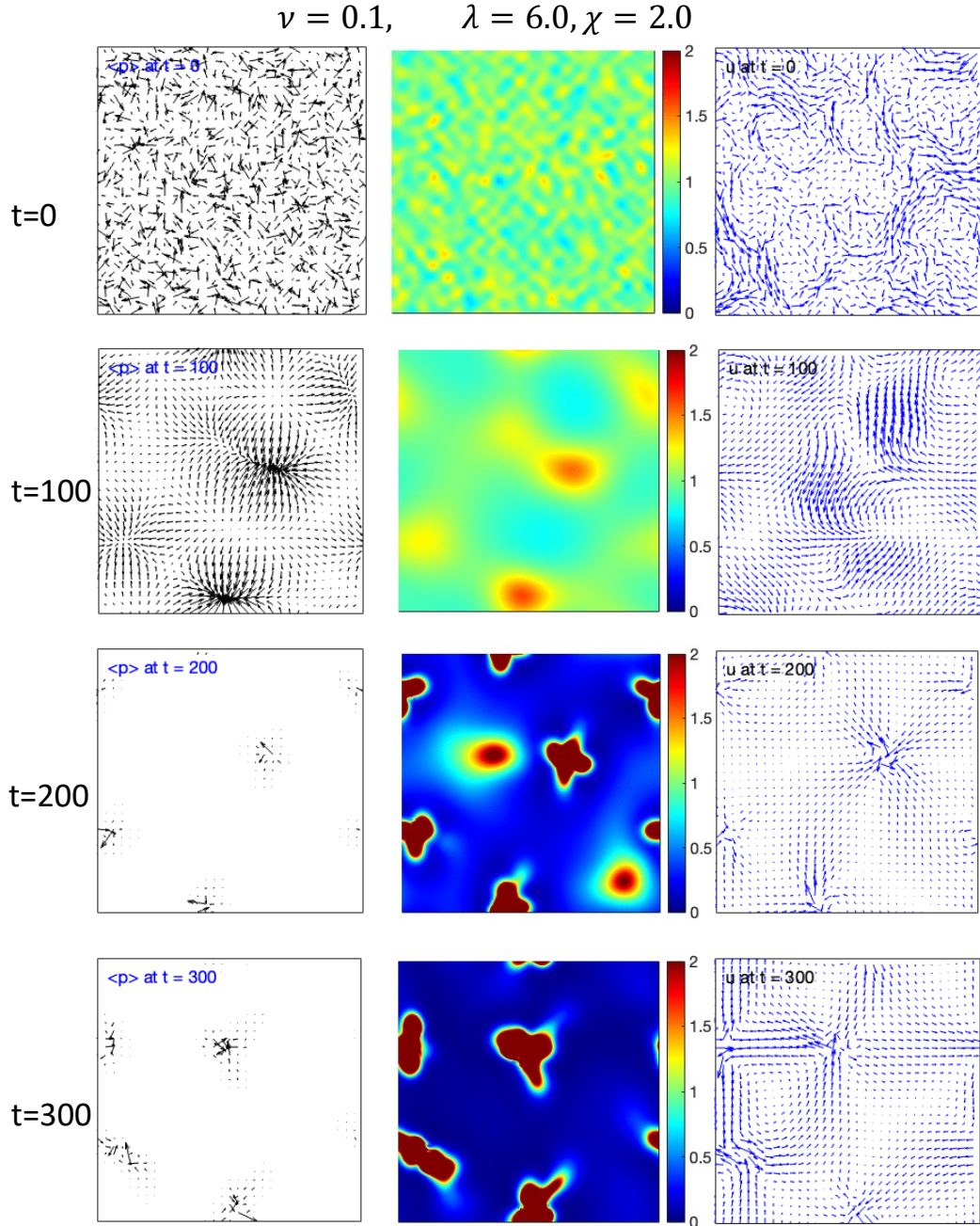
Figure 3.16 The average swimmer director $< \mathbf{p} >$, concentration Φ and fluid velocity $\mathbf{u}$ at times $t = 0, 100, 200, 300$ for autochemotactic swimmers with $\lambda_0 = 6.0, \chi = 2.0, \beta_1 = 0.1 = \beta_2$ and $\nu = 0.1$.

$$\nu = 0.2, \qquad \lambda = 6.0, \chi = 2.0$$
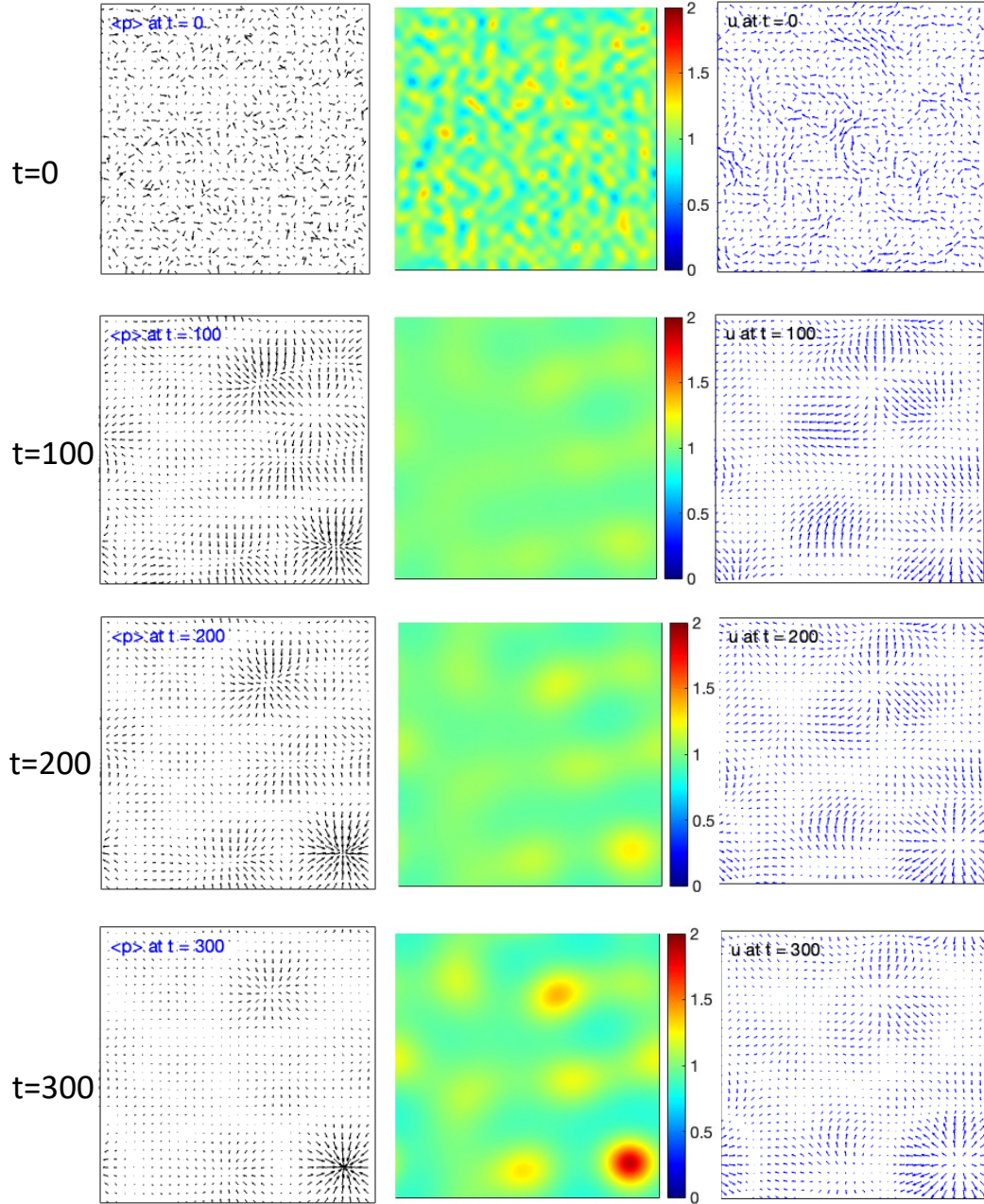
Figure 3.17 The average swimmer director $< \mathbf{p} >$, concentration Φ and fluid velocity $\mathbf{u}$ at times $t = 0, 100, 200, 300$ for autochemotactic swimmers with $\lambda_0 = 6.0, \chi = 2.0, \beta_1 = 0.1 = \beta_2$ and$\nu = 0.2$.

$$\nu = 0.3, \qquad \lambda = 6.0, \chi = 2.0$$
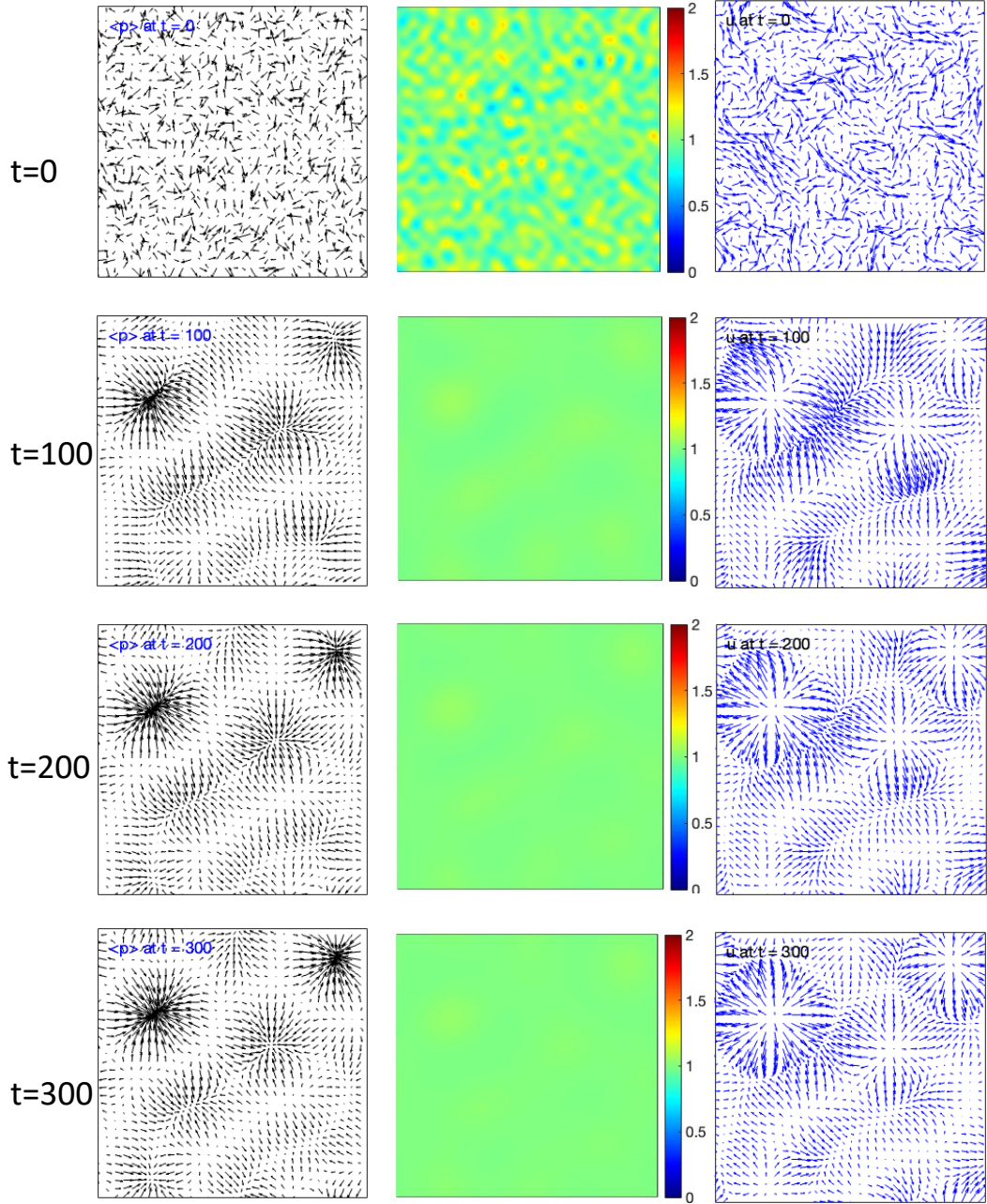
Figure 3.18 The average swimmer director $< \mathbf{p} >$, concentration Φ and fluid velocity $\mathbf{u}$ at times $t = 0, 100, 200, 300$ for autochemotactic swimmers with $\lambda_0 = 6.0, \chi = 2.0, \beta_1 = 0.1 = \beta_2$ and $\nu = 0.3$.

Examining snapshots of the dynamics in Figures 3.15 to 3.18, we observe that resistance appears to inhibit auto-chemotactic aggregation. As the hydrodynamic resistance parameter ν increases, the aggregates become weaker, with their magnitude diminishing. This inhibitory effect becomes more pronounced at $\nu = 0.3$ where the aggregates are barely visible, even though present.

We quantify these observed effects of the Brinkman resistance in the formation and sustenance of these motile pusher aggregates in Figures 3.19 and 3.20.
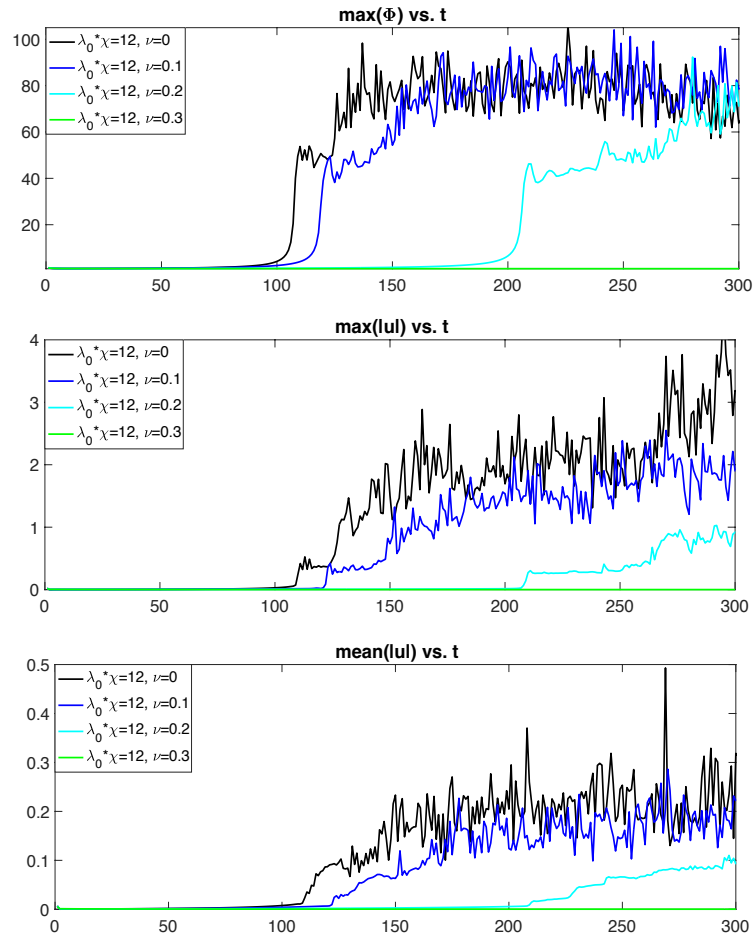
Figure 3.19 Comparisons over a long time of $max(\mathbf{\Phi})$, $max(|\mathbf{u}|)$, and $mean(|\mathbf{u}|)$ for autochemotactic swimmers with $\lambda_0 = 6.0, \chi = 2.0, \beta_1 = 0.1 = \beta_2$ for various ν.
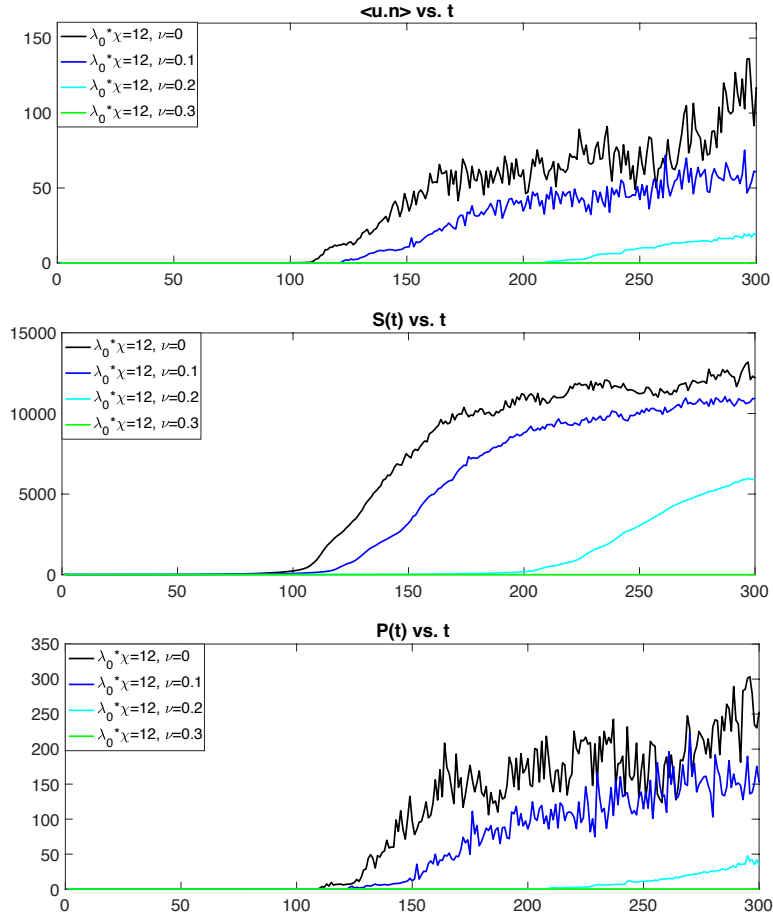
Figure 3.20 Comparisons over a long time of $< \mathbf{u} \cdot \mathbf{n} >$, $S(t)$, and $P(t)$ ffor autochemotactic swimmers with $\lambda_0 = 6.0, \chi = 2.0, \beta_1 = 0.1 = \beta_2$ for various ν.

It is important to note that in the linear theory analysis, resistance was solely present in the hydrodynamic dispersion relation while being absent from the chemotactic dispersion relation. This decoupling implied that resistance primarily influenced the hydrodynamic collective swimming state. However, in the full system where the resistance, hydrodynamics and chemotaxis becomes intricately coupled, we see that resistance also significantly impacts the chemotactic aggregation. Resistance hinders the formation of clusters by impeding the hydrodynamic interaction and the motion of swimmers, and ultimately affects the swimmers ability to aggregate.

3.4   Summary and Discussion

In this chapter, we considered the dynamics of a pusher swimmer suspension that undergoes chemotaxis. We presented a continuum model that coupled run-and-tumble chemotaxis to the flows generated by collective swimming.

Tumbling alone typically acts as a stabilizer of pusher suspension dynamics. It introduces a rotational motion that counteracts the formation and persistence of concentration bands. This tumbling behavior disrupts the fluid flow patterns generated by the swimmers, leading to a more stable and less chaotic suspension.

Auto-chemotaxis, on the other hand, introduces another instability in the swimmer suspension known as aggregation. This occurs due to the swimmers' tendency to move towards the chemo-attractants produced by the colony. The gradient of the chemo-attractants serves as a guiding force, causing the swimmers to aggregate and form clusters within the suspension.

Linear stability analysis of a uniform and isotropic auto-chemotactic pusher suspension with quasi-static chemo-attractant revealed two separate dispersion relations, due to hydrodynamics and chemotaxis processes respectively. Resistance appears only in the hydrodynamic dispersion relation as it affects only the hydrodynamic interactions.

The results from linear theory help us identify parameter ranges for instabilities and nontrivial system states. From these parameter ranges we construct a phase diagram of the expected dynamics of auto-chemotactic pusher suspensions. We identify four distinct dynamics states depending on the presence of either hydrodynamic or chemotaxis instabilities: hydrodynamic collective swimming, dynamical aggregation, auto-chemotactic aggregation, and uniform. Resistance acts as a suppressor for all of these dynamical states, and for sufficiently large resistance values it can completely suppress them.

Through full simulations, we observe that the hydrodynamic and auto-chemotaxis instabilities can enhance each other when present. This interaction leads to the dynamical aggregation of pusher swimmers, resulting in the formation of larger and more coherent clusters within the suspension. However, resistance inhibits swimmer motion and thus aggregation, acting as a suppressor for dynamics resulting from either the hydrodynamic or auto-chemotactic instabilities, or their combined effects.

In addition, resistance inhibits chemotactic accumulation in initially isotropic pusher suspensions. It impedes the movement of swimmers towards chemo-attractants and disrupts the formation of concentration gradients, thus hindering the accumulation of swimmers in specific regions.

The interplay between hydrodynamics, tumbling, auto-chemotaxis and resistance is intricate. These factors contribute to the formation and evolution of the concentration bands and clusters in ways that linear theory alone cannot predict. Studying these processes through nonlinear simulations separately and together gives more insights into their effects on the stability and dynamics of chemotactic pusher swimmer suspensions.

CHAPTER 4

BACTERIAL SPREAD IN A POROUS WET MEDIUM

We previously examined the collective swimming and auto-chemotactic aggregation in pusher suspensions whose initial configuration was a perturbation from the uniform isotropic state. Here we consider a different starting configuration where the micro-swimmers are already accumulated and arranged in a line. We aim to observe and analyze the subsequent spread of the swimmers into the surrounding domain its properties. This different initial state provides another opportunity to investigate the interplay of hydrodynamic, auto-chemotaxis and resistance.

The inspiration for the work comes from the recent experiments in the Datta lab to study the migration and chemotaxis of *E. coli* bacteria in porous environments consisting of hydrogel beads [18, 19, 17, 16, 1, 113]. The group found that the run-and-tumble motility is dramatically altered in a porous medium as cells navigate the porous space where they are intermittently trapped, and in the long terms the cells exhibit diffusive behavior [18, 19]. Bacteria is injected in the porous hydrogel matrix in a line-like formation, and from there it spreads into the 3D domain. Auto-chemotactic bacterial populations smooth out large-scale perturbations in their overall morphology allowing the cells to better migrate together and spread [17, 16, 1]. The interplay of competition for nutrients with growth-driven colony expansion, can lead to morphological instabilities and roughening into broccoli-like fronts [113].

Though the pore-scale confinement in the experiments is of a different scale from what we can model with in our Brinkman approximation, we try simulations approximating experimental setup to gain some insight into the effects of hydrodynamic collective swimming, auto-chemotaxis, nutrients, and resistance on the emergent behavior of such a complex system.

4.1 Spread of a Bacterial Accumulation

We consider first the case of a non-chemotactic non-tumbling pusher suspension ($\alpha = -1, \gamma = 1$), in a periodic box with size $L = 25$. We take the initial configuration to be a perturbation with random orientations about a *Gaussian line* concentration in space centered at $\mathbf{x} = L/2$ and satisfying $\overline{\Psi(\mathbf{x}, \mathbf{p}, t)} = \Psi_0$. In Figures 4.1-4.4 we show snapshots of the evolution of the concentration field for various resistance values ν.

Without resistance in Figure 4.1, the swimmers spread throughout the domain via diffusion, eventually resulting in the quasi-chaotic dynamics studied in Chapter 2. Resistance alters the collective dynamics when the swimmers are already clustered primarily by restricting the swimmer spread away from the cluster into the rest of the domain. This inhibition arises from the resistance's hindrance to swimmer motion.

The swimmer cluster starts to spread out and away from the center in both directions, though non-uniformly for low ν, reflecting the random perturbations of the starting state. With increasing resistance ν the perturbations in the spreading fronts tend to smooth out and the concentration field becomes quasi-one-dimensional and also symmetrical about the initial mean position. Moreover, we see the emergence of distinct several concentration waves trailing the initial spreading fronts. Higher resistance visibly delays the advancement of the first fronts and gives an opportunity to the trailing concentration waves to catch up. The first fronts collide at $t \approx 15$, and, as the system is periodic, continue in their respective directions towards another imminent collision near $\mathbf{x} = L/2$. The magnitude of the concentration profile continues to diminish due to diffusion.

Interestingly, resistance has a significant effect on this system's dynamics for values of ν much larger than the $\nu \approx 0.27$ that linear theory predicted to fully suppress hydrodynamic instabilities in an initially uniform isotropic suspension. This examples is another reminder on the system's nonlinearity and the initial condition's crucial and difficult-to predict effects on the emergent dynamics.

$$\lambda = 0.0, \chi = 0.0$$
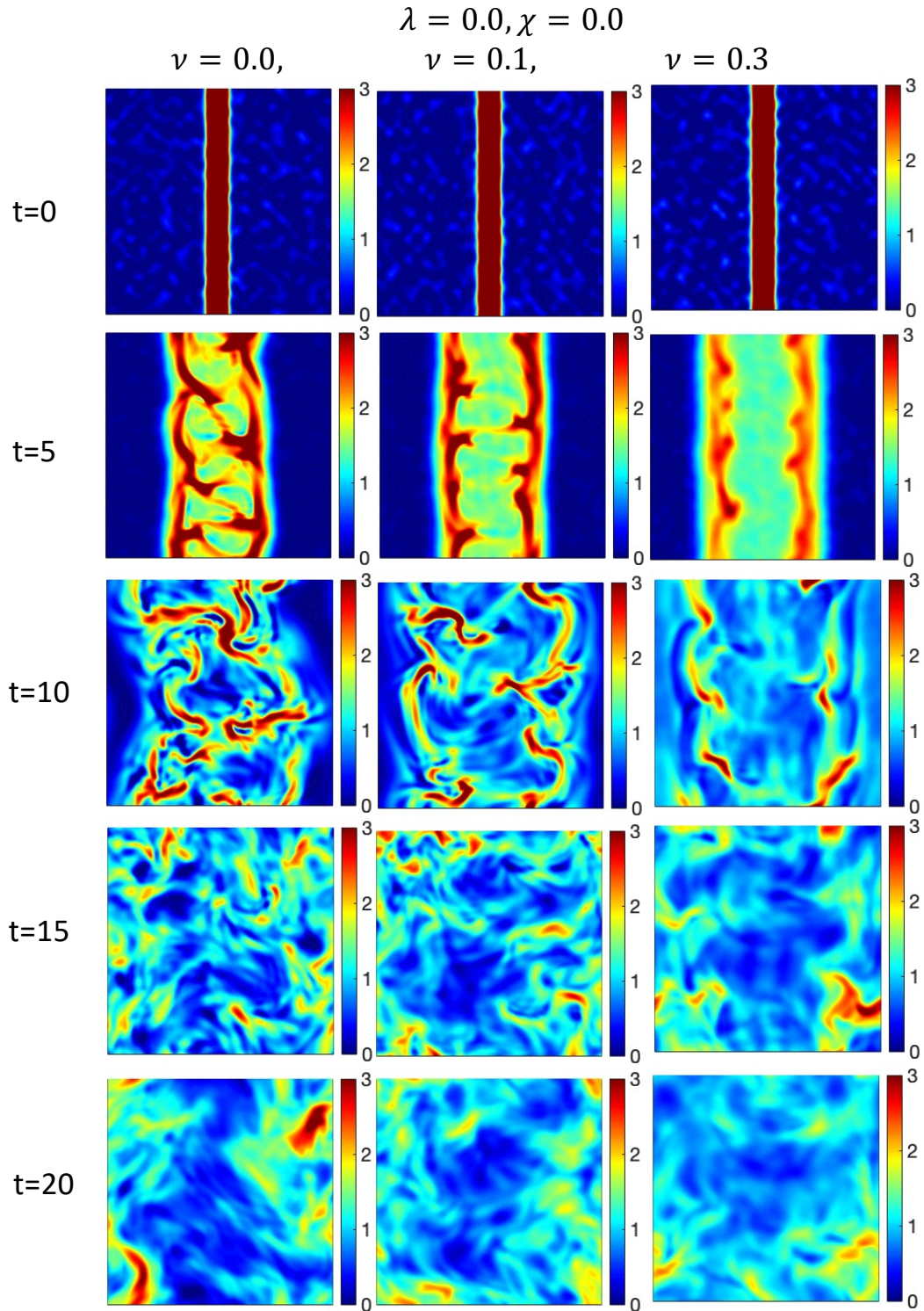
$\nu = 0.0,$ $\nu = 0.1,$ $\nu = 0.3$

Figure 4.1 The spreading swimmer concentration $\Phi(x, y)$ at different times for $\nu = 0, 0.1, 0.3$.
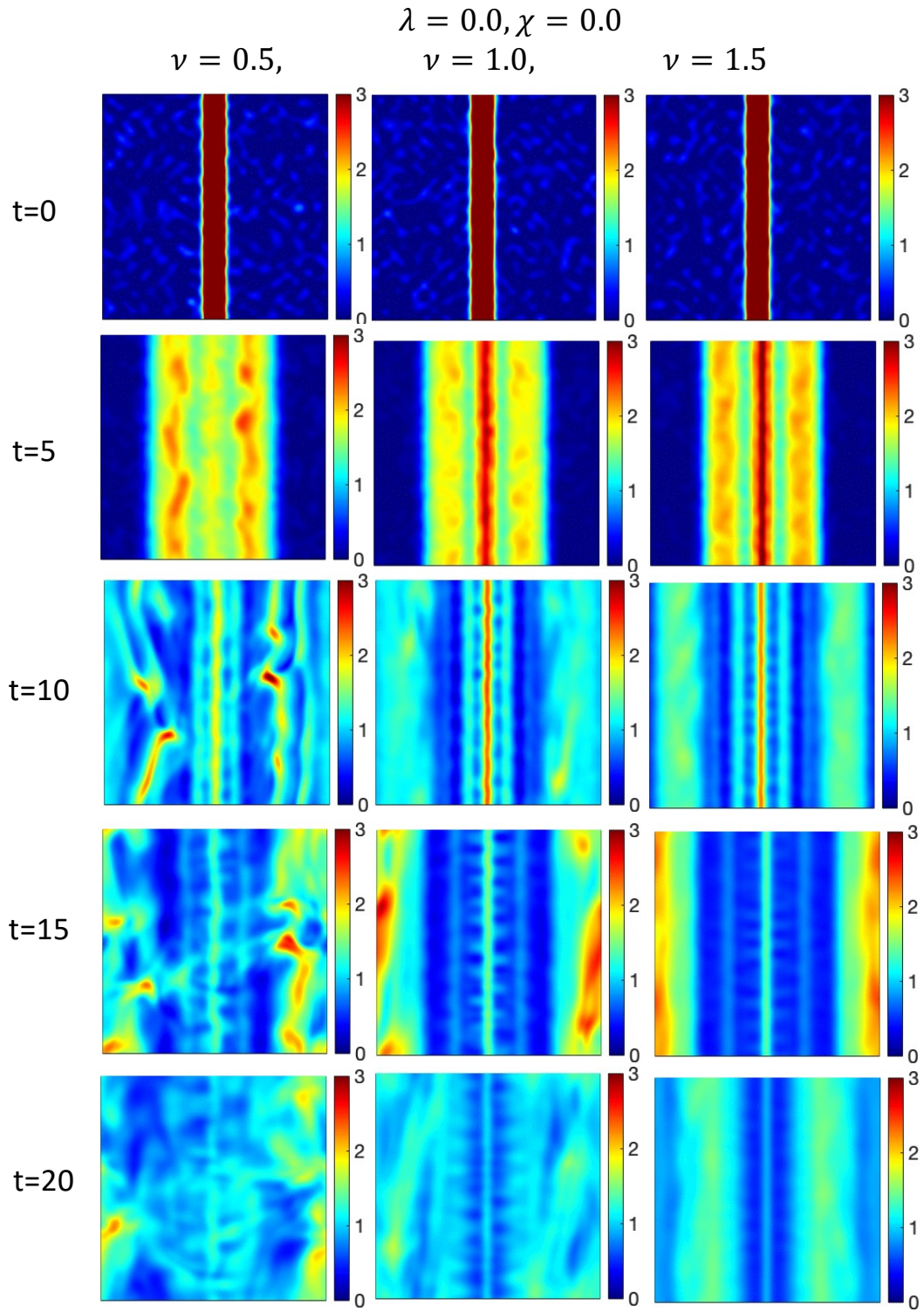
Figure 4.2 The spreading swimmer concentration $\Phi(x, y)$ at different times for $\nu = 0.5, 1, 1.5$.
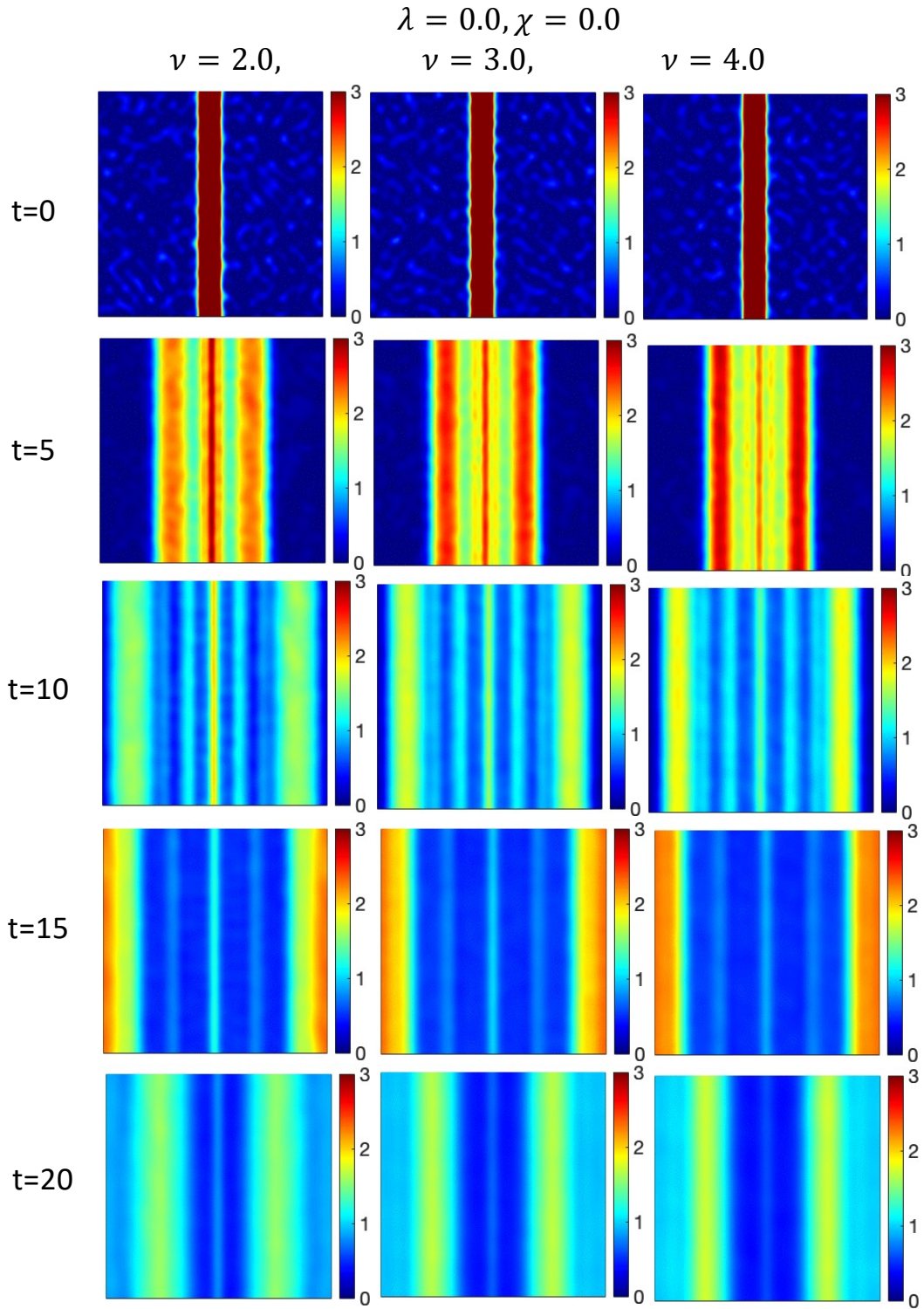
Figure 4.3 The spreading swimmer concentration $\Phi(x, y)$ at different times for $\nu = 2, 3, 4$.
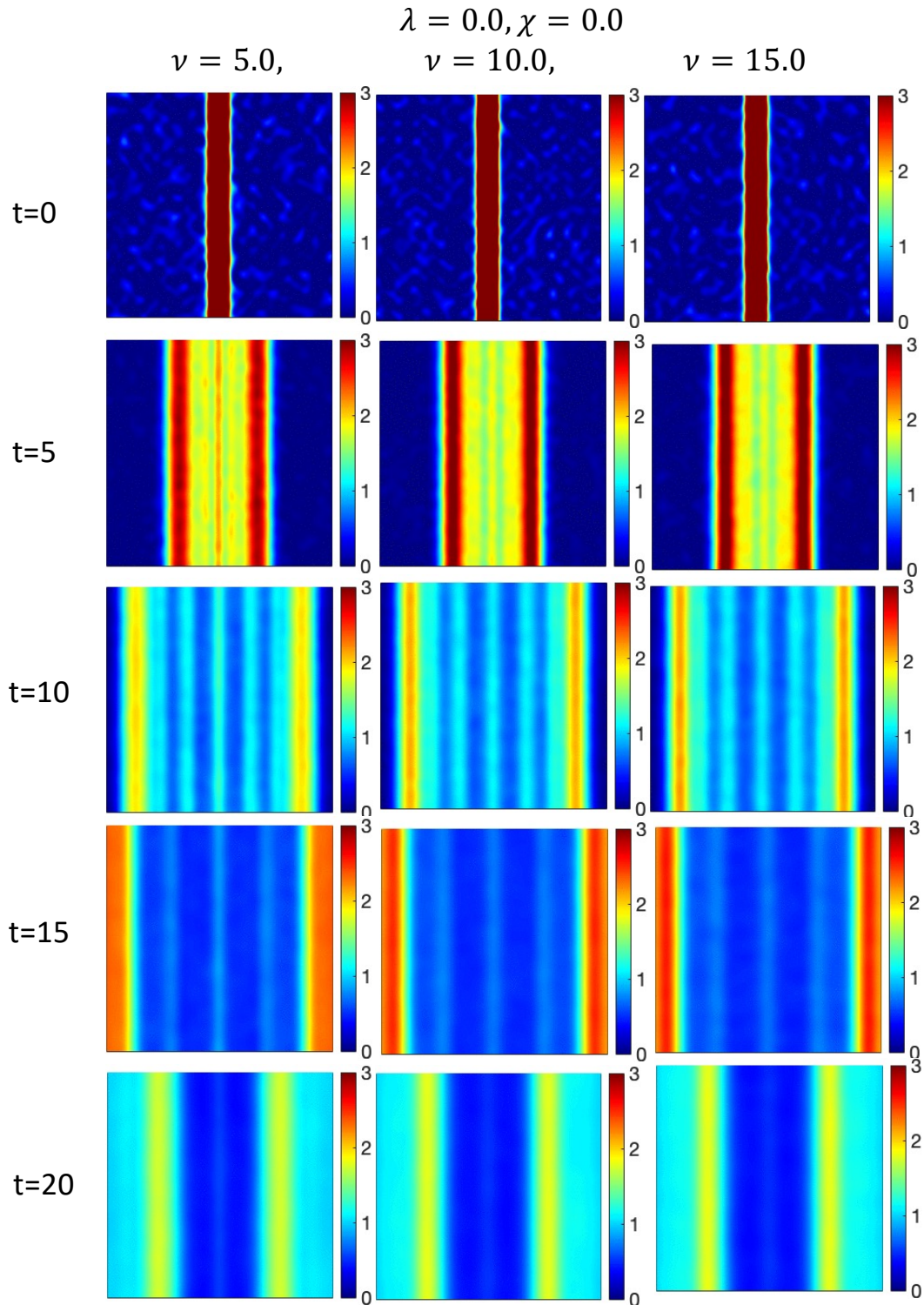
Figure 4.4 The spreading swimmer concentration $\Phi(x,y)$ at different times for $\nu = 5, 10, 15$.

4.2 Effects of auto-chemotaxis on the bacterial spread

When considering an auto-chemotactic suspension $(C(\mathbf{x}, 0) = \beta_2/\beta_1 \Phi(\mathbf{x}, 0))$ in the case of no resistance, an intriguing behavior emerges, as seen in Figure 4.5. Since the swimmers are already clustered, they tend to further aggregate and form accumulations with a characteristic length-scale determined by the specific parameters of the system [106]. However, in regions where the concentration of pusher swimmers is high, the collectively generated fluid flows become nontrivial. These fluid flows exert forces on the aggregate, causing it to break apart and undergo movement. As a consequence, the aggregates exhibit motility and take on a "squiggly" appearance, as observed in Chapter 3 Figures 3.15 to 3.18. This behavior highlights the interplay between auto-chemotaxis, fluid flows, and the formation and motion of aggregates.

From Chapter 3, we know resistance inhibits swimmer motion and auto-chemotactic aggregation in initially uniform isotropic pusher suspensions. In this context, as seen in Figures 4.5 to 4.8, resistance not only restricts the diffusive spread of the pusher swimmers, but also hinders the breaking of the line aggregate. By suppressing the hydrodynamic instability that would otherwise yield "squiggly" aggregates, resistance plays a significant role in maintaining the integrity of the aggregate and inhibiting its movement from the center. Consequently, the effects of resistance extend beyond impeding swimmer motion and aggregation; they also dampen the dynamic behavior and motility of the aggregates themselves. Moreover, for higher resistance ν, the line aggregate of swimmers eventually breaks off into circular clusters of size similar to those auto-chemotaxis would induce in the absence of hydrodynamics [106].

These examples, though not modeling the setup and environments in the experiments [17, 16, 1], still show that resistance tends to smooth out the morphology of the spreading micro-swimmer front.
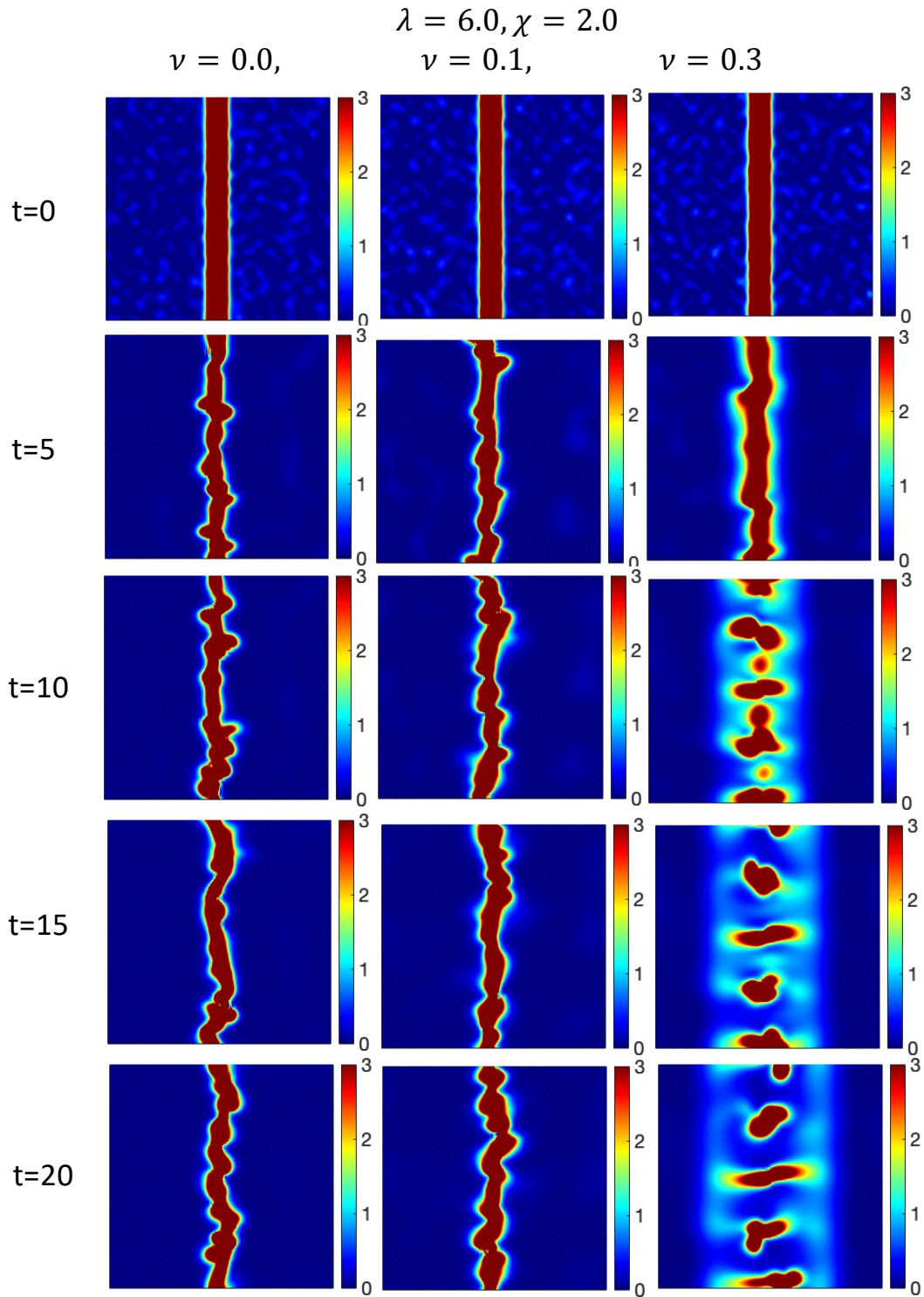
Figure 4.5 The spreading of auto-chemotactic swimmers, their concentration $\Phi(x, y)$ at different times for $\nu = 0, 0.1, 0.3$.
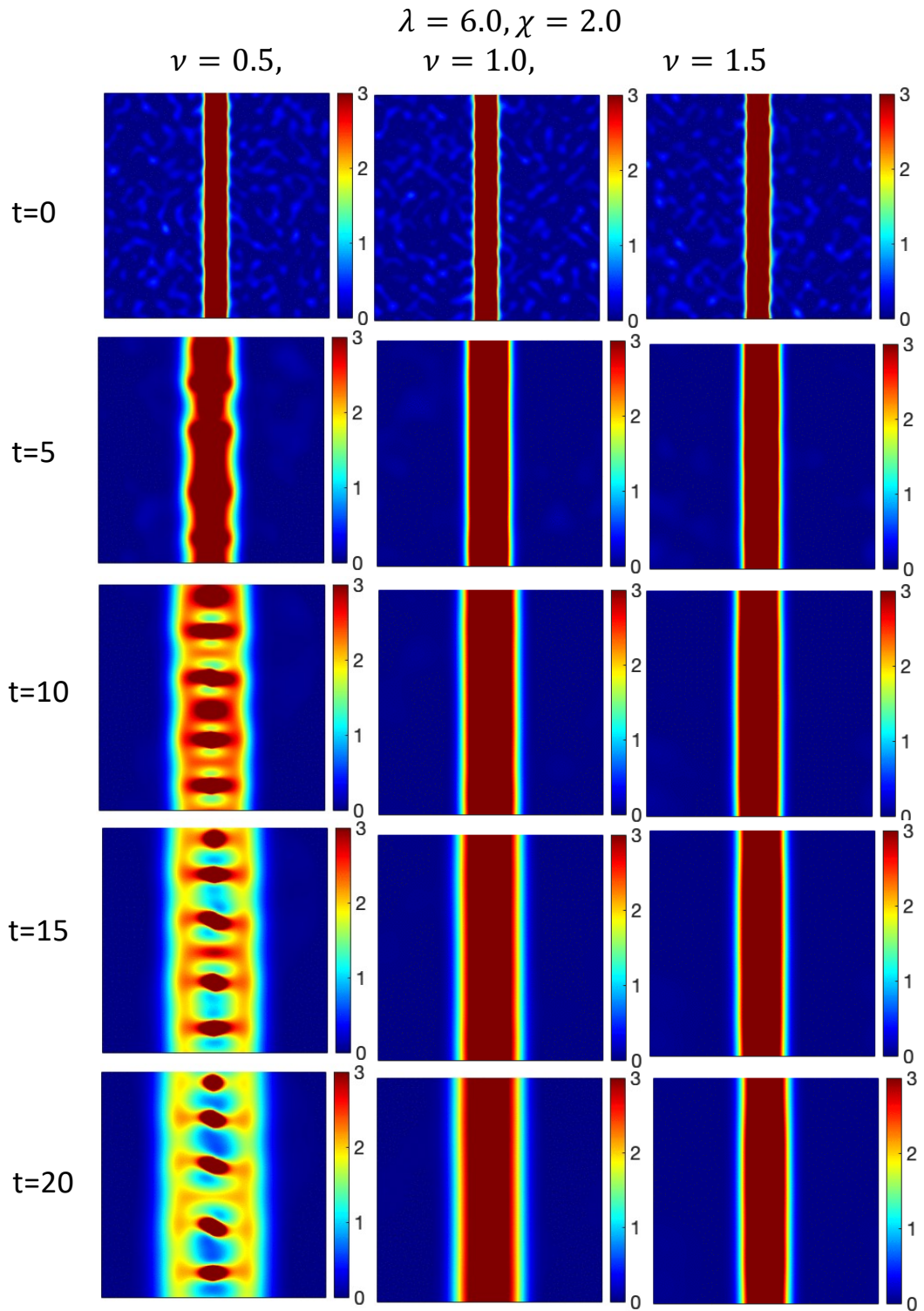
Figure 4.6 The spreading of auto-chemotactic swimmers, their concentration $\Phi(x,y)$ at different times for $\nu = 0.5, 1, 1.5$.
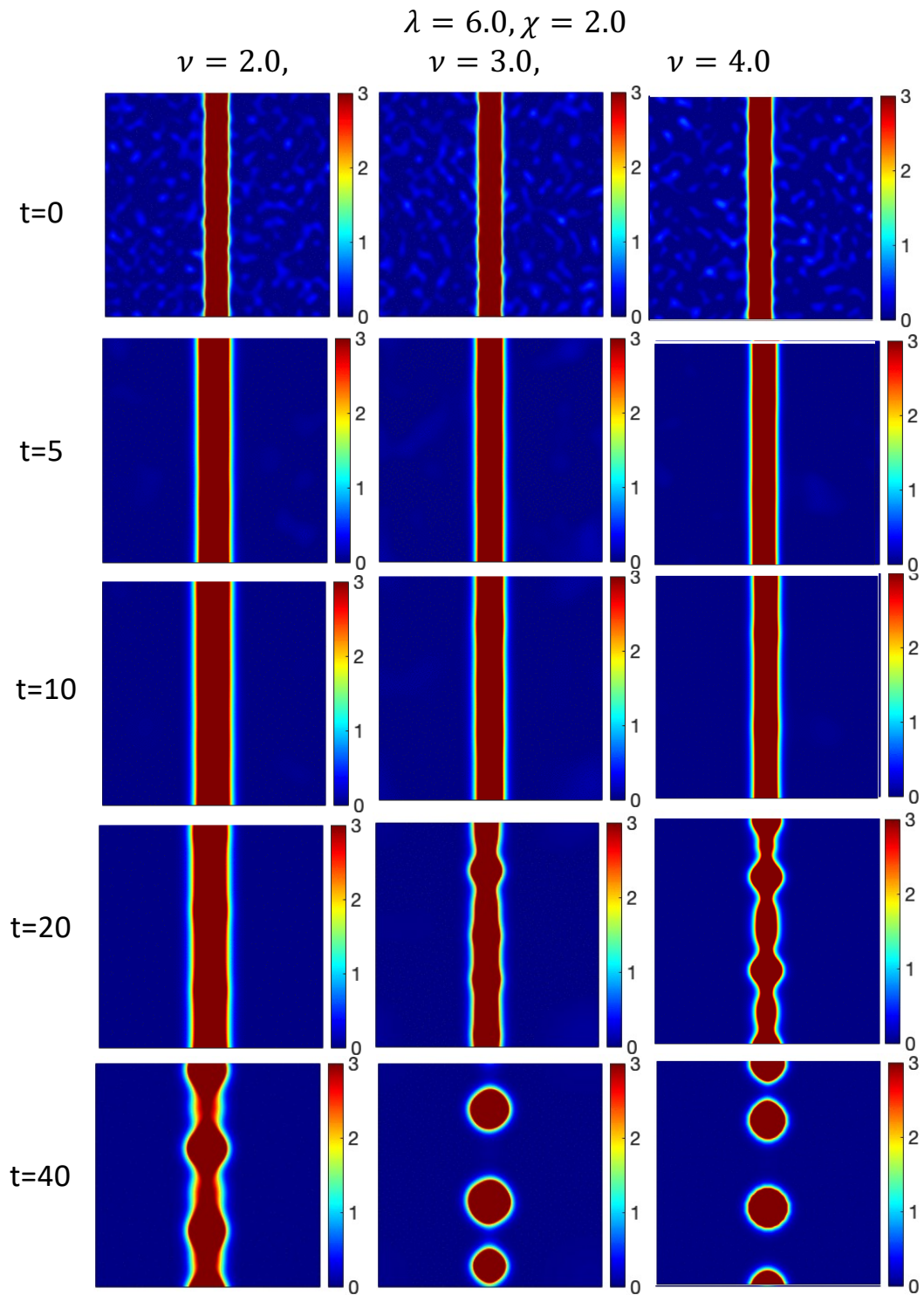
Figure 4.7 The spreading of auto-chemotactic swimmers, their concentration$\Phi(x, y)$ at different times for $\nu = 2, 3, 4$.
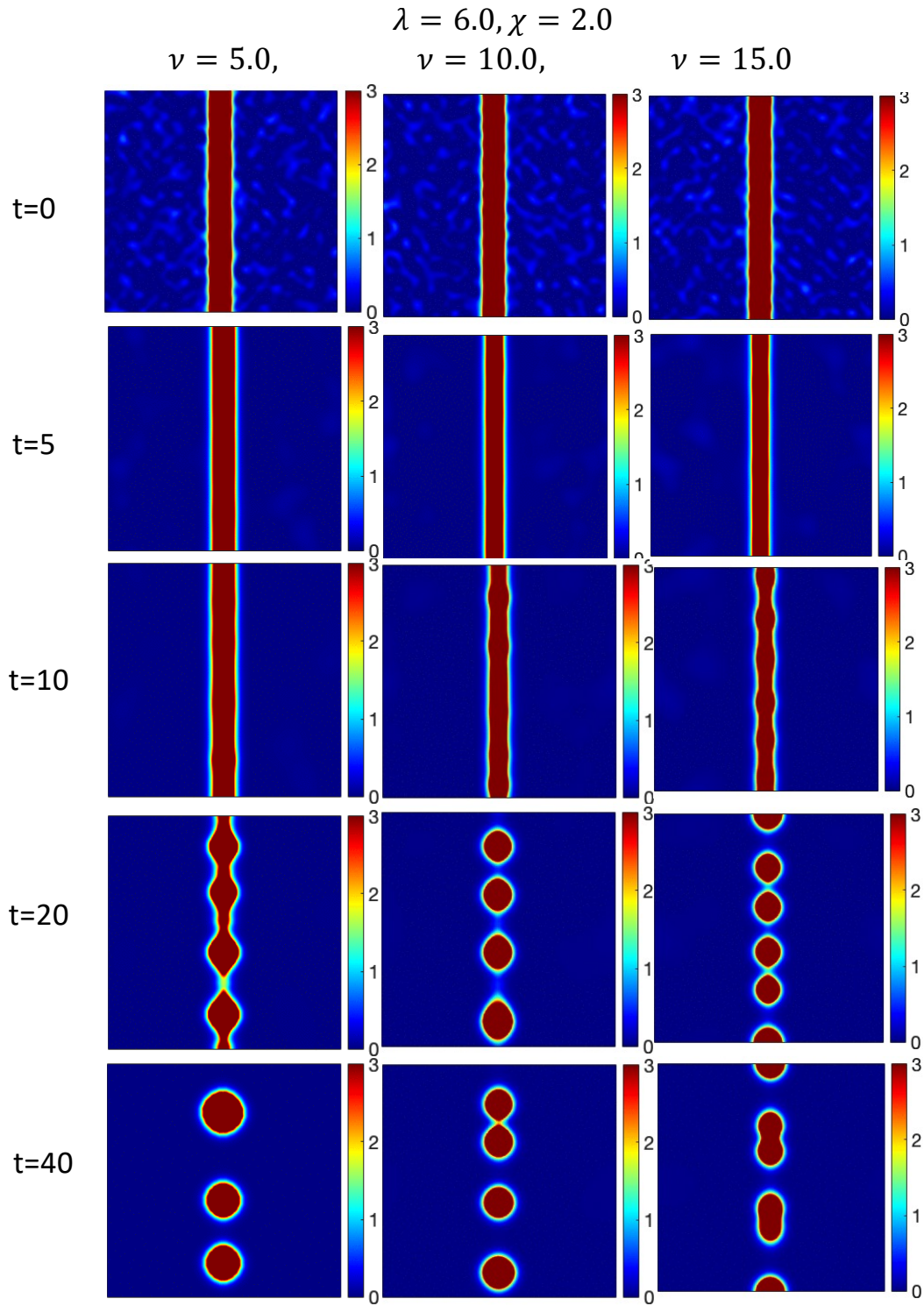
Figure 4.8 The spreading of auto-chemotactic swimmers, their concentration $\Phi(x,y)$ at different times for $\nu = 5, 10, 15$.

4.3 Effects of nutrients on the bacterial spread

Lastly, we consider the effect of an externally-supplied chemo-attractant, e.g., a nutrient, on an accumulation of pusher micro-swimmers that are tumbling with a basic tumbling rate but not generating their own chemo-attractant. The example is a relevant exercise because most experiments are performed in environments containing agar, and moreover the bacterial colonies need to consume oxygen to move.

We consider the initial swimmer configuration with Gaussian-line concentration profile as before. We use parameters $\chi^E = 2.0$, $\lambda_0 = 6.0$, $\beta_1 = 0.1$, $D_c = 0.4$, but $\beta_2 = -0.5 < 0$, denoting consumption of the nutrient in proportion to the local swimmer concentration. We take an initial nutrient profile $C^E(\mathbf{x}, t) = 5 = |\beta_2/\beta_1|\overline{\Phi}$ that is constant and uniform throughout the domain. This initial supply of the nutrient is not replenished and can only diminish due to the degradation with constant rate β_1, diffusion with constant D_c, and most importantly consumption by the swimmers. However, it can be advected by any collectively-generated fluid flows.

In Figures 4.9 to 4.11 we show the dynamics of the swimmer concentration in time for various resistance values ν. We also show the y-direction averaged profiles of the swimmer concentration and the chemo-attractant field.

Unsurprisingly and in line with intuition, we see that in the absence of resistance, the swimmers quickly spread in both directions to consume the nutrient. Chasing the nutrient which is still available in the untravelled areas, tends to help the swimmer spread, as can be seen by the sharper concentration fronts and also the disappearance of the trailing waves. Resistance inhibits the spread of the swimmers and smooths out the fluctuations in the spreading concentration fronts, leading to quasi-1D and more symmetric concentration profiles. The competition between these two factors gives rise to the curious dynamics seen here.
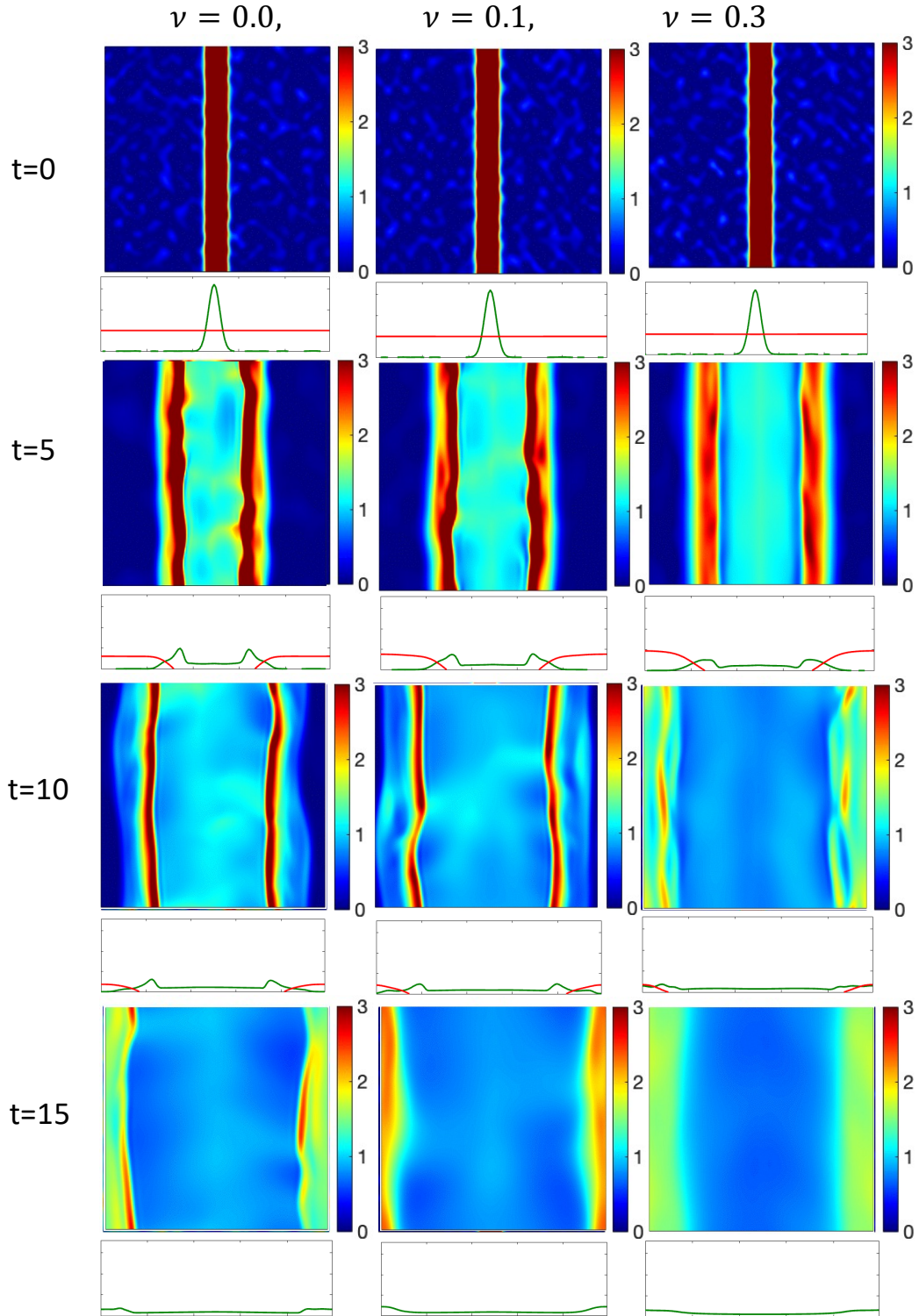
Figure 4.9 The swimmer concentration $\Phi(x, y)$, its averaged profile $< \Phi >_y$ (green line), and the nutrient averaged profile $< C^E >_y$ (red line) for $\nu = 0, 0.1, 0.3$.
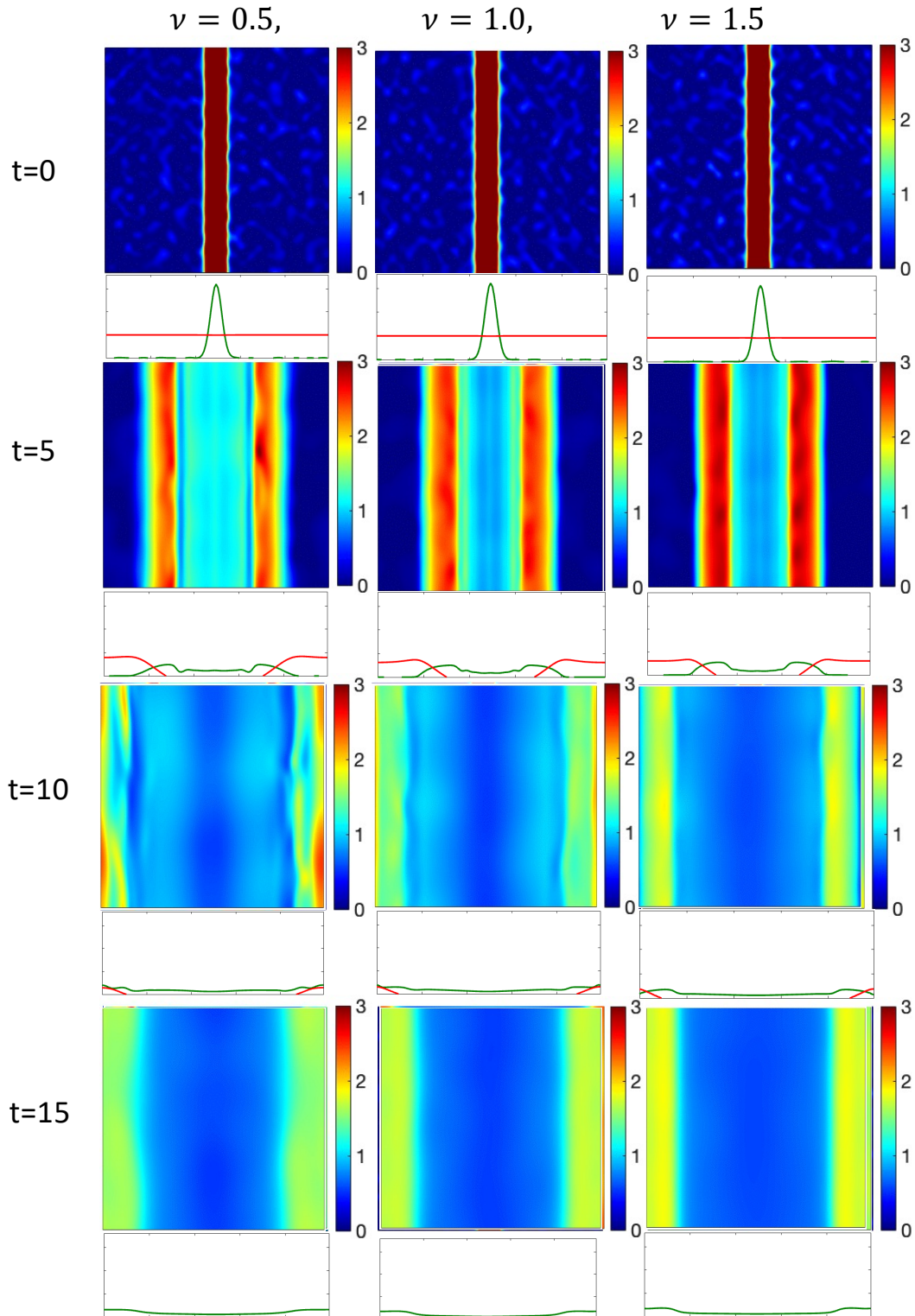
Figure 4.10   The swimmer concentration $\Phi(x, y)$, its averaged profile $< \Phi >_y$(green line), and the nutrient averaged profile $< C^E >_y$ (red line) for $\nu = 0.5, 1, 1.5$.
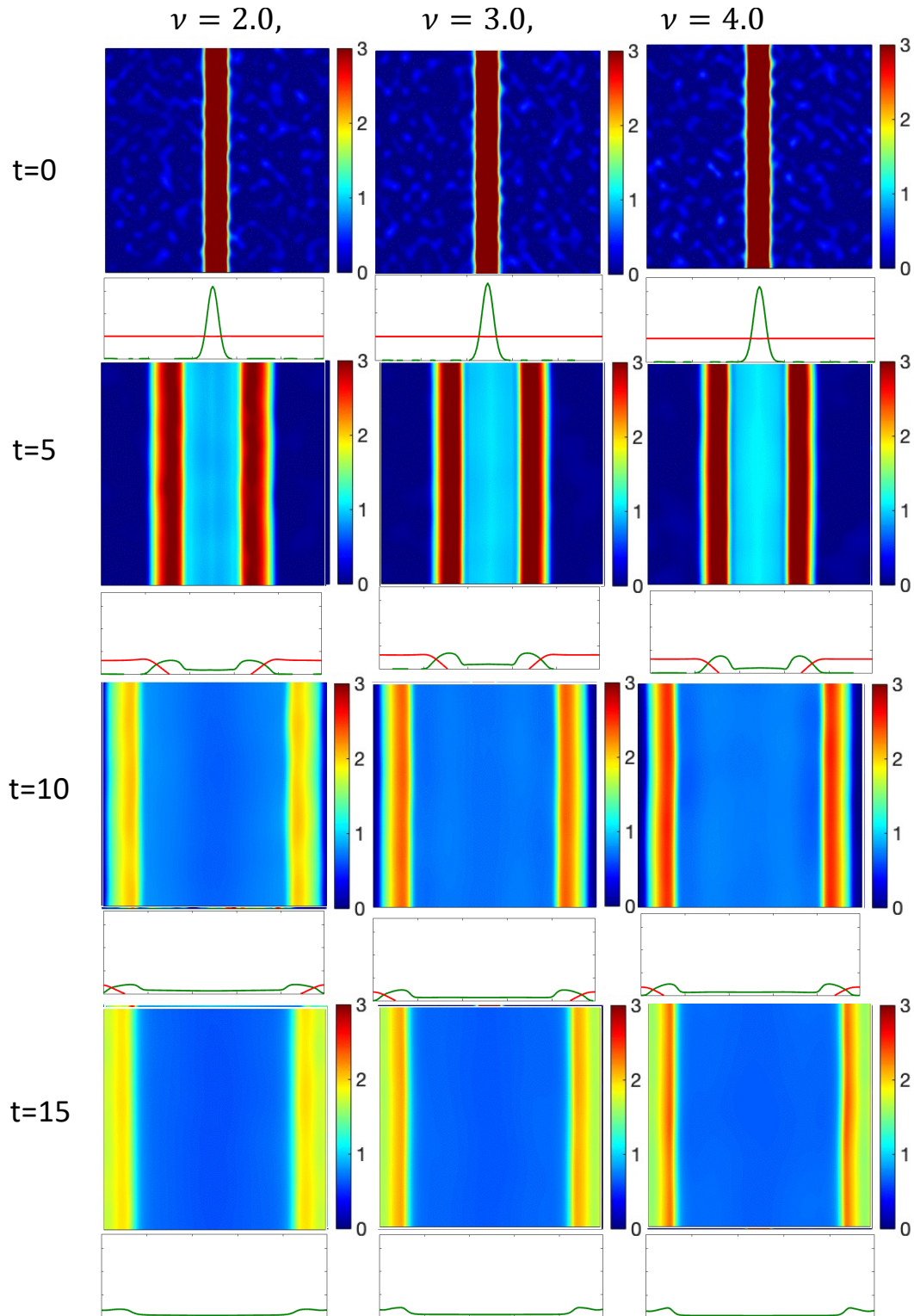
Figure 4.11 The swimmer concentration $\Phi(x, y)$, its averaged profile $< \Phi >_y$ (green line), and the nutrient averaged profile $< C^E >_y$ (red line) for $\nu = 2, 3, 4$.

4.4 Summary and Discussion

We studied the spread on a line accumulation of pusher micro-swimmers in environments of increasing resistance for the cases when the swimmers are non-tumbling non-chemotactic, auto-chemotactic, and in the presence of a nutrient they consume.

In the absence of auto-chemotaxis and nutrients, the swimmers spread away from the line cluster into the domain due to diffusion, and resistance tends to hinder this spread. Resistance smoothes out the perturbations in the spreading concentration front and overall stabilizes these fronts into quasi-1D and symmetric profiles.

Auto-chemotaxis, the process where the swimmers respond to self-generated chemo-attractant gradients and results in aggregation, has the curious effect of producing a "squiggling" accumulation line for zero or low resistance. We notice the emergence of transverse movement in the swimmers' accumulation line due to the swimmers auto-chemotactic tendency to cluster into circular spots. The clustering is countered by the diffusive processes that encourage outward spreading. Increasing resistance inhibits swimmer motion and smooths out the concentration fronts. The competing processes of auto-chemotactic clustering, diffusion and resistance give curious results: for intermediate resistance we see the formation of non-line non-circular accumulations that did not manage to spread far before "solidifying", see Figures 4.5 to 4.6, and for very high resistance we see the line accumulation break into centered circular spots, see Figures 4.7 to 4.8.

Externally supplied nutrient can act as an incentive for swimmers to move away from the initial accumulation, and thus enhances spreading expected by diffusive processes alone. Resistance counters both these factors by hindering the spread. Note that the effects are dependent on the amount of the initially-supplied nutrient and the parameters for its evolution dynamics, however the example highlights that nutrients can affect the micro-swimmer spread and can perhaps be used to control it.

The examples considered here show that we see that bacterial spreading and eventual state depend delicately on the balance of all these factors: auto-chemotaxis ability of the colony, the presence of nutrients, as well as the resistance encountered in the porous environment. Understanding of the effects of each one of these factors can help us understand their contributions to the dynamics observed in experiments. Better understanding of these processes and their non-trivial interactions can help us fine-tune their effects and perhaps can suggest ways to control the dynamics and spread of micro-swimmer colonies.

CHAPTER 5

CONCLUSION AND FUTURE WORK

5.1   Summary

The dissertation primarily focuses on studying micro-swimmers and their collective behavior in inhomogeneous viscous environments. In Chapter 1, we introduce the concept of these environments and their prevalence in nature, particularly among microorganisms like bacteria and algae. We also discuss the significance of low Reynolds number flow singularities, which arise due to the high viscosity and low fluid velocity in such environments.

In Chapter 2, we focus on understanding the collective motion of micro-swimmers in a fluid with resistance using mathematical modeling, analysis, and numerical simulations. A continuum model is presented to describe the collective dynamics of micro-swimmers, where their motion is coupled to the fluid dynamics through a Stokes-Brinkman equation with an active stress term.

The analysis of the entropy equations and stability of the linearized system reveals that Brinkman hydrodynamic resistance dampens the dynamics of a pusher micro-swimmer suspension. The suspension undergoes a transition from a long-wave instability to a finite-range instability, leading to weakened collective motion. The linear analysis also provides insights into parameter ranges that can result in fluctuations in the system of a specific size.

Numerical simulations of the full nonlinear system show that low resistance leads to the emergence of concentration bands of swimmers that dynamically form, merge, and break up in a quasi-periodic manner, accompanied by mixing fluid flow. However, as resistance increases, the motion of the swimmers and the formation of these concentration bands are inhibited. High resistance values can completely

suppress dynamics, leading to a uniform state. Resistance hinders the movement of swimmers, disrupts fluid flow patterns, and impedes hydrodynamic interactions, thus suppressing macroscopic collective motion.

Chapter 3 explores the dynamics of a pusher swimmer suspension undergoing chemotaxis, utilizing a continuum model that couples run-and-tumble chemotaxis with the flows generated by collective swimming. Tumbling behavior acts as a stabilizer, counteracting the formation of concentration bands and leading to a more stable suspension. On the other hand, auto-chemotaxis introduces an instability known as aggregation, causing swimmers to move towards chemo-attractants and form clusters within the suspension.

Linear stability analysis of an auto-chemotactic pusher suspension identifies two separate dispersion relations for hydrodynamics and chemotaxis processes, with resistance affecting only the hydrodynamic interactions. A phase diagram is constructed, showing four distinct dynamic states depending on the presence of hydrodynamic or chemotaxis instabilities, all of which are suppressed by resistance at sufficiently high values.

Full simulations reveal that hydrodynamic and auto-chemotaxis instabilities can mutually enhance each other, leading to the aggregation of swimmers. However, resistance acts as an inhibitor, suppressing dynamics resulting from these instabilities or their combined effects. Additionally, resistance hinders chemotactic accumulation in initially isotropic pusher suspensions by disrupting the movement of swimmers towards chemo-attractants and the formation of concentration gradients.

The interplay between hydrodynamics, tumbling, auto-chemotaxis, and resistance is complex and impacts the formation and evolution of concentration bands and clusters. Nonlinear simulations provide deeper insights into their effects on the stability and dynamics of chemotactic pusher swimmer suspensions.

Chapter 4 explores the spread of a line accumulation of pusher micro-swimmers in environments with increasing resistance. Three scenarios are considered: non-tumbling non-chemotactic swimmers, auto-chemotactic swimmers, and swimmers in the presence of a nutrient they consume.

In the absence of auto-chemotaxis and nutrients, swimmers spread away from the line cluster due to diffusion, and resistance hinders this spread, stabilizing the fronts into quasi-1D and symmetric profiles.

Auto-chemotaxis leads to a "squiggling" accumulation line for low resistance, with swimmers clustering into circular spots and diffusive processes promoting outward spreading. Increasing resistance inhibits swimmer motion and smoothes out concentration fronts, resulting in non-line and non-circular accumulations for intermediate resistance and centered circular spots for very high resistance.

Externally supplied nutrients incentivize swimmers to move away from the initial accumulation, enhancing spreading driven by diffusion. However, resistance counters both factors, hindering the spread. Understanding the delicate balance of auto-chemotaxis, nutrients, and resistance is crucial for controlling the dynamics and spread of micro-swimmer colonies.

5.2   Future Directions

In the current study, we investigate the collective motion of micro-swimmers in a fluid with resistance. The continuum model we employ describes the dynamics of these swimmers, with parameters such as swimming speed, chemotactic sensitivity, and tumbling frequency assumed to be constant to simplify the analysis. However, it is worth noting that in experimental settings, these parameters have been observed to exhibit non-linear dependencies on factors such as swimmer and chemo-attractant concentrations. Experimental studies have shown that a micro-swimmer's individual velocity is dependent on the local concentration of chemo-attractant, denoted as $U_0 =$

$U_0(C)$. The swimmers' velocity increases with higher chemo-attractant concentration until reaching a saturation point [157]. These non-linear dependencies on chemo-attractant concentration can have significant effects on the overall behavior of the swimmer colony e.g., Karmakar et al., [77] demonstrated that the swimming speed of bacteria increases with higher concentrations of repellent, consequently enhancing the drift velocity. As stated before, in our current model, we treat certain variables, such as the chemotactic parameters β_1, β_2, and χ, as constants. However, in reality, these variables may exhibit variations and dependencies on other factors [167]. To provide a more comprehensive analysis, it is necessary to consider these variables as functions that can capture the nuanced influences and complexities of the system. By incorporating variable dependencies, we can potentially capture more realistic and dynamic behaviors of the swimmers, enabling a deeper understanding of their collective motion and response to chemo-attractant gradients [167].

Collective motion in systems of micro-swimmers is a fascinating phenomenon that has been the subject of extensive research [141, 164, 171, 112, 149, 1, 88]. While hydrodynamic interactions have been shown to play a crucial role in explaining some aspects of collective behavior, it is important to recognize that experiments often involve high volume fractions where steric interactions between neighboring swimmers become significant and cannot be overlooked. These close interactions can have a profound impact on the dynamics and emergent properties of the system. But these are difficult to model properly in continuum theories, so various approximations of various effectiveness are often employes. For example, Ezhilan et al. [50] approximates the effects of steric collisions between swimmers by using an aligning potential, and studies how this aligning impacts the emerging collective swimmer dynamics. Other active matter models include various aligning interactions; more examples and discussions on them can be seen in these reviews and articles [141, 112, 48, 1].

The continuum model considered in this dissertation does not consider the close interactions between swimmers, or the swimmers and obstacles and other structures. This simplified approach still allowed us to gain insights into the effects of inhomogeneity on the collective motion of swimmers at a macroscopic level, capturing the overall emerging behavior and patterns. However, it is known that collisions and direct interactions between swimmers and other structures are crucial, especially in confined environments [108, 33, 174], so to better understand confined collective dynamics one should consider alternative approaches that explicitly account for these close interactions. Therefore, direct simulations of micro-swimmer suspensions are preferred to understand collective dynamics, but they are computationally challenging and expensive. Numerical simulations, like boundary integral methods [75], dumbbell models [57], slender-body models [143], immersed boundary [107, 108, 174] or Lattice-Boltzmann approaches [161] and Stokesian dynamics [64] include particle-fluid interactions and often particle-particle interactions have been considered to study micro-swimmer suspensions, with many of them obtain qualitative features observed in experiments. By accounting for both the hydrodynamic and steric interactions at a microscopic level, particle-level simulations can provide a more comprehensive view of the system's behavior and allow us to investigate the intricate interplay between hydrodynamics, steric effects, and emergent collective phenomena.

Previous studies have explored the motion of individual swimmers in various environments, for example 2D obstacle arrays [109] and 3D Brinkman media [93]. More recently, there has been a growing interest in understanding the behavior of active matter in structured or unstructured environments [159, 139, 161]. For example, active matter flow can be controlled by macroscopic boundaries [108, 130] or micro-patterned structures [166], and the navigation of micro-swimmer colonies can be routed through 2D structured porous media [42]. More thorough description of recent advances and open questions on this topic can be found in the review articles,

for example on micro-swimmers in Newtonian or complex fluids [93, 60, 149, 50, 54, 92, 98, 160], soft active matter and active turbulence [141, 112, 1], collective motion and emergent behavior of active particles [171, 180], active particles and matter in complex environments [11, 114, 27].

Building upon the work in this dissertation and the aforementioned studies, we will study micro-swimmer collective navigation through spaces with heterogeneous resistance or friction, whether these structures are organized or randomly distributed. To do so, we can make the hydrodynamic resistance or friction term ν depend on space, $\nu(x)$, and, as we can no longer use Fourier methods to solve the fluid equations, would need to develop alternative numerical schemes, e.g. finite difference or element ones [162]. As swimmers or active particles can more easily move through areas of lower friction, one could consider various questions, e.g. how to optimize the geometry of micro-structured environments to modulate and direct or active flow, see for example the sketch in Figure (5.1). As 3D porous environments with controllable properties can be realized in the labs [4], it may become feasible to design environments of variable porosity and study micro-swimmer navigation through them. By studying the influence of resistance and friction in particular, and heterogenous environments in general, we can gain better insight into how the presence of structured obstacles or varying frictional properties affects the collective motion and emergent behavior of the swimmers and other types of active particles. Moreover, this insight will guide us into developing better strategies to control and direct the micro-swimmer motion and active matter flow for future technological applications.

Figure 5.1 Examples of space-dependent friction, e.g., a square or hexagonal lattice of circular Gaussians (left), a square lattice of ellipsoidal Gaussians (top-right) and a random forest distribution for $\nu(x, y)$. Possible paths for the flow of an active suspension are indicated.

APPENDIX A

BRINKMAN EQUATIONS IN PERIODIC DOMAINS

We outline how to solve the Brinkman equations for the fluid velocity in a periodic domain. This solution or its idea is used in our analyses and simulations.

The Brinkman equations with a general force are

$$-\nabla^2\mathbf{u} + \nabla q + \nu^2\mathbf{u} = \mathbf{f}, \qquad \nabla\cdot\mathbf{u} = 0. \tag{A.1}$$

Taking the divergence of the momentum equations and using the incompressibility condition yields a Laplace's Equation for the pressure $\nabla^2 q = \nabla\cdot\mathbf{f}$. Applying the Fourier transform to this equation, we can solve for the Fourier mode $\hat{q}$ for the pressure q:

$$-k^2\hat{q} = i\mathbf{k}^T\hat{\mathbf{f}} \qquad \implies \hat{q} = \frac{-i}{k^2}\mathbf{k}^T\hat{\mathbf{f}}. \tag{A.2}$$

Applying Fourier transform to the momentum Equation (A.1), we obtain

$$k^2\hat{\mathbf{u}} + i\mathbf{k}\hat{q} + \nu^2\hat{\mathbf{u}} = \hat{\mathbf{f}}. \tag{A.3}$$

Putting all these results together,

$$(k^2 + \nu^2)\hat{\mathbf{u}} = \hat{\mathbf{f}} - i\mathbf{k}\hat{q} = \left(\mathbf{I} - \frac{\mathbf{k}\mathbf{k}^T}{k^2}\right)\hat{\mathbf{f}},$$

and hence

$$\hat{\mathbf{u}} = \frac{1}{k^2 + \nu^2} \left(\mathbf{I} - \frac{\mathbf{k}\mathbf{k}^T}{k^2} \right) \hat{\mathbf{f}}. \tag{A.4}$$

We make use of this result or related ones in our linear analysis and also numerical simulations in periodic domains, specifically to solve for the fluid flow generated by a suspension micro-swimmers immersed in environments with various resistance.

APPENDIX B

ASYMPTOTIC SOLUTIONS

B.1 Asymptotic Solution of the Hydrodynamic Dispersion Relation

Below we present the *Maple* scripts for how to find asymptotic solutions for the growth rate $\sigma(k)$ from the dispersion relation Equation (2.42). Figures B.1 to B.4 show how to solve for the two branches Equations (2.43) and Equation (2.44). Asymptotic solutions of Equations (3.13) and (3.14) are obtained from the dispersion relation Equation (3.11) in a similar way.

**Asymptotic expansion of the growth rate σ(k) for small k
for the Brinkman hydrodynamic dispersion relation F(σ,k)=0.**

Note that we make the assumption ν = τ*k.

**We are looking for a small k expansion for σ= σ0+ σ1*k+σ2*k^2+...
First find a series expansion of F(σ,k) for small k, and gather the terms for each power of k,
i.e. F(σ,k) = F0(σ) + F1(σ)*k^1 + F2(σ)*k^2 +...**

**Note that because F(s,k)=0, we get equations F0(σ) =0, F1(σ)=0, F2(σ)=0, and so on.
Solving these equations systematically for σ0, σ1, σ2, we get the asymptotic expansion for σ(k).**

For the first/upper branch, we try an expansion of the equation F(σ,k)=0 for σ ~(-αγ)/5.

```
>  restart;
>  a := (σ + D·k²)/(I·k) :
>  F := (4·k·(1 + τ²))/(3·I·(−α·γ)) + 2·a³ − 4/3 ·a + (a⁴ − a²)·( − 2/a − 2/(3·a³) − 2/(5·a⁵) − 2/(7·a⁷) − 2/(9·a⁹) ) :
>  σ := σ0 + σ1·k + σ2·k² + σ3·k³ + σ4·k⁴ :
>  F := simplify(F) :
>  FS := series(F, k = 0, 6) :
>  FS := simplify(%)
```

$$FS := \frac{\frac{4I}{15}\,(5\,\sigma0\,\tau^2 + \alpha\gamma + 5\,\sigma0)}{\sigma0\,\alpha\,\gamma}\,k + \frac{-\frac{4I}{15}\,\sigma1}{\sigma0^2}\,k^2 + \frac{\frac{4I}{105}\,(-3 - 7\,(D + \sigma2)\,\sigma0 + 7\,\sigma1^2)}{\sigma0^3}\,k^3 \qquad \text{(1)}$$
$$+ \frac{\frac{4I}{105}\,(-7\,\sigma3\,\sigma0^2 + 14\,\sigma1\,(D + \sigma2)\,\sigma0 - 7\,\sigma1^3 + 9\,\sigma1)}{\sigma0^4}\,k^4$$
$$+ \frac{\frac{4I}{315}\,\left(-21\,\sigma4\,\sigma0^3 + 21\,(2\,\sigma3\,\sigma1 + (D + \sigma2)^2)\,\sigma0^2 - 63\,(D + \sigma2)\left(\sigma1^2 - \frac{3}{7}\right)\sigma0 + 21\,\sigma1^4 - 54\,\sigma1^2 + 5\right)}{\sigma0^5}\,k^5$$
$$+ O(k^6)$$

Figure B.1 Maple script for the first asymptotic solution of the Hydrodynamic Dispersion Relation, part 1.

> $Eq0 := \dfrac{\frac{4I}{15}\,(5\,\sigma0\,\tau^2 + \gamma\alpha + 5\,\sigma0)}{\sigma0\,\alpha\,\gamma}$; $solve(Eq0, \sigma0\,)$;

$$Eq0 := \frac{\frac{4I}{15}\,(5\,\sigma0\,\tau^2 + \alpha\gamma + 5\,\sigma0)}{\sigma0\,\alpha\,\gamma}$$

$$-\frac{\alpha\gamma}{5\,(\tau^2 + 1)} \qquad\qquad (2)$$

> $\sigma0 := \dfrac{(-\alpha\gamma)}{5\,(\tau^2 + 1)}$:

> $Eq1 := \dfrac{-\frac{4I}{15}\,\sigma1}{\sigma0^2}$; $solve(Eq1, \sigma1)$;

$$Eq1 := \frac{-\frac{4I}{15}\,(5\,\tau^2 + 5)^2\,\sigma1}{\alpha^2\,\gamma^2}$$

$$0 \qquad\qquad (3)$$

> $\sigma1 := 0$:

> $Eq2 := \dfrac{\frac{4I}{105}\,(-3 - 7\,(D + \sigma2)\,\sigma0 + 7\,\sigma1^2)}{\sigma0^3}$; $solve(Eq2, \sigma2)$;

$$Eq2 := \frac{-\frac{4I}{105}\,\left(-3 + \frac{7\,(D + \sigma2)\,\alpha\gamma}{5\,\tau^2 + 5}\right)(5\,\tau^2 + 5)^3}{\alpha^3\,\gamma^3}$$

$$-\frac{7D\,\alpha\gamma - 15\,\tau^2 - 15}{7\,\alpha\,\gamma} \qquad\qquad (4)$$

> $\sigma2 := -D + \dfrac{15\cdot(\tau^2 + 1)}{7\cdot(-\alpha\gamma)}$:

> $Eq3 := \dfrac{\frac{4I}{105}\,(-7\,\sigma3\,\sigma0^2 + 14\,\sigma1\,(D + \sigma2)\,\sigma0 - 7\,\sigma1^3 + 9\,\sigma1)}{\sigma0^4}$; $solve(Eq3, \sigma3)$;

$$Eq3 := \frac{-\frac{4I}{15}\,\sigma3\,(5\,\tau^2 + 5)^2}{\alpha^2\,\gamma^2}$$

$$0 \qquad\qquad (5)$$

> $\sigma3 := 0$:

> $Eq4 := \dfrac{\frac{4I}{315}\,\left(-21\,\sigma4\,\sigma0^3 + 21\,(2\,\sigma3\,\sigma1 + (D + \sigma2)^2)\,\sigma0^2 - 63\,(D + \sigma2)\left(\sigma1^2 - \frac{3}{7}\right)\sigma0 + 21\,\sigma1^4 - 54\,\sigma1^2 + 5\right)}{\sigma0^5}$;

$solve(Eq4, \sigma4)$;

$$Eq4 := \frac{-\frac{4I}{315}\,\left(\frac{21\,\sigma4\,\alpha^3\,\gamma^3}{(5\,\tau^2 + 5)^3} + \frac{675\,(\tau^2 + 1)^2}{7\,(5\,\tau^2 + 5)^2} + \frac{405\,(\tau^2 + 1)}{7\,(5\,\tau^2 + 5)} + 5\right)(5\,\tau^2 + 5)^5}{\alpha^5\,\gamma^5}$$

$$-\frac{17875\,(\tau^6 + 3\,\tau^4 + 3\,\tau^2 + 1)}{147\,\alpha^3\,\gamma^3} \qquad\qquad (6)$$

> $factor\left(-\dfrac{17875\,(\tau^6 + 3\,\tau^4 + 3\,\tau^2 + 1)}{147\,\alpha^3\,\gamma^3}\right)$;

$$-\frac{17875\,(\tau^2 + 1)^3}{147\,\alpha^3\,\gamma^3} \qquad\qquad (7)$$

> $\sigma4 := -\dfrac{17875\,(\tau^2 + 1)^3}{147\,\alpha^3\,\gamma^3}$:

The upper branch of the hydrodynamic relation then is

$$\sigma = \frac{(-\alpha\gamma)}{5\,(\tau^2 + 1)} + \left(\frac{15\cdot(\tau^2 + 1)}{7\cdot(-\alpha\gamma)} - D\right)k^2 + \frac{17875\,(\tau^2 + 1)^3}{147\,(-\alpha\gamma)^3}k^4 + O(k^5)$$

Figure B.2 Maple script for the first asymptotic solution of the Hydrodynamic Dispersion Relation, part 2.

117

Asymptotic expansion of the growth rate σ(k) for small k
for the Brinkman hydrodynamic dispersion relation F(σ,k)=0.

For the second/lower branch, we try an expansion of the equation F(σ,k)=0 for σ ~0.

```
> restart;
> σ := σ1·k + σ2·k² + σ3·k³ + σ4·k⁴ :
> a := (σ + D·k²)/(I·k) :
> a := simplify(a);
```

$$a := -\mathrm{I}\left(k^3\,\sigma4 + k^2\,\sigma3 + \mathrm{D}\,k + k\,\sigma2 + \sigma1\right) \tag{1}$$

```
> F := (4·k·(1+τ²))/(−3·I·α·γ) + 2·a³ − (4/3)·a + (a⁴ − a²)·log((a−1)/(a+1)) :
> F := simplify(F) :
> FS := series(F, k=0, 3) :
> FS := simplify(FS);
```

$$FS := \frac{\sigma1\left(3\ln\left(\dfrac{-\mathrm{I}+\sigma1}{\mathrm{I}+\sigma1}\right)\sigma1^3 + 6\,\mathrm{I}\,\sigma1^2 + 3\,\sigma1\ln\left(\dfrac{-\mathrm{I}+\sigma1}{\mathrm{I}+\sigma1}\right) + 4\,\mathrm{I}\right)}{3} \tag{2}$$

$$+ \frac{4}{3}\frac{1}{\alpha\gamma}\left(1 + 3\,\gamma(\mathrm{D}+\sigma2)\right)\left(\sigma1^2 + \frac{1}{2}\right)\alpha\,\sigma1\ln\left(\frac{-\mathrm{I}+\sigma1}{\mathrm{I}+\sigma1}\right) + 6\,\mathrm{I}\,\gamma(\mathrm{D}+\sigma2)\left(\sigma1^2\right.$$

$$\left. + \frac{1}{6}\right)\alpha + \mathrm{I}\,\tau^2\Bigg)k + 12\frac{1}{(1+\sigma1)^2(1-\sigma1)^2}\Bigg((\sigma1^2$$

$$+ 1)\left(\frac{(\sigma1^2+1)\left(\dfrac{2\,\sigma1^3\,\sigma3}{3} + (\mathrm{D}+\sigma2)^2\,\sigma1^2 + \dfrac{\sigma3\,\sigma1}{3} + \dfrac{(\mathrm{D}+\sigma2)^2}{6}\right)\ln\left(\dfrac{-\mathrm{I}+\sigma1}{\mathrm{I}+\sigma1}\right)}{2}\right.$$

$$\left. + \frac{2\,\mathrm{I}\,\sigma1^4\,\sigma3}{3} + \mathrm{I}(\mathrm{D}+\sigma2)^2\,\sigma1^3 + \frac{7\,\mathrm{I}\,\sigma1^2\,\sigma3}{9} + \frac{5\,\mathrm{I}(\mathrm{D}+\sigma2)^2\,\sigma1}{6} + \frac{\mathrm{I}\,\sigma3}{9}\right)\Bigg)k^2 + \mathrm{O}(k^3)$$

```
> Eq1 := (σ1(3 ln((−I+σ1)/(I+σ1)) σ1³ + 6 I σ1² + 3 σ1 ln((−I+σ1)/(I+σ1)) + 4 I))/3 ; solve(Eq1, σ1);
```

$$Eq1 := \frac{\sigma1\left(3\ln\left(\dfrac{-\mathrm{I}+\sigma1}{\mathrm{I}+\sigma1}\right)\sigma1^3 + 6\,\mathrm{I}\,\sigma1^2 + 3\,\sigma1\ln\left(\dfrac{-\mathrm{I}+\sigma1}{\mathrm{I}+\sigma1}\right) + 4\,\mathrm{I}\right)}{3}$$

$$0, \ \frac{\mathrm{I}\left(-e^{RootOf\left(-(e\_Z)^3 + 6\_Z(e\_Z)^2 - 9(e\_Z)^2 + 6\_Z e\_Z + 9\,e\_Z + 1\right)} - 1\right)}{e^{RootOf\left(-(e\_Z)^3 + 6\_Z(e\_Z)^2 - 9(e\_Z)^2 + 6\_Z e\_Z + 9\,e\_Z + 1\right)} - 1} \tag{3}$$

We choose the first solution because that's the only one that satisfies the integral.

```
> σ1 := 0 :
```

Figure B.3 Maple script for the second asymptotic solution of the Hydrodynamic Dispersion Relation, part 1.

> $\sigma 1 := 0:$
> $FS;$

$$\frac{4\left(I + I\gamma(D + \sigma 2)\,\alpha + I\tau^2\right)}{3\,\alpha\,\gamma}\,k + \left(I\left(D + \sigma 2\right)^2\pi + \frac{4\,I\,\sigma 3}{3}\right)k^2 + O(k^3) \qquad (4)$$

> $Eq2 := \left(\dfrac{4\left(I + I\gamma(D + \sigma 2)\,\alpha + I\tau^2\right)}{3\,\alpha\,\gamma}\right);\ solve(Eq2,\sigma 2);$

$$Eq2 := \frac{4\left(I + \gamma(D + \sigma 2)\,\alpha I + \tau^2 I\right)}{3\,\alpha\,\gamma}$$

$$-\frac{D\,\gamma\,\alpha + \tau^2 + 1}{\alpha\,\gamma} \qquad (5)$$

> $\sigma 2 := \dfrac{\tau^2 + 1}{(-\alpha\,\gamma)} - D:$

> $Eq3 := \left(I\left(D + \sigma 2\right)^2\pi + \dfrac{4\,I\,\sigma 3}{3}\right);\ solve(Eq3,\sigma 3);$

$$Eq3 := \frac{I\left(\tau^2 + 1\right)^2\pi}{\alpha^2\,\gamma^2} + \frac{4\,I\,\sigma 3}{3}$$

$$-\frac{3\,\pi\left(\tau^4 + 2\,\tau^2 + 1\right)}{4\,\alpha^2\,\gamma^2} \qquad (6)$$

> $factor\left(-\dfrac{3\,\pi\left(\tau^4 + 2\,\tau^2 + 1\right)}{4\,\alpha^2\,\gamma^2}\right)$

$$-\frac{3\left(\tau^2 + 1\right)^2\pi}{4\,\alpha^2\,\gamma^2} \qquad (7)$$

> $\sigma 3 := -\dfrac{3\,\pi\left(\tau^2 + 1\right)^2}{4\cdot(-\alpha\,\gamma)^2}:$

>

The lower branch of the hydrodynamic relation then is

$$\sigma := \left(\frac{\tau^2 + 1}{(-\alpha\,\gamma)} - D\right)k^2 - \frac{3\,\pi(\tau^2 + 1)^2}{4(-\alpha\,\gamma)^2}k^3 + \frac{3\left(\tau^2 + 1\right)^3\left(3\,\pi^2 - 8\right)}{8(-\alpha\,\gamma)^3}k^4 + O(k^5)$$

Figure B.4 Maple script for the second asymptotic solution of the Hydrodynamic Dispersion Relation, part 2.

B.2 Asymptotic Solution of the Chemotactic Dispersion Relation

Below we present the *Maple* scripts used to find asymptotic solutions for the growth rate $\sigma(k)$ from the dispersion relation Equation (3.12). Figures B.5 and B.6 show how to solve and find the expression shown in Equation (3.15).

Asymptotic expansion of the growth rate σ(k) for small k
for the Chemotactic dispersion relation G(σ,k)=0.

We are looking for a small k expansion for σ= σ0+ σ1*k+σ2*k^2+...
First find a series expansion ofG(σ,k) = G0(σ) + G1(σ)*k^1 + G2(σ)*k^2 +...
We get equations G0(σ) =0, G1(σ)=0, G2(σ)=0, and so on.
Solving these equations systematically for σ0, σ1, σ2, we get the asymptotic expansion for σ(k).

Recall that $R = \dfrac{X}{1 + Ck^2} \sim X \cdot (1 - C \cdot k^2 + C^2 \cdot k^4 + \dots)$ **for small k, where** $X = \dfrac{\chi\beta2}{\beta1}$ **and** $C = \dfrac{D\_c}{\beta1}$

```
>  restart;
```

$$> \quad a := \frac{(\sigma + \lambda)}{I \cdot k} :$$

$$> \quad R := X \cdot (1 - C \cdot k^2 + C^2 \cdot k^4) :$$

$$> \quad G := \frac{2}{\lambda} \cdot I \cdot k - 2 \cdot R \cdot I \cdot k - (R \cdot a \cdot I \cdot k - 1) \cdot \left(-\frac{2}{a} - \frac{2}{3 \cdot a^3} - \frac{2}{5 \cdot a^5} - \frac{2}{7 \cdot a^7} - \frac{2}{9 \cdot a^9} - \frac{2}{11 \cdot a^{11}} \right) :$$

$$> \quad \sigma := \sigma0 + \sigma1 \cdot k + \sigma2 \cdot k^2 + \sigma3 \cdot k^3 + \sigma4 \cdot k^4 :$$

$$> \quad G := simplify(G) :$$

$$> \quad GS := series(G, k = 0, 5);$$

$$GS := \left(\frac{2\,I}{\lambda} - 2\,IX + \frac{2\,I\,(X\,(\lambda + \sigma0) - 1)}{\lambda + \sigma0} \right) k + \left(-\frac{2\,I\,(X\,(\lambda + \sigma0) - 1)\,\sigma1}{(\lambda + \sigma0)^2} + \frac{2\,IX\,\sigma1}{\lambda + \sigma0} \right) k^2 \qquad \textbf{(1)}$$

$$+ \left(2\,IXC - (X\,(\lambda + \sigma0) - 1) \left(\frac{\dfrac{2\,I\,\sigma2}{\lambda + \sigma0} - \dfrac{2\,I\,\sigma1^2}{(\lambda + \sigma0)^2}}{\lambda + \sigma0} + \frac{2\,I}{3\,(\lambda + \sigma0)^3} \right) - \frac{2\,IX\,\sigma1^2}{(\lambda + \sigma0)^2} \right.$$

$$\left. + \frac{2\,I\,(X\,\sigma2 - CX\,(\lambda + \sigma0))}{\lambda + \sigma0} \right) k^3 + \left(-(X\,(\lambda + \sigma0)) \right.$$

$$- 1) \left(\frac{\dfrac{2\,I\,\sigma3}{\lambda + \sigma0} - \dfrac{2\,I\,\sigma1\,\sigma2}{(\lambda + \sigma0)^2} - \dfrac{2\,I\,(\sigma2\,\lambda + \sigma2\,\sigma0 - \sigma1^2)\,\sigma1}{(\lambda + \sigma0)^3}}{\lambda + \sigma0} - \frac{2\,I\,\sigma1}{(\lambda + \sigma0)^4} \right)$$

$$- X\,\sigma1 \left(\frac{\dfrac{2\,I\,\sigma2}{\lambda + \sigma0} - \dfrac{2\,I\,\sigma1^2}{(\lambda + \sigma0)^2}}{\lambda + \sigma0} + \frac{2\,I}{3\,(\lambda + \sigma0)^3} \right) - \frac{2\,I\,(X\,\sigma2 - CX\,(\lambda + \sigma0))\,\sigma1}{(\lambda + \sigma0)^2}$$

$$\left. + \frac{2\,I\,(-CX\,\sigma1 + X\,\sigma3)}{\lambda + \sigma0} \right) k^4 + O(k^5)$$

Figure B.5 Maple script for the second asymptotic solution of the Chemotactic Dispersion Relation, part 1.

Asymptotic expansion of the growth rate σ(k) for small k
for the Chemotactic dispersion relation G(σ,k)=0.

We are looking for a small k expansion for σ= σ0+ σ1*k+σ2*k^2+...
First find a series expansion ofG(σ,k) = G0(σ) + G1(σ)*k^1 + G2(σ)*k^2 +...
We get equations G0(σ) =0, G1(σ)=0, G2(σ)=0, and so on.
Solving these equations systematically for σ0, σ1, σ2, we get the asymptotic expansion for σ(k).

Recall that $R = \dfrac{X}{1 + Ck^2} \sim X \cdot (1 - C \cdot k^2 + C^2 \cdot k^4 + ...)$ for small k, where $X = \dfrac{\chi\beta 2}{\beta 1}$ and $C = \dfrac{D\_c}{\beta 1}$

```
>  restart;
```

$$> \quad a := \frac{(\sigma + \lambda)}{I \cdot k} :$$

$$> \quad R := X \cdot (1 - C \cdot k^2 + C^2 \cdot k^4) :$$

$$> \quad G := \frac{2}{\lambda} \cdot I \cdot k - 2 \cdot R \cdot I \cdot k - (R \cdot a \cdot I \cdot k - 1) \cdot \left(-\frac{2}{a} - \frac{2}{3 \cdot a^3} - \frac{2}{5 \cdot a^5} - \frac{2}{7 \cdot a^7} - \frac{2}{9 \cdot a^9} - \frac{2}{11 \cdot a^{11}} \right) :$$

$$> \quad \sigma := \sigma 0 + \sigma 1 \cdot k + \sigma 2 \cdot k^2 + \sigma 3 \cdot k^3 + \sigma 4 \cdot k^4 :$$

$$> \quad G := simplify(G) :$$

$$> \quad GS := series(G, k = 0, 5);$$

$$GS := \left(\frac{2\,I}{\lambda} - 2\,I X + \frac{2\,I\,(X\,(\lambda + \sigma 0) - 1)}{\lambda + \sigma 0} \right) k + \left(-\frac{2\,I\,(X\,(\lambda + \sigma 0) - 1)\,\sigma 1}{(\lambda + \sigma 0)^2} + \frac{2\,I X \sigma 1}{\lambda + \sigma 0} \right) k^2 \qquad \textbf{(1)}$$

$$+ \left(2\,I X C - (X\,(\lambda + \sigma 0) - 1) \left(\frac{\dfrac{2\,I \sigma 2}{\lambda + \sigma 0} - \dfrac{2\,I \sigma 1^2}{(\lambda + \sigma 0)^2}}{\lambda + \sigma 0} + \frac{2\,I}{3\,(\lambda + \sigma 0)^3} \right) - \frac{2\,I X \sigma 1^2}{(\lambda + \sigma 0)^2} \right.$$

$$\left. + \frac{2\,I\,(X\sigma 2 - C X\,(\lambda + \sigma 0))}{\lambda + \sigma 0} \right) k^3 + \left(-(X\,(\lambda + \sigma 0)) \right.$$

$$- 1) \left(\frac{\dfrac{2\,I \sigma 3}{\lambda + \sigma 0} - \dfrac{2\,I \sigma 1\,\sigma 2}{(\lambda + \sigma 0)^2} - \dfrac{2\,I\,(\sigma 2\,\lambda + \sigma 2\,\sigma 0 - \sigma 1^2)\,\sigma 1}{(\lambda + \sigma 0)^3}}{\lambda + \sigma 0} - \frac{2\,I \sigma 1}{(\lambda + \sigma 0)^4} \right)$$

$$- X \sigma 1 \left(\frac{\dfrac{2\,I \sigma 2}{\lambda + \sigma 0} - \dfrac{2\,I \sigma 1^2}{(\lambda + \sigma 0)^2}}{\lambda + \sigma 0} + \frac{2\,I}{3\,(\lambda + \sigma 0)^3} \right) - \frac{2\,I\,(X\sigma 2 - C X\,(\lambda + \sigma 0))\,\sigma 1}{(\lambda + \sigma 0)^2}$$

$$\left. + \frac{2\,I\,(-C X \sigma 1 + X \sigma 3)}{\lambda + \sigma 0} \right) k^4 + O(k^5)$$

Figure B.6 Maple script for the second asymptotic solution of the Chemotactic Dispersion Relation, part 2.

APPENDIX C

LINEAR ANALYSIS IN 2D

Similar to the linear stability analysis for the 3D case in Section 2.3.1, we analyze the stability of nearly-uniform and isotropic ($\Psi_0 = 1/2\pi$) suspension in 2D. Again we consider a suspension of swimmers with no diffusion $D = d_r = 0$. Here we have only one turning angle $\theta \in [0, 2\pi)$ and the direction vector is $\mathbf{p} = [\cos\theta, \sin\theta]$.

The linearized distribution equation is

$$\frac{\partial \Psi}{\partial t} = -\mathbf{p} \cdot \nabla\Psi + 2\gamma\mathbf{p}^T\mathbf{E}\mathbf{p} - \lambda_0\Psi + \frac{\lambda_0\chi}{2\pi}\mathbf{p}\cdot\nabla C + \frac{\lambda_0}{2\pi}\int_0^{2\pi}\Psi' d\theta. \qquad \text{(C.1)}$$

We consider plane-wave perturbations for the distribution

$$\Psi(\mathbf{x}, \mathbf{p}, t) = 1/2\pi + \epsilon\tilde{\Psi}(\mathbf{p}, \mathbf{k})\exp(i\mathbf{k}\cdot\mathbf{x} + \sigma t)$$

$$C(\mathbf{x}, t) = \beta_1/\beta_2 + \epsilon\tilde{C}(\mathbf{k})\exp(i\mathbf{k}\cdot\mathbf{x} + \sigma t) \qquad \text{(C.2)}$$

with $|\epsilon| << 1$, $\mathbf{k}$ the wavenumber and σ the growth rate.

Substituting the solution for $\tilde{C}$ and $\tilde{\Sigma}^p$ from the quasi-static chemo-attractant equation and solution to the fluid equations respectively, we arrive at

$$(\sigma + \lambda_0 + ik\sin\theta)\tilde{\Psi} = \frac{-\alpha\gamma k^2}{\pi(k^2 + \nu^2)}\sin\theta\cos\theta\int_0^{2\pi}\tilde{\Psi}'\sin\theta'\cos\theta' d\theta'$$

$$+ \frac{\lambda_0}{2\pi}ik\sin\theta\frac{\chi\beta_2}{\beta_1 + k^2 D_c}\int_0^{2\pi}\tilde{\Psi}' d\theta' + \frac{\lambda_0}{2\pi}\int_0^{2\pi}\tilde{\Psi}' d\theta' \qquad \text{(C.3)}$$

where we have let $\mathbf{k} = k\hat{\mathbf{k}}$. This gives a linear equation for $\tilde{\Psi}$

$$\tilde{\Psi} = \frac{-\alpha\gamma k^2}{\pi(k^2 + \nu^2)} \frac{\sin\theta\cos\theta}{(\sigma + \lambda_0 + ik\sin\theta)} \int_0^{2\pi} \tilde{\Psi}' \sin\theta' \cos\theta' d\theta'$$
$$+ \frac{\lambda_0}{2\pi} ik \frac{\chi\beta_2}{(\beta_1 + k^2 D_c)} \frac{\sin\theta}{(\sigma + \lambda_0 + ik\sin\theta)} \int_0^{2\pi} \tilde{\Psi}' d\theta'$$
$$+ \frac{\lambda_0}{2\pi} \frac{1}{(\sigma + \lambda_0 + ik\sin\theta)} \int_0^{2\pi} \tilde{\Psi}' d\theta' \tag{C.4}$$

Therefore,

$$1 = \frac{-\alpha\gamma k^2}{\pi(k^2 + \nu^2)} \int_0^{2\pi} \frac{\sin^2\theta\cos^2\theta}{(\sigma + \lambda_0 + ik\sin\theta)} d\theta. \tag{C.5}$$

For the auto-chemotaxis relation, we just integrate Equation (C.4) in θ and obtain

$$1 = \frac{\lambda_0}{2\pi} ik \frac{\chi\beta_2}{(\beta_1 + k^2 D_c)} \int_0^{2\pi} \frac{\sin\theta}{(\sigma + \lambda_0 + ik\sin\theta)} d\theta$$
$$+ \frac{\lambda_0}{2\pi} \int_0^{2\pi} \frac{1}{(\sigma + \lambda_0 + ik\sin\theta)} d\theta. \tag{C.6}$$

We can do the integrals in the hydrodynamics and auto-chemotaxis dispersion relations in Equations (C.5) and (C.6) exactly by using contour integrals and residue calculations. The details of this, while long, are omitted here. The resulting equations are

$$1 = \frac{-\alpha\gamma}{ik} \frac{k^2}{k^2 + \nu^2} \left[2a^3 - a \pm 2a^2\sqrt{a^2 - 1} \right] \tag{C.7}$$

for the hydrodynamics relation, and

$$1 = \lambda_0 \frac{\chi \beta_2}{(\beta_1 + k^2 D_c)} \left[1 \pm \frac{a}{\sqrt{a^2 - 1}} \right] \pm \frac{\lambda_0}{ik} \frac{1}{\sqrt{a^2 - 1}} \tag{C.8}$$

which can be re-arranged as

$$0 = \mathcal{F}(\sigma, k) := \frac{-ik}{-\alpha \gamma} \frac{(k^2 + \nu^2)}{k^2} + \left[2a^3 - a \pm 2a^2 \sqrt{a^2 - 1} \right] \tag{C.9}$$

$$0 = \mathcal{G}(\sigma, k) := \frac{-ik}{\lambda_0} + \frac{\chi \beta_2 ik}{(\beta_1 + k^2 D_c)} \left[1 \pm \frac{a}{\sqrt{a^2 - 1}} \right] \pm \frac{1}{\sqrt{a^2 - 1}}, \tag{C.10}$$

for the auto-chemotaxis relation. We have again let $a = (\sigma + \lambda_0)/ik$, and recognize here as well the factor $R = \chi \beta_2 / (\beta_1 + k^2 D_c)$.

The first equation is the hydrodynamic dispersion relation in 2D. It is a cubic equation for a and can be solved exactly for a and thus for σ, though we have to take care that the solution satisfies the integral relation in Equation (2.49). From the two cases arising from the $\pm$, only the minus case is feasible [61, 103]. We obtain these roots

$$\sigma_{H1} = -\frac{A}{\Delta} + \frac{B\Delta}{A} + \frac{\Delta}{12}$$

$$\sigma_{H2} = \frac{A}{2\Delta} - \frac{2B\Delta}{A} + \frac{\Delta}{12} \pm \frac{i\sqrt{3}}{2} \left(-\frac{A}{2\Delta} - \frac{B\Delta}{A} \right) \tag{C.11}$$

where for simplicity of the formula we have let $\Delta = (-\alpha \gamma)/(1 + \tau^2)$ and

$$A = \frac{1}{12} \left[-\Delta^4 + 36\Delta^2 k^2 - 216k^4 + 24\Delta^2 k^3 \sqrt{-3\Delta^2 + 81k^2} \right]^{1/3}$$

$$B = \frac{1}{6} \left[k^2 - \frac{\Delta^2}{24} \right].$$

As for the auto-chemotaxis relation, we can solve it for the growth rate $\sigma(k)$ and get two branches

$$\sigma = -\lambda_0 + \frac{\lambda_0^2 R}{2R\lambda_0 - 1} \pm \frac{\sqrt{R^2\lambda_0^4 + (2R\lambda_0 - 1)[(2R\lambda_0 - 1)^2 k^2 - \lambda_0^2]}}{2R\lambda_0 - 1}. \tag{C.12}$$

Note that for small k, the solutions above give

$$\sigma_{C-} \approx \frac{1}{2\lambda_0}(\overline{\chi}\lambda_0 - 1)k^2 + O(k^4)$$

$$\sigma_{C+} \approx -\lambda_0 \frac{\overline{\chi}\lambda_0 - 1}{2\overline{\chi}\lambda_0 - 1} + O(k^2)$$

for $\overline{\chi} = \chi/\beta_1$. However, the second $(C+)$ branch does not satisfy the integral relation Equation (C.6) and it is a spurious solution. To see this clearly, consider the no-auto-chemotaxis case $\chi = 0$ and $k = 0$ for which the above is $\sigma_C = -\lambda_0$, but the integrand in the integral relation Equation (C.6) has a zero denominator and thus no solution can be found. Thus the only auto-chemotaxis solution in 2D is

$$\sigma_C = -\lambda_0 + \frac{\lambda_0^2 R}{2R\lambda_0 - 1} - \frac{\sqrt{R^2\lambda_0^4 + (2R\lambda_0 - 1)[(1 - R\lambda_0)^2 k^2 - \lambda_0^2]}}{2R\lambda_0 - 1}. \tag{C.13}$$

REFERENCES

[1] R. Alert, J. Casademunt, and J. Joanny. Active turbulence. *Annual Review of Condensed Matter Physics*, 13(1):143–170, 2022.

[2] W. Alt. Biased random walk models for chemotaxis and related diffusion approximations. *Journal of Mathematical Biology*, 9:147, 1980.

[3] M. Ben Amar. Collective chemotaxis and segregation of active bacterial colonies. *Scientific Reports*, 6:21269, 2016.

[4] D.B. Amchin, J.A. Ott, T. Bhattacharjee, and S.S. Datta. Influence of confinement on the spreading of bacterial populations. *PLoS Computational Biology*, 18(5):e1010063, 2022.

[5] I. S. Aranson, A. Sokolov, J. O. Kessler, and R. E. Goldstein. Model for dynamical coherence in thin films of self-propelled microorganisms. *Physical Review E*, 75:040901, 2007.

[6] A. Baskaran and M. C. Marchetti. Statistical mechanics and hydrodynamics of bacterial suspensions. *Proceedings of the National Academy of Sciences of the United States of America*, 106:15567, 2009.

[7] B. L. Bassler. Small talk. cell-to-cell communication in bacteria. *Cell*, 109:421, 2002.

[8] G. Batchelor. Slender-body theory for particles of arbitrary cross-section in stokes flow. *Journal of Fluid Mechanics*, 44:419–440, 1970.

[9] G. K. Batchelor. The stress system in a suspension of force-free particles. *Journal of Fluid Mechanics*, 41:545, 1970.

[10] R. N. Bearon and T. J. Pedley. Modelling run-and-tumble chemotaxis in a shear flow. *Bulletin of Mathematical Biology*, 62:775, 2000.

[11] C. Bechinger, R. Di Leonardo, H Lowen, C. Reichhardt, G. Volpe, and G. Volpe. Active particles in complex and crowded environments. *Reviews of Modern Physics*, 88:045006, 2016.

[12] A. Bejan. *Advanced engineering thermodynamics*. Wiley, New York, 4th edition, 2013.

[13] H. Berg and E. Purcell. Chemotaxis in bacteria. *Annual Review of Biophysics and Bioengineering*, 1(1):27–58, 1972.

[14] H. C. Berg and D. A. Brown. Chemotaxis in escherichia coli analyzed by three-dimensional tracking. *Nature*, 239:500, 1972.

[15] H.C. Berg. *Random Walks in Biology.* Princeton University Press, 1993.

[16] T. Bhattacharjee, D. B. Amchin, R. Alert J. A. Ott, and S.S. Datta. Chemotactic smoothing of collective migration. *eLife*, 11:e71226, 2022.

[17] T. Bhattacharjee, D.B. Amchin, J.A. Ott, F. Kratz, and S.S. Datta. Chemotactic migration of bacteria in porous media. *Biophysical Journal*, 120:3483–3497, 2021.

[18] T. Bhattacharjee and S. S. Datta. Bacterial hopping and trapping in porous media. *Nature Communications*, 1:2, 2019.

[19] T. Bhattacharjee and S. S. Datta. Confinement and activity regulate bacterial motion in porous media. *Soft Matter*, 15:9920–9930, 2019.

[20] J. Blake. A spherical envelope approach to ciliary propulsion. *Journal of Fluid Mechanics*, 46:199–208, 1971.

[21] J. R. Blake and A. T. Chwang. Fundamental singularities of viscous flow. *Journal of Engineering Mathematics*, 8:23, 1974.

[22] Y. Bozorgi and P. T. Underhill. Role of linear viscoelasticity and rotational diffusivity on the collective behavior of active particles. *Journal of Rheology*, 57:511–533, 2013.

[23] Y. Bozorgi and P. T. Underhill. Effects of elasticity on the nonlinear collective dynamics of self-propelled particles. *Journal of Non-Newtonian Fluid Mechanics*, 214:69–77, 2014.

[24] C.J. Brokaw. Chemotaxis of bracken spermatozoids. the role of bimalate ions. *Journal of Experimental Zoology*, 35:192, 1958.

[25] Q. Brosseau, F. Balboa Usabiaga, E. Lushi, Y. Wu, L. Ristroph, M. D. Ward, M. J. Shelley, and J. Zhang. Metallic microswimmers driven up the wall by gravity. *Soft Matter*, 17:6597–6602, 2021.

[26] Q. Brosseau, F. Balboa Usabiaga, E. Lushi, Y. Wu, L. Ristroph, J. Zhang, M. Ward, and M.J. Shelley. Coherent structures and dynamics in confined active nematics. *Physical Review Letters*, 123:178004, 2019.

[27] L.H. Cai, S.S. Datta, and X. Cheng. Active matter in complex environments. *Frontiers in Physics*, 10:1005146, 2022.

[28] H. Callen. *Thermodynamics and an introduction to thermostatistics.* New York, Wiley, 2nd edition, 1985.

[29] N.W. Charon, E.P. Greenberg, M.B. Koopman, and R.J. Limberger. Spirochete chemotaxis, motility, and the structure of the spirochetal periplasmic flagella. *Research in Microbiology*, 143(6):597, 1992.

[30] K.C. Chen, R.M. Ford, and P.T. Cummings. Cell balance equation for chemotactic bacteria with a biphasic tumbling frequency. *Journal of Mathematical Biology*, 47:518, 2003.

[31] S. Childress. Viscous flow past a random array of spheres. *The Journal of Chemical Physics*, 56:2527–2539, 1972.

[32] L. H. Cisneros, R. Cortez, C. Dombrowski, R. E. Goldstein, and J. O. Kessler. Fluid dynamics of self-propelled microorganisms, from individuals to concentrated populations. *Experiments in Fluids*, 43:737, 2007.

[33] M. Contino, E. Lushi, I. Tuval, V. Kantsler, and M. Polin. Microalgae scatter off solid surfaces by hydrodynamic and contact forces. *Physical Review Letters*, 115:258102, 2015.

[34] R. Cortez, B. Cummins, K. Leiderman, and D. Varela. Computation of three-dimensional brinkman flows using regularized methods. *Journal of Computational Physics*, 229:7609–7624, 2010.

[35] A. Daddi-Moussa-Ider, Y. Hosaka, A. Vilfan, and R. Golestanian. Axisymmetric monopole and dipole flow singularities in proximity of a stationary no-slip plate immersed in a brinkman fluid. *arXiv preprint*, page 2305.07669, 2023.

[36] A. Daddi-Moussa-Ider, B. Nasouri, A. Vilfan, and R. Golestanian. Optimal swimmers can be pullers, pushers or neutral depending on the shape. *Journal of Fluid Mechanics*, 922:R5, 2021.

[37] C. Datt, G. Natale, S. Hatzikiriakos, and G. Elfring. An active particle in a complex fluid. *Journal of Fluid Mechanics*, 823:675–688, 2017.

[38] C. Datt, L. Zhu, G. Elfring, and O. Pak. Squirming through shear-thinning fluids. *Journal of Fluid Mechanics*, 784:R1, 2015.

[39] A. Dehkharghani, N. Waisbord, J. Dunkel, and J. S. Guasto. Bacterial scattering in microfluidic crystal flows reveals giant active taylor–aris dispersion. *Proceedings of the National Academy of Sciences*, 116(23):11119–11124, 2019.

[40] A. Dehkharghani, N. Waisbord, and J. S. Guasto. Self-transport of swimming bacteria is impaired by porous microstructure. *Communications Physics*, 6:18, 2023.

[41] R. Dillon, L. Fauci, and D. Gaver. A microscale model of bacterial swimming, chemotaxis and substrate transport. *Journal of Theoretical Biology*, 177:325, 1995.

[42] M. Doi and S. Edwards. *The Theory of Polymer Dynamics*. Oxford University Press, New York, 1986.

[43] C. Dombrowski, L. Cisneros, S. Chatkaew, R. E. Goldstein, and J. O. Kessler. Self-concentration and large-scale coherence in bacterial dynamics. *Physical Review Letters*, 93:098103, 2004.

[44] K. Drescher, J. Dunkel, L. Cisneros, S. Ganguly, and R. Goldstein. Fluid dynamics and noise in bacterial cell–cell and cell–surface scattering. *Proceedings of the National Academy of Sciences of the United States of America*, 108:10940–10945, 2011.

[45] K. Drescher, R. Goldstein, N. Michel, M. Polin, and I. Tuval. Direct measurement of the flow field around swimming microorganisms. *Physical Review Letters*, 105:168101, 2010.

[46] R. Dreyfus, J. Baudry, M. L. Roper, H. A. Stone, M. Fermigier, and J. Bibette. Microscopic artificial swimmers. *Nature (London)*, 437:862, 2005.

[47] M. Driscoll, B. Delmotte, M. Youssef, S. Sacanna, A. Donev, and P. Chaikin. Unstable fronts and motile structures formed by microrollers. *Nature Physics*, 13(4):375–379, 2017.

[48] J. Dunkel, S. Heidenreich, K. Drescher, H. H. Wensink, M. Bär, and R. E. Goldstein. Fluid dynamics of bacterial turbulence. *Physical Review Letters*, 110:228102, 2013.

[49] L. Durlofsky and J. Brady. Analysis of the brinkman equation as a model for flow in porous media. *Physics of Fluids*, 30:3329–3341, 1987.

[50] J. Elgeti, R. G. Winkler, and G. Gompper. Physics of microswimmers—single particle motion and collective behavior: a review. *Reports on Progress in Physics*, 78:056601, 2015.

[51] B. Ezhilan, A. A. Pahlavan, and D. Saintillan. Chaotic dynamics and oxygen transport in thin films of aerotactic bacteria. *Physics of Fluids*, 24(9):091701, 2012.

[52] B. Ezhilan, M. J. Shelley, and D. Saintillan. Instabilities and nonlinear dynamics of concentrated active suspensions. *Physics of Fluids*, 25:070607, 2013.

[53] L. J. Fauci and R. Dillon. Biofluid mechanics of reproduction. *Annual Review of Fluid Mechanics*, 38:371–94, 2006.

[54] R.E. Goldstein. Batchelor prize lecture fluid dynamics at the scale of the cell. *Journal of Fluid Mechanics*, 807:1–39, 2016.

[55] J. Guasto, K. Johnson, and J. Gollub. Oscillatory flows induced by microorganisms swimming in two dimensions. *Physical Review Letters*, 105:168102, 2010.

[56] J. Hernandez-Ortiz, C. Stoltz, and M. Graham. Dynamics of confined suspensions of swimming particles. *Journal of Physics*, 21:204107, 2009.

[57] J.P. Hernandez-Ortiz, P.T. Underhill, and M.D. Graham. Dynamics of confined suspensions of swimming particles. *Journal of Physics: Condensed Matter*, 21:204107, 2007.

[58] N.A. Hill and T.J. Pedley. Bioconvection. *Fluid Dynamics Research*, 37:1, 2005.

[59] E. Hinch. Hydrodynamics at low reynolds number: a brief and elementary introduction disorder and mixing. *North Atlantic Treaty Organization Advanced Studies Institute*, 1:4355, 1988.

[60] C. Hohenegger and M. J. Shelley. Dynamics of complex biofluids. *Oxford University Press, New York*, 92:66–94, 2011.

[61] C. Hohenegger and M.J. Shelley. On the stability of active suspensions. *Physical Review E*, 81(4):046311, 2010.

[62] Y. Hong, N.M.K. Blackman, N.D. Kopp, A. Sen, and D. Velegol. Chemotaxis of non-biological nanorods. *Physical Review Letters*, 99:178103, 2007.

[63] M.M. Hopkins and L.J. Fauci. A computational model of the collective fluid dynamics of motile micro-organisms. *Journal of Fluid Mechanics*, 455:149, 2002.

[64] T. Ishikawa and T. J. Pedley. Diffusion of swimming model micro-organisms in a semi-dilute suspension. *Journal of Fluid Mechanics*, 588:437, 2007.

[65] T. Ishikawa and T. J. Pedley. The rheology of a semi-dilute suspension of swimming model micro-organisms. *Journal of Fluid Mechanics*, 588:399, 2007.

[66] T. Ishikawa and T. J. Pedley. Coherent structures in monolayers of swimming particles. *Physical Review Letters*, 100:088103, 2008.

[67] T. Ishikawa, T. J. Pedley, and T. Yamaguchi. Orientational relaxation time of bottom-heavy squirmers in a semi-dilute suspension. *Journal of Theoretical Biology*, 249:296, 2007.

[68] T. Ishikawa, M. P. Simmonds, and T. J. Pedley. Hydrodynamic interaction of two swimming model micro-organisms. *Journal of Fluid Mechanics*, 568:119, 2006.

[69] G. B. Jeffrey. The motion of ellipsoidal particles immersed in a viscous fluid. *Proceedings of the Royal Society*, 102:161, 1922.

[70] C. Jeznach and S. D. Olson. Dynamics of swimmers in fluids with resistance. *Fluids*, 5, 2020.

[71] R. Johnson. An improved slender-body theory for stokes flow. *Journal of Fluid Mechanics*, 99:411–431, 1980.

[72] S. Jung. Caenorhabditis elegans swimming in a saturated particulate system. *Physics of Fluids*, 22:1, 2010.

[73] D. Kagan, R. Laocharoensuk, M. Zimmerman, C. Clawson, S. Balasubramanian, D. Bishop, S. Sattayasamitsathit, L. Zhang, and J. Wang. Rapid delivery of drug carriers propelled and navigated by catalytic nanoshuttles. *Small*, 6:2741, 2010.

[74] S. Kamdar, S. Shin, P. Leishangthem, LF Francis, X. Xu, and X. Cheng. The colloidal nature of complex fluids enhances bacterial motility. *Nature*, 603:819–823, 2022.

[75] A. Kanevsky, M. J. Shelley, and A. Tornberg. Modeling simple locomotors in stokes flow. *Journal of Computational Physics*, 229:958, 2010.

[76] H. Karani, G. Pradillo, and P. M. Vlahovska. Tuning the random walk of active colloids: From individual run-and-tumble to dynamic clustering. *Physical Review Letters*, 123(20):208002, 2019.

[77] R. Karmakar, R.V.S. Uday Bhaskar, R.E. Jesudasan, M.S. Tirumkudulu, and K.V. Venkatesh. Enhancement of swimming speed leads to a more-efficient chemotactic response to repellent. *Applied and Environmental Microbiology*, 82:1205–1214, 2015.

[78] T. V. Kasyap and D. L. Koch. Chemotaxis driven instability of a confined bacterial suspension. *Physical Review Letters*, 108(3):038101, 2012.

[79] T. V. Kasyap and D. L. Koch. Instability of an inhomogeneous bacterial suspension subjected to a chemoattractant gradient. *Journal of Fluid Mechanics*, 741:619–657, 2014.

[80] U.B. Kaupp, J. Solzin, E. Hildebrand, J.E. Brown, A. Helbig, V. Hagen, M. Beyermann, F. Pampaloni, and I. Weyand. The signal flow and motor response controlling chemotaxis of sea urchin sperm. *Nature Cell Biology*, 5:109, 2003.

[81] E. F. Keller and L. A. Segel. Initiation of slime mold aggregation viewed as an instability. *Journal of Theoretical Biology*, 26:399, 1970.

[82] E. F. Keller and L. A. Segel. Model for chemotaxis. *Journal of Theoretical Biology*, 30:225, 1971.

[83] J. Keller and S. Rubinow. Slender-body theory for slow viscous flow. *Journal of Fluid Mechanics*, 75:705–714, 1976.

[84] M. J. Kim and K. S. Breuer. Enhanced diffusion due to motile bacteria. *Physics of Fluids*, 16:L78, 2004.

[85] M.J. Kim and K.S. Breuer. Controlled mixing in microfluidic systems using bacterial chemotaxis. *Analytical Chemistry*, 79:955, 2007.

[86] Z. Kos and M. Ravnik. Elementary flow field profiles of micro-swimmers in weakly anisotropic nematic fluids: Stokeslet, stresslet, rotlet and source flows. *Fluids*, 3:1–2, 2018.

[87] D. E. Koshland. *Bacterial chemotaxis as a model behavior system*. Raven Press, 1980.

[88] D. Krishnamurthy and G. Subramanian. Collective motion in a suspension of micro-swimmers that run-and-tumble and rotary diffuse. *Journal of Fluid Mechanics*, 781:422–466, 2015.

[89] M. Kumar, J. S. Guasto, and A. M. Ardekani. Transport of complex and active fluids in porous media. *Journal of Rheology*, 66(2):375–397, 2022.

[90] P. Kundu and I. Cohen. *Fluid mechanics*. Academic Press, Massachusetts, 6th edition, 2016.

[91] R. Larson. *The Structure and Rheology of Complex Fluids*. Oxford University Press, New York, 1995.

[92] E. Lauga. Bacterial hydrodynamics. *Annual Review of Fluid Mechanics*, 48:105, 2016.

[93] E. Lauga and T.R. Powers. The hydrodynamics of swimming microorganisms. *Reports on Progress in Physics*, 72:096601, 2009.

[94] K. Leiderman and S. D. Olson. Swimming in a two-dimensional brinkman fluid: Computational modeling and regularized solutions. *Physics of Fluids*, 28:1, 2016.

[95] R. Di Leonardo, L. Angelani, D. Dell'Arciprete, G. Ruocco, V. Iebba, S. Schippa, M. P. Conte, F. Mecarini, F. De Angelis, and E. Di Fabrizio. Bacterial ratchet motors. *Proceedings of the National Academy of Sciences of the United States of America*, 107:9541–9545, 2010.

[96] A. M. Leshansky. Enhanced low-reynolds-number propulsion in heterogeneous viscous environments. *Phys. Rev. E 80*, 80, 2009.

[97] G. Li and A. Ardekani. Collective motion of microorganisms in a viscoelastic fluid. *Physical Review Letters*, 117(11):118001, 2016.

[98] G. Li, E. Lauga, and A. Ardekani. Microswimming in viscoelastic fluids. *Journal of Non-Newtonian Fluid Mechanics*, 297:104655, 2021.

[99] B. Liebchen and H. Löwen. Synthetic chemotaxis and collective behavior in active matter. *Accounts of Chemical Research*, 51:2982–2990, 2018.

[100] J. Lighthill. *Mathematical Biofluiddynamics*. SIAM, Philadelphia, PA, 1975.

[101] J. Lighthill. Flagellar hydrodynamics—the john von neumann lecture, 1975. *SIAM Review*, 18:161–230, 1976.

[102] J. Lighthill. On the squirming motion of nearly spherical deformable bodies through liquids at very small reynolds numbers. *SIAM Review*, 18:161–230, 1976.

[103] E. Lushi. *Chemotaxis and other effects in active particle suspensions*. PhD thesis, New York University, 2011.

[104] E. Lushi. Stability and dynamics of anisotropically tumbling chemotactic swimmers. *Physical Review E*, 94:022414, 2016.

[105] E. Lushi, R. E. Goldstein, and M. J. Shelley. Collective chemotactic dynamics in the presence of self-generated fluid flows. *Physical Review E*, 86:040902, 2012.

[106] E. Lushi, R. E. Goldstein, and M. J. Shelley. Nonlinear concentration patterns and bands in autochemotactic suspensions. *Physical Review E*, 98:052411, 2018.

[107] E. Lushi and C. Peskin. Modeling and simulation of active suspensions containing large numbers of interacting micro-swimmers. *Computers and structures*, 122:4–9, 2013.

[108] E. Lushi, H. Wioland, and R. Goldstein. Fluid flows created by swimming bacteria drive self-organization in confined suspensions. *Proceedings of the National Academy of Sciences of the United States of America*, 111:9734, 2014.

[109] R. M. Macnab and D. E. Koshland. The gradient-sensing mechanism in bacterial chemotaxis. *Proceedings of the National Academy of Sciences USA*, 69:2509, 1972.

[110] T. Majmudar, E. Keaveny, J. Zhang, and M. J. Shelley. Experiments and theory of undulatory locomotion in a simple structured medium. *Journal of the Royal Society Interface*, 9:1809–1823, 2012.

[111] K. Manesh and J. Wang. Motion control at the nanoscale. *Small*, 6:338, 2010.

[112] M. C. Marchetti, J. F. Joanny, S. Ramaswamy, T. B. Liverpool, J. Prost, Madan Rao, and R. Aditi Simha. Hydrodynamics of soft active matter. *Reviews of Modern Physics*, 85:1143, 2013.

[113] A. Martinez-Calvo, T. Bhattacharjee, R.K. Bay, H.N. Luu, A.M. Hancock, N.S. Wingreen, and S.S. Datta. Morphological instability and roughening of growing 3d bacterial colonies. *Proceedings of the National Academy of Sciences U.S.A.*, 119 (43):e2208019119, 2022.

[114] A. Martinez-Calvo, C. Trenado-Yuste, and S.S. Datta. Active transport in complex environments. *arXiv*, page 2108.07011, 2021.

[115] S. Michelin. Self-propulsion of chemically active droplets. *Annual Review of Fluid Mechanics*, 55:77–101, 2023.

[116] G. Mino, T.E. Mallouk, T. Darnige, M. Hoyos, J. Dauchet, J. Dunstan, R. Soto, Y. Wang, A. Rousselet, and E. Clement. Enhanced diffusion due to active swimmers at a solid surface. *Physical Review Letters*, 106:061916, 2011.

[117] N. Mittal, E. O. Budrene, M. P. Brenner, and A. van Oudenaarden. Motility of escherichia coli cells in clusters formed by chemotaxis. *Proceedings of the National Academy of Sciences USA*, 100:13259, 2003.

[118] D. Mondal, A. G. Prabhune, S. Ramaswamy, and P. Sharma. Strong confinement of active microalgae leads to inversion of vortex flow and enhanced transport. *eLife*, 2003.02040:2, 2021.

[119] J. Moran and J. Posner. Microswimmers with no moving parts. *Phys. Today 72*, 5:45, 2019.

[120] A. Morozov. From chaos to order in active fluids. *Science*, 355:1262–1263, 2017.

[121] N. Murugan and A. Roy. Instability of an autochemotactic active suspension. *Journal of Fluid Mechanics*, 934:A21, 2022.

[122] H. Nganguia and O. S. Pak. Squirming motion in a brinkman medium. *Journal of Fluid Mechanics*, 855:554, 2018.

[123] H. Nganguia, L. Zhu, D. Palaniappan, and O. S. Pak. Squirming in a viscous fluid enclosed by a brinkman medium. *Physical Review E*, 101:063105, 2020.

[124] H. Nguyen, K. Leiderman, and S. Olson. A three-dimensional model of flagellar swimming in a brinkman fluid. *Journal of Fluid Mechanics*, 864:1088–1124, 2019.

[125] H. Nguyen, S. Olson, and K. Leiderman. A fast method to compute triply-periodic brinkman flows. *Computers and Fluids*, 133:55–67, 2016.

[126] H. Nguyen, S. Olson, and K. Leiderman. Computation of a regularized brinkmanlet near a plane wall. *Journal of Engineering Mathematics*, 114:19–41, 2019.

[127] H.G. Othmer, S.R. Dunbar, and W. Alt. Models of dispersal in biological systems. *Journal of Mathematical Biology*, 26:263, 1988.

[128] S. Park, P. M. Wolanin, E. A. Yuzbashyan, P. Silberzan, J. B. Stock, and R. H. Austin. Motion to form a quorum. *Science*, 301:188, 2003.

[129] C.S. Patlak. Random walk with persistence and external bias. *Bulletin of Mathematical Biophysics*, 15:311, 1953.

[130] W. F. Paxton, K. C. Kistler, C. C. Olmeda, A. Sen, S. K. St. Angelo, Y. Cao, T. E. Mallouk, P. E. Lammert, and V. H. Crespi. Engineering bacterial vortex lattice via direct laser lithography. *Nature Communications*, 9:4486, 2018.

[131] W.F. Paxton, P.T. Baker, T.R. Kline, Y. Wang, T.E. Mallouk, and A. Sen. Catalytically induced electrokinetics for motors and micropumps. *Journal of the American Chemical Society*, 128:46, 2006.

[132] W.F. Paxton and K.C. Kistler. Catalytic nanomotors: Autonomous movement of striped nanorods. *Journal of the American Chemical Society*, 126:13424, 2004.

[133] W.F. Paxton, A. Sen, and T.E. Mallouk. Motility of catalytic nanoparticles through self-generated forces. *Chemistry - A European Journal*, 11:6462, 2005.

[134] T. Pedley. Spherical squirmers: models for swimming micro-organisms. *Institute of mathematics and its applications of applied mathematics*, 81:488–521, 2016.

[135] T. J. Pedley and J. O. Kessler. Hydrodynamic phenomena in suspensions of swimming microorganisms. *Annual Review of Fluid Mechanics*, 24:313, 1992.

[136] T.J. Pedley. Instability of uniform micro-organism suspensions revisited. *Journal of Fluid Mechanics*, 647:335, 2010.

[137] A. Petroff and A. Libchaber. Fast-moving bacteria self-organize into active two-dimensional crystals of rotating cells. *Physical Review Letters*, 114:158102, 2015.

[138] M. Polin, I. Tuval, K. Drescher, J. Gollub, and R. Goldstein. Chlamydomonas swims with two gears in a eukaryotic version of run-and-tumble locomotion. *Science*, 325:487–490, 2009.

[139] C. Pozrikidis. *Boundary Integral and Singularity Methods for Linearized Viscous Flow*. Cambridge University Press, New York, first edition, 1992.

[140] E. Purcell. Life at low reynolds number. *American Journal of Physics*, 45:3–11, 1977.

[141] S. Ramaswamy. The mechanics and statistics of active matter. *Annual Review of Condensed Matter Physics*, 1:323–345, 2010.

[142] R.J. Redfield. Is quorum sensing a side-effect of diffusion sensing? *Trends in Microbiology*, 19:365, 2002.

[143] F. Rojas-Pérez, B. Delmotte, and S. Michelin. Hydrochemical interactions of phoretic particles: a regularized multipole framework. *Journal of Fluid Mechanics*, A22:919, 2021.

[144] R. Rusconi, S. Lecuyer, L. Guglielmini, and H.A. Stone. Laminar flow around corners triggers the formation of biofilm streamers. *Journal of the Royal Society Interface*, 7:1293, 2010.

[145] D. Saintillan. Kinetic models for biologically active suspensions. In *Proceedings of IMA*, 2010.

[146] D. Saintillan and M. J. Shelley. Orientational order and instabilities in suspensions of self-locomoting rods. *Physical Review Letters*, 99:058102, 2007.

[147] D. Saintillan and M. J. Shelley. Instabilities and pattern formation in active particle suspensions: Kinetic theory and continuum simulations. *Physical Review Letters*, 100:178103, 2008.

[148] D. Saintillan and M. J. Shelley. Instabilities, pattern formation, and mixing in active suspensions. *Physics of Fluids*, 20:123304, 2008.

[149] D. Saintillan and M. J. Shelley. Active suspensions and their nonlinear models. *Comptes Rendus Physique*, 16:318–334, 2015.

[150] D. Saintillan and M.J. Shelley. Emergence of coherent structures and large-scale flows in motile suspensions. *Journal of the Royal Society Interface*, 2011.

[151] J. Saragosti, V. Calvez, N. Bournaveas, B. Perthame, A. Buguin, and P. Silberzan. Directional persistence of chemotactic bacteria in a traveling concentration wave. *Proceedings of the National Academy of Sciences*, 108:16235–16240, 2011.

[152] M. J. Schnitzer. Theory of continuum random walks and application to chemotaxis. *Physical Review E*, 48:2553, 1993.

[153] A. Sen, M. Ibele, Y. Hong, and D. Velegol. Chemo and phototactic nano/microbots. *Faraday Discussions*, 2009.

[154] O. Sipos, K. Nagy, R. Di Leonardo, and P. Galajda. Hydrodynamic trapping of swimming bacteria by convex walls. *Physical Review Letters*, 114:258104, 2015.

[155] A. Sokolov, M. M. Apodaca, B. A. Grzybowski, and I. S. Aranson. Swimming bacteria power microscopic gears. *Proceedings of the National Academy of Sciences of the United States of America*, 107:969–974, 2010.

[156] A. Sokolov, I. S. Aranson, J. O. Kessler, and R. E. Goldstein. Concentration dependence of the collective dynamics of swimming bacteria. *Physical Review Letters*, 98:158102, 2007.

[157] A. Sokolov, R.E. Goldstein, F.I. Feldstein, and I.S. Aranson. Enhanced mixing and spatial instability in concentrated bacteria suspensions. *Physical Review E*, 80:031903, 2009.

[158] S. E. Spagnolie and E. Lauga. Hydrodynamics of self-propulsion near a boundary: predictions and accuracy of far-field approximations. *Journal of Fluid Mechanics*, 700:105–147, 2012.

[159] S. E. Spagnolie, G. R. Moreno-Flores, D. Bartolo, and E. Lauga. Geometric capture and escape of a microswimmer colliding with an obstacle. *Soft Matter*, 11:1, 2015.

[160] S. E. Spagnolie and P. T. Underhill. Swimming in complex fluids. *Annual Review of Condensed Matter Physics*, 14(1):381–415, 2023.

[161] J. Stenhammar, C. Nardini, R. W. Nash, D. Marenduzzo, and A. Morozov. Role of correlations in the collective behavior of microswimmer suspensions. *Physical Review Letters*, 119:028005, 2017.

[162] R. L. Stoop, N. Waisbord, V. Kantsler, V. Heinonen, J. Guasto, and J. Dunkel. Disorder-induced topological transition in porous media flow networks. *Journal of Non-Newtonian Fluid Mechanics*, 268:66–74, 2019.

[163] G. Subramanian and D. L. Koch. Critical bacterial concentration for the onset of collective swimming. *Journal of Fluid Mechanics*, 632:359, 2009.

[164] G. Subramanian and D. L. Koch. Collective hydrodynamics of swimming microorganisms: Living fluids. *Annual Review of Fluid Mechanics*, 43:637–659, 2011.

[165] S. Sundararajan, S. Sengupta, M. Ibele, and A. Sen. Drop-off of colloidal cargo transported by catalytic pt-au nanomotors via photochemical stimuli. *Small*, 6:1479, 2010.

[166] K. Thijssen, D. Khaladj, Aghvami, S. Ali, M.A. Gharbi, S. Fraden, J. Yeomans, L. Hirst, and T. Shendruk. Submersed micropatterned structures control active nematic flow, topology and concentration. *Proceedings of the National Academy of Sciences of the United States of America*, 2102.10184:13, 2021.

[167] M.J. Tindall, P.K. Maini, S.L. Porter, and J.P. Armitage. Overview of mathematical approaches used to model bacterial chemotaxis i: the single cell. *Bulletin of Mathematical Biology*, 70:1525, 2008.

[168] T. Traverso and S. Michelin. Collective dynamics and rheology of confined phoretic suspensions. *Journal of Fluid Mechanics*, A21:943, 2022.

[169] I. Tuval, L. Cisneros, C. Dombrowski, C.W. Wogelmuth, J.O.Kessler, and R.E. Goldstein. Bacterial swimming and oxygen transport near contact lines. *Proceedings of the National Academy of Sciences of the United States of America*, 102:2277, 2005.

[170] P. T. Underhill, J. P. Hernandez-Ortiz, and M. D. Graham. Diffusion and spatial correlation in suspensions of swimming particles. *Physical Review Letters*, 100:248101, 2008.

[171] T. Vicsek and A. Zafeiris. Collective motion. *Physics Reports*, 517:71–140, 2012.

[172] A. Villa-Torrealba, S. Navia, and R. Soto. Kinetic modeling of the chemotactic process in run-and-tumble bacteria. *Physical Review E*, 107:034605, 2023.

[173] G. Volpe, I Buttinoni, D. Vogt, J-H Kummerer, and C. Bechinger. Microswimmers in patterned environments. *Soft Matter*, 7:8810–8815, 2011.

[174] H. Wioland, E. Lushi, and R. E. Goldstein. Directed collective motion of bacteria under channel confinement. *New Journal of Physics*, 18:075002, 2016.

[175] H. Wioland, F. Woodhouse, J. Dunkel, J. Kessler, and R. Goldstein. Confinement stabilizes a bacterial suspension into a spiral vortex. *Physical Review Letters*, 110:268102, 2013.

[176] X.-L. Wu and A. Libchaber. Particle diffusion in a quasi-two-dimensional bacterial bath. *Physical Review Letters*, 84:3017, 2000.

[177] G. T. Yates. How microorganisms move through water. *American Scientist*, 74:358–65, 1986.

[178] J. M. Yeomans, D.O. Pushkin, and H. Shum. An introduction to the hydrodynamics of swimming microorganisms. *The European Physical Journal Special Topics*, 223:1771–1785, 2014.

[179] H.P. Zhang, A. Be'er, E.L. Florin, and H.L. Swinney. Collective motion and density fluctuations in bacterial colonies. *Proceedings of the National Academy of Sciences of the United States of America*, 107:10731, 2010.

[180] A. Zottl and H. Stark. Emergent behavior in active colloids. *Journal of Physics: Condensed Matter*, 2016.

[181] V. Škultéty, C. Nardini, J. Stenhammar, D. Marenduzzo, and A. Morozov. Swimming suppresses correlations in dilute suspensions of pusher microorganisms. *Physical Review X*, 10:031059, 2020.